Development of a new composite powder material of cement additive with Polyamide 12 for selective laser sintering

A thesis

submitted to

Cardiff University

For the degree of

Doctor of Philosophy

by

Saleh Ahmed Aldahsh

Manufacturing Engineering Centre

School of Engineering

Cardiff University

United Kingdom

2011

Abstract

Applications of rapid prototyping are expanding to new domains. This is particularly true of the selective laser sintering (SLS) process. In order for that process to be competitive and become a strong candidate for new applications, such as rapid manufacturing, the material used needs to be improved. The aim of the work presented in this thesis was to develop a new composite material made up of Polyamide 12 (a common SLS material) and cement, an inexpensive additive, for the purpose of improving the mechanical properties, as well as reducing the cost of the sintered components.

An experimental study was conducted of the thermal properties of the cement-Polyamide 12 composite material with different proportions of cement and Polyamide 12. The purpose of the study was to determine optimal SLS parameters to produce good quality fabricated SLS specimens. The research also involved an experimental investigation of the mechanical properties (Young's modulus, tensile, flexural, compression and impact strengths, and density) as a function of the proportion of cement additive to Polyamide 12. Finally, a method of quickly and inexpensively producing test specimens by casting instead of using SLS was developed and experiments conducted to demonstrate the similarity in properties between cast and SLS specimens.

This research has shown that adding cement to Polyamide 12 yields a composite material that enables the production of sintered specimens with mechanical properties that are superior to those of pure Polyamide 12 specimens. As cement is much cheaper than Polyamide 12, the composite material is also obviously less expensive than pure Polyamide 12.

Acknowledgements

I would like to express my sincere gratitude to Allah for giving me the opportunity to complete the writing of this thesis. I am also grateful to my wife, Jawaher, my daughter, Shekhah and my little son, Ahmed for their patience, giving me their love and supporting that I needed.

I am heartily thankful to my supervisor Professor D T Pham (OBE), Director of Manufacturing Engineering Centre (MEC), for his valued supervision, advice, availability, support and encouragement enabled this thesis to be written and will always be deeply appreciated.

To all colleagues and friends at the Mechanical and Manufacturing Engineering, I would like to express my gratitude for their patience and continuous support. Special thanks go to Dr. Shwe Soe, Dr. Sam Evans, Mr. Justin for their constant assistance through technical help, endless discussion and unquestionable support. Also my thanks go to Mr. Rod Bottom and Dr. Steve Holding.

Lastly, I also express my warmest appreciation to all of those who supported me in any respect during the completion of the research.

Declaration

This work has not previously been accepted in substance for any degree and is not concurrently being submitted in candidature for any degree.

Signed:…… (Saleh Ahmed Aldahsh) Date :……..

Statement 1

This thesis is being submitted in partial fulfilment of the requirements for the degree of PhD.

Signed:…… (Saleh Ahmed Aldahsh) Date :……..

Statement 2

This thesis is the result of my own independent work/investigation, except where otherwise stated. Other sources are acknowledged by explicit references.

Signed:…… (Saleh Ahmed Aldahsh) Date :……..

Statement 3

I hereby give consent for my thesis, if accepted, to be available for photocopying and for inter-library loan and for the title and summary to be made available to outside organisations.

Signed:…… (Saleh Ahmed Aldahsh) Date :……..

Table of contents

List of figures

List of tables

Abbreviations

ABS	Acrylonitrile butadiene styrene
AL2O3	Aluminum Oxide
CAD	Computer aided design
CaO	Calcium Oxide
CCD	Charge Coupled Device
CRT	Cathode Ray Tube
CSA	Cross Sectional Area
CuPA	Copper Polyamide
DSLS	Direct Selective Laser Sintering
Dp	Penetration Depth
3DP	Three-Dimensional Printing
DSC	Differential scanning calorimetry
3D	Three dimensions
EOS	Electro Optical Systems
FDM	Fused Deposition Modelling
Fe2O3	Iron Oxide
GF	Glass filled
GPC	Gel permeation chromatography
IR	Sensor
ISO	International Organization for Standards
LOM	Laminated Object Manufacturing

LS	Laser Sintering
MFR	Melt flow rate
PA12	Polyamide 12
PC	Polycarbonate
PP	Polypropylene
PE	Polyethylene
RM	Rapid manufacturing
RP	Rapid prototyping
RT	Rapid tooling
RW	Road Width
SEM	Scanning electron microscope
SiC	Silicon Carbide
SiO2	Silicon Dioxide
SLA	Stereolithography
SLS	Selective Laser Sintering
STL	Stereolithography Interface Format
UTS	Ultimate Tensile Strength
UV	Ultraviolet
WT	Weight Fractions

Nomenclature

Symbol	Description	Unit
ε	Strain value	%
η_0	Viscosity	Pa.s
ρ	powder density	g/cm^3
σf	Flexural stress	MPa
σM	Tensile strength	MPa
Δd	Difference in deflection corresponding to the difference in force ΔF	mm
ΔE	Activation energy	kJ/mol
ΔF	Difference in force	N
ΔLo	Increase in the specimen length	mm
A	Initial cross-sectional area of the specimen	mm
*a*iN	Izod impact strength of notched specimens	KJ/m^2
*b*N	Remaining width of the test specimen	mm
b	Width of the specimen	mm
C	Specific heat	J/g.ºC
Db	Diameter of laser beam on the part-bed	mm
*E*c	Energy absorbed by breaking the test specimen	J
*E*f	Flexural modulus	GPa
Et	Young's modulus	MPa
F	Force applied	N
h	Thickness of the specimen	mm

lf	Latent melting heat	J/kg
Lo	Length of the test specimen	mm
Lp	Laser powder	Watt
Ls	Laser speed	mm/sec
L	Span of two points	mm
M_w	Average molecular weight	g/mol
R	Gas constants	J/ mol.K
r	Radius of the particles	μm
Scsp	Scan spacing	mm
Tb	Part bed temperature	^oC
T_c	Crystalline temperature	^oC
T_g	Glass transition temperature	^oC
T_m	Melting temperature	^oC
T	Absolute temperature	Kelvin
ν	Growth rate	μm/min
x	Size of neck growth	μm

Chapter 1

Introduction

1.1 Background

One of the most common rapid prototyping (RP) techniques in existence is selective laser sintering (SLS) which is capable of producing very complex part-geometry directly from three-dimensional CAD software. SLS employs powder-processing in the construction of parts. Sintered parts are fabricated when the surface tension of particles is overcome in the heat of an infrared laser beam and they subsequently fuse together. The powder is supplied by two feed-cartridges which distribute a thin layer of powder over the build-area with a rotating roller, so that the next layer of powder may be added. The process continues in this way until the part is completed.

One of the main advantages of the SLS process is that numerous materials and indeed, any material that can be triturated, may be used in the SLS process via a low melting temperature binder such as a polymer, for a high melting point phase in order to produce a geometrically accurate sintered part (Vail et al., 1996; Hon & Gill, 2003). The flexibility of material and shape which SLS technology produces

potentially has practical and effective applications in specific areas (Maeda & Childs, 2004).

One of the key factors which make thermoplastics attractive for engineering applications is the possibility of property enhancement through reinforcement. Composites produced through additive reinforcement have enabled thermoplastics to satisfactorily meet demands in the aerospace and automobile industries (Crawford, 1987). Thermoplastics such as Polyamide 12 (PA12) have been developed as SLS materials for various applications.

However, the purpose of the work presented in this thesis concerns the relatively low strength and high price of Polyamide 12. The focus of the research is to create new composite material from cement additive with Polyamide 12 so as to reduce cost, as well as to considerably improve the mechanical properties of the sintered specimen. The addition of rigid particles to polymers can produce a number of attractive effects in the mechanical properties of specimens, such as increased flexural strength, compression, hardness, rigidity, improvement in fracture toughness, creep resistance and, in some cases, tensile strength, while impact strength is decreased with increasing filler (Kohan, 1995; Gill & Hon, 2004).

1.2 Aim and objectives

The aim of this research was to test the hypothesis that adding cement to Polyamide 12 yields a composite material enabling the production of sintered parts with mechanical properties that are superior to those made from pure Polyamide 12. As cement is much cheaper than Polyamide 12, naturally, the composite material will be less expensive than pure Polyamide 12.

The objectives of the research are:

- To investigate the properties of Polyamide 12 powder and cement powder in varying proportions, as the new composite powder material is based on SLS.
- To expand a methodology for controlling SLS parameters, in order to obtain consistent and good quality fabricated SLS specimens.
- To obtain homogeneous powder mixtures which offer consistency in density and the mechanical properties of the sintered parts, by developing a methodology for controlling the mixture of composite powder material.
- To develop a casting method to produce specimens with properties similar to those of SLS parts in the same material, in order to reduce the time and quantities of material involved when testing new materials.
- To study how cement powder influences mechanical properties of sintered components when added to Polyamide 12.

- To improve the mechanical properties of functional parts by increasing the proportion of cement.

The research mainly involved experimentation with composite material having different proportions of additive to Polyamide 12. Tests were also carried out to determine the mechanical properties of specimens produced using the new composite material.

1.3 Organisation of the thesis

Chapter 2 reviews common rapid prototyping processes with emphasis on a description of Selective Laser Sintering (SLS) technology which is considered one of the more common rapid prototyping techniques. During the SLS process, the main fabrication parameters which influence the quality of sintered parts are described. Some of the common materials used to produce RM and RP parts by SLS are presented. The problems found in parts produced through the sintering process are mentioned in this chapter. Additionally, some previous studies of composite materials used in SLS are reviewed**.** In Chapter 3, the experimental procedure, equipment and measurements used to characterise the behaviour of composite material as powder and sintered specimens are introduced. Additionally, the composite material used in this thesis is described. The composite material used in this work comprises cement additives with Polyamide 12.

Chapter 4 This chapter discusses the properties of cement and Polyamide 12 composite, as well as the thermal behaviour, melt flow rate, and molecular weight of this material. This chapter focuses on understanding the thermal properties of different proportions of composite material of cement and PA12 to determine the optimum parameters of the SLS process. In addition, the thermal and physical of used or un-sintered powder are studied to develop a methodology for controlling SLS parameters, and consequently to obtain consistent and good quality in fabricated SLS specimens.

Chapter 5 discusses the interactions between cement and Polyamide 12 particles and between Polyamide 12 themselves. It describes an experimental study of tensile, Young's modulus, flexural, compression, impact and density specimens, in order to determine the effects of varying energy density and varying proportions of composite material of cement additive with Polyamide 12 on the density and mechanical properties of sintered specimens. The effect of using un-sintered powder on MFR and mechanical properties is investigated to determine the validity of the powder. In addition, it compares the mechanical properties of actual parts produced using SLS with data-sheet values for PA12 material so as to generate confidence in the measured mechanical properties. Furthermore, it explains the effects of various energy densities on composite material properties by examining the physical construction of the specimens presented. The optimum energy density for producing parts with maximum density, strength and stiffness has been determined in this chapter.

Chapter 6 presents a method of casting to produce parts with similar mechanical properties to those of components fabricated by SLS. Tensile, Young's modulus, flexural and compression strength measurements used in the casting method to assess the effect of varying proportions of composite material of cement additive with Polyamide 12 on the mechanical properties of specimens. The mechanical properties of parts produced using casting are compared with those of parts created in SLS using the same materials. The main purpose of this chapter is to investigate whether or not a correlation can be made between the mechanical properties of parts produced via casting methods and those manufactured through SLS.

Finally, chapter 7 concludes the thesis by summarising the contributions and findings of the research and proposing areas for further study.

Chapter 2

Literature Review

2.1 Preliminaries

Rapid prototyping (RP) methods denote a family of technologies capable of producing very complex part-geometry directly from three-dimensional CAD software, using a swift, highly automated and flexible manufacturing procedure (Kai & Fai, 1997; Pham & Dimov, 2000; Cooper, 2001). These technologies are also known as 'Solid Freeform Fabrication', 'Layer Manufacturing' and 'Computer Automated Manufacturing' (Beaman et al., 1997; Ilkgun, 2005).

RP systems operate on the principle of layer-by-layer construction (see Figure 2.1). Through a computer interface, the system receives the STL (Standard Triangulation Language) model CAD data relating to the object to be produced. The STL file is very simple as it consists solely of a list of planar triangles: a wide range of input in any 3D geometric form can be converted to a triangulated model due to the broad applicability of available-surface triangulation algorithms (Kumar & Dutta, 1997). The STL model is sliced virtually into thin even layers by software inside the RP

system. The model is then reconstructed physically layer by layer, with each layer being fused to the previous one gradually to generate an object.

These RP technologies have a broad range of applications in different fields, including aerospace, electronics and biomedical engineering. Consequently, they offer a unique and versatile process (Pham & Dimov, 2003; Salmoria et al., 2007). RP processes differ from conventional manufacturing processes in that production time is shorter when using the former and a wide range of materials can be used to a high degree of accuracy due to the additive, layered nature of RP. This enables objects with complicated internal features to be created, which conventional machinery cannot manufacture directly. In addition, RP builds parts by adding material layer-by-layer, thus avoiding tooling, reorientation and fixturing problems. When the bottom layer is attached to a platform, the part is produced without any reorientation or refixturing needed during manufacture. In contrast to this, traditional machining methods involve the removal of unwanted material from a solid block. Generally, a complex object built using traditional machining requires that complex tooling and tool-path planning be designed and constructed in advance. Furthermore, difficult fixturing techniques and reorientation of complex objects are necessary during the fabrication process. In addition to prototypes, however, RP techniques can also be utilised in tool-making (referred to as 'rapid tooling') and even in the manufacture of certain production-quality parts (rapid manufacturing) (King & Tansey 2003; Ilkgun, 2005).

A large numbers of rapid prototyping techniques exists, but only a few of them are widely used and predominant in the market (Pham & Gault, 1998). In the following sections, the following most common processes are presented:

Laminated Object Manufacturing (LOM)

Stereolithography (SLA)

Fused Deposition Modelling (FDM)

Three-Dimensional Printing (3DP)

Selective Laser Sintering (SLS)

Each of these technologies is explained with a brief description and an outline of their building strategies. This current study focuses on SLS technology. In this process, a wide variety of materials can be used to build parts, and so it has an advantage over some of the other RP processes. A number of these materials and their applications are presented in this study. Furthermore, some of the problems found in parts produced through SLS are mentioned, and finally, a description of previous studies of composite material used in SLS is given.

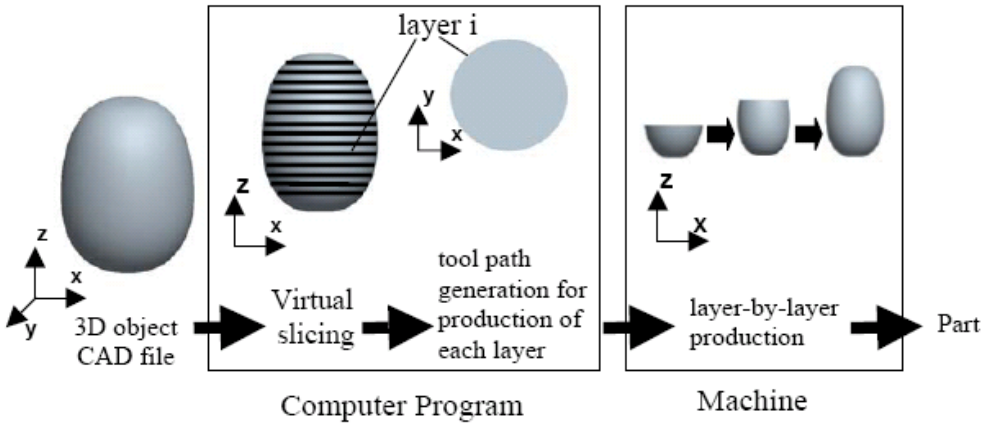

Figure 2.1: Layer-by-Layer Production (Ilkgun, 2005).

2.2 Classification of Common Rapid Prototyping Technologies

In the following sections, common rapid prototyping (RP) processes are classified. In addition, a brief description of each, together with their building approaches and the major advantages and disadvantages of these approaches, are also presented.

2.2.1 Laminated Object Manufacturing

Laminated Object Manufacturing (LOM) is one of the RP techniques that mainly adopt the process of 'laminated forming'. Thin layers of laminate are used to produce parts during this process. The materials used are paper, plastic, ceramic and composites: the most common material being paper. Layers are bonded by coating the sheets with heat sensitive adhesives, allowing layer-by-layer bonding through hot roller compression.

As illustrated in Figure 2.2, the sheets of material are supplied and fed from a material-supply roll and transferred to a take-up roll located in a facing position. The contours of each layer are cut with a CO2 laser controlled by a CAD system. A laser beam is carefully modulated to penetrate precisely to the depth of one layer. Any material that is not part of the specimen is trimmed into a rectangular shape by the laser to facilitate its removal when fabrication of the part is later completed. The rectangular shape remains in place as an external support during the building process.

The LOM process generally has advantages over other RP technologies. For example, the part does not require a support structure as it is supported by its own material. It is also simple to use and poses no environmental concerns. Furthermore, it prevents distortion, shrinkage and deformation due to the very low levels of internal tension within LOM parts. In contrast however, a high level of effort is applied to decubing, finishing and sealing parts. Papers are easily peeled off at the adhesion layer and bubbles can appear between layers. The part can either be burnt due to overheating, or be subject to integration failure due to insufficient heat. The control of parts' accuracy in the *Z*-dimension is relatively complicated for paper LOM parts, due to a swelling effect (‘*Z* growth'). Remains of material supporting the part are scrapped after building and the cost of such waste can be significant (Mueller & Kochan, 1999; Pham & Dimov, 2003).

2.2.2 Stereolithography (SLA)

Parts built using SLA are based on a photosensitive liquid resin which forms a solid polymer when exposed to ultraviolet (UV) light. SLA systems consist of a build-platform positioned inside a vat of resin and an ultraviolet laser. The first position of the platform is on top of the surface of the resin, before being lowered to the planned thickness of the first layer of the part, where it is imaged on the resin surface by the laser using information obtained from the three-dimensional solid CAD model. Once an ultraviolet laser has drawn the layer structure on the surface of the resin, the scanned resin is allowed to polymerise and solidify. The next layer is then scanned so

another layer can be built. The process is repeated until the part is completely fabricated (see Figure 2.3). The vat and excess resin are drained and the part removed from its build-platform. Any parts produced through SLA have overhangs which require support structures to prevent them from swaying and becoming deformed in the liquid environment. The supports are removed after the part has been completed. In some cases the support structures are not removed, for example, where a fabrication part has internal cavities with few or no access points (Kai & Fai, 1997; Pham & Dimov, 2000).

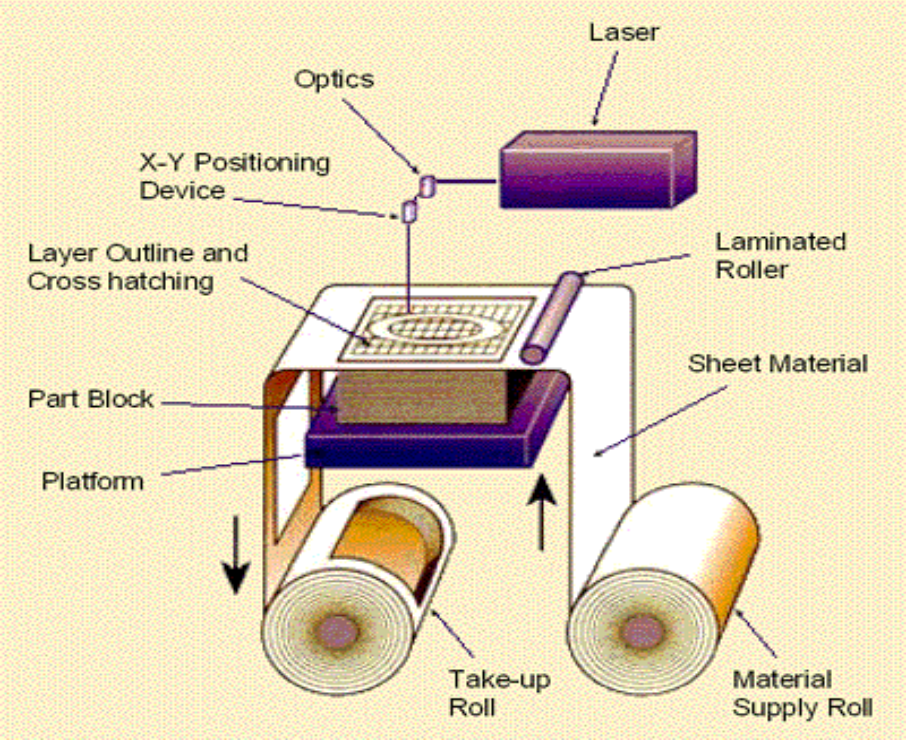

Figure 2.2: Laminated Object Manufacturing Process (Liao, et al., 2005).

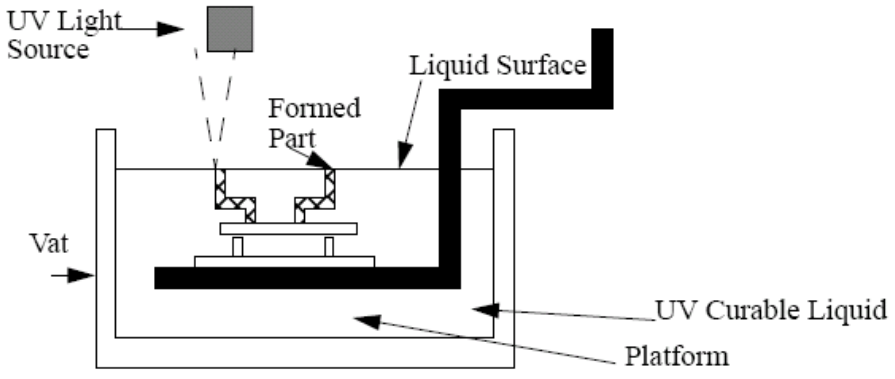

Figure 2.3: Stereolithography Process (Kietzman, 1999).

2.2.3 Fused Deposition Modelling

Fused Deposition Modelling (FDM) requires a nozzle tip to build the part and a base platform for support and building. The material which is used in this process is thermoplastic filament or wax. The filament material is fed by a temperature-controlled extruder to force out and deposit the material onto a platform in a layer-by-layer process, as shown in Figure 2.4. Once the first layer is finished, the base platform is lowered and the next layer is deposited. Each added layer bonds to the previous one as a result of thermal fusion. Consequently, the building process needs to be maintained at a temperature just below solidification point to ensure proper adhesion between subsequently added layers. The designed object is fabricated as a three-dimensional part from computer-generated solid or surface models, as in a typical RP process based exclusively on the precise deposition of thin layers of extrudate. In this process, the road width (RW) is controlled by flow parameters at a temperature set above the melting-point of the thermoplastic material and also by the precise dimensions of the nozzle tip used (Jamal, 2001; Castle, 2008).

2.2.4 Three-Dimensional Printing

Three Dimensional Printing (3DP) is one of the rapid prototype techniques which employ powder-processing in the construction of parts. In this process, many types of powder can be used, including metals, ceramics and polymers. The 3DP machine consists of a print-head which has X–Y axes suspended over a vertical piston plate,

providing control over three directions of motion as shown in Figure 2.5. A thin layer of powder is spread onto a piston plate and levelled by a roller controlled by a CAD system. Binding material is passed through a nozzle affixed to the fast-axis carriage with a back and forth motion over the powder-bed, in order to selectively print droplets which bind the powder particles together. The piston plate lowers the piece of work and the roller spreads the next layer of powder. The process is repeated until the part is completed. A schematic of the process is shown in Figure 2.5. Once building is complete, excess powder which has been supporting the model is removed to reveal the fabricated part. Any possible overhangs in the part therefore do not require the design and fabrication of support structures (Kai & Fai, 1997; Katstra et al., 2000).

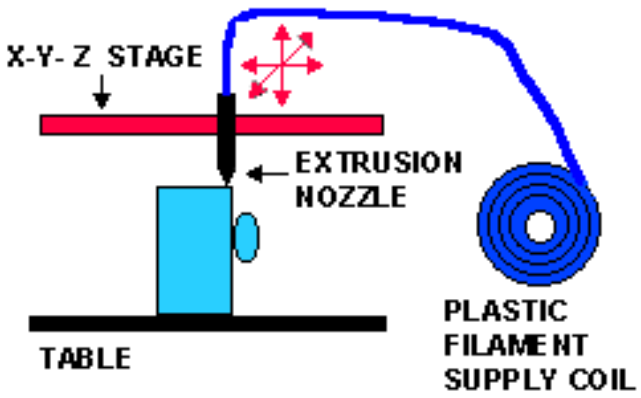

Figure 2.4: Fused Deposition Modelling Process (Castle, 2008).

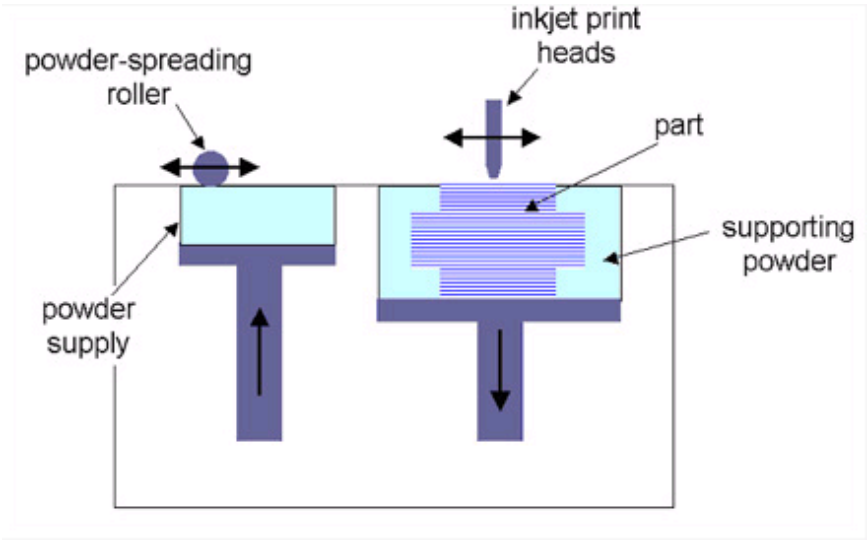

Figure 2.5: Three-Dimensional Printing Process (Xpress 3D, 2005).

2.2.5 Selective Laser Sintering

Selective Laser Sintering (SLS) is one of the more common rapid prototype techniques. It was developed and originally patented by the University of Texas, Austin, and was licensed to the DTM Corporation. DTM introduced the first commercially available system in 1992, and the latest SLS system by DTM is the Sinterstation 2500 Plus (Kai & Fai, 1997; Pham & Dimov, 2000). A summary of specifications for Sinterstation 2500 Plus and Sinterstation 2000 is given in Table 2.1.

SLS employs powder-processing in the construction of parts. In this process, many types of powders can be used, including polymers, ceramics, metals and composites. SLS parts are fabricated when the surface tension of particles is overcome in the heat of an infrared laser beam and they subsequently fuse together. The powder is supplied by two feed-cartridges which distribute a thin layer of powder over the build-area, using a rotating roller. The build-area is also supported by a movable piston (see Figure 2.6) (Pham & Dimov, 2003).

The SLS process begins by transferring CAD data files in STL file format to the SLS machine, where they are sliced as shown in Figure 2.1. Build-parameters and manipulation of the laser are controlled by data processing with the computer system. In addition to this, the computer system is used to regulate nitrogen, thus creating an inert environment so as to eliminate the possibility of powder oxidation and explosion. This is followed by heating the powder to a temperature just below the

melting-point of the material concerned, using a heater located above the part-bed. This minimises thermal distortion, reduces heat stress to the lowest possible degree and prevents the fabricated part from warping. In this way, fusion to the previous layer is also facilitated. The temperature of the powder feed-cartridges is controlled to allow powder to be transferred freely by a rotating roller. A very thin layer (between 100 μm to 125μm) is spread by the roller across the part during the build process. The transverse speed of the roller is an adjustable machine parameter (Kumar & Dutta, 1997; Yusoff, 2007).

The SLS machine uses a CO2 laser with a capacity of up to 50 watts (Kai & Fai, 1997). The laser beam is guided by two mirrors onto the surface of the powder build-area, thereby enabling it to scan specific areas of powder corresponding to a particular slice of the object's design geometry (see Figure 2.6). The interaction of the laser beam with the powder fuses the powder particles to produce the first layer of LS parts (Neal, 1994; Yusoff, 2007). The part-build cylinder lowers slightly and one of the feed-cartridges rises so that the next layer of powder may be added. The process continues in this way until the part is completed. The sintered powder forms the part while the un-sintered powder remains in the part-build during fabrication, surrounding the sintered powder as a support.

Table 2.1: Specifications of Sinterstation 2000 and 2500plus.

Model	Sinterstation 2000 System	Sinterstation 2500plus System
Process	Selective Laser Sintering	Selective Laser Sintering
Laser type	CO2	CO2
Laser power (W)	50	50
Spot size (mm)	0.4	0.42
Scan speed (mm/s)	914	5000
Work volume (mm)	300 Ø × 380 Z	381w × 330d × 457h
Computer system	Pentium-based; Unix System	Pentium-based controller
Power supply	240 VAC, single phase	240 VAC, 3-phase

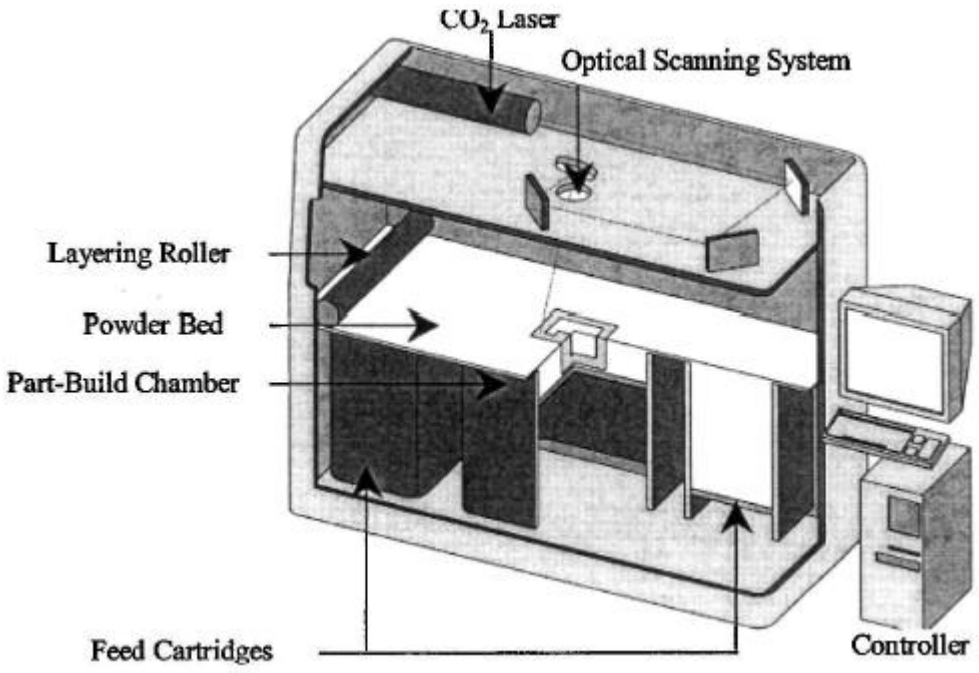

Figure 2.6: Selective Laser Sintering (Pham & Dimov, 2003).

2.2.5.1 Common fabrication parameters

The SLS process has many fabrication parameters which influence the quality of sintered parts, such as geometric problems, or mechanical and physical properties. These parameters are set differently according to powder properties and the requirements of the application (Gibson & Shi, 1997). Consequently, the default values for all process parameters based on the material used in the process have been specified by SLS manufacturers as DTM and EOS. In the following section, the most common fabrication parameters are described.

2.2.5.1.1 Fill-laser power

Fill-laser power takes into account an important SLS parameter available to the CO2 laser beam at the part-bed surface. The input value of fill-laser power depends on the type of material and thickness of the layer relevant to the part being built (Ilkgun, 2005). This parameter should be set to ensure that the powder at part-bed surface is heated to a temperature close to its melting-point in order to allow bonding between adjacent powder particles. To determine the optimum laser power for the material used in SLS, test parts are fabricated using various levels of laser power (Gibson & Shi, 1997; Jamal, 2001). Relatively low laser power is used to sinter the powder in each successive cross-section of the part, because the part-bed temperature is close to the melting-point of the material. Excessive laser power energy will cause large thermal penetration into the powder and will consequently affect powder beyond the

cross-section of the part, thus causing growth. Conversely, insufficient laser energy will not fuse the part completely, therefore resulting in porous and weak parts (DTM, 1997). Fill-laser power (*P*) can be calculated approximately using the following equation:

$$P = \frac{BS * p * Db * h * [\, C * (Tm - Tb) + lf \,]}{(1 - R)} \qquad \text{(Eq.2.1)}$$

where *BS* represents laser beam speed; *p* is powder density; *Db* is the diameter of the laser beam on the part-bed; *h* is slice thickness; *C* is specific heat; *Tm* is melting temperature; *Tb* is part-bed temperature; *lf* is latent melting heat, and *R* is reflectivity, i.e. the refraction of laser light by the powder (Gibson & Shi, 1997).

2.2.5.1.2 Laser beam speed

Laser beam speed is the scan-speed of laser movement across the surface of the part on the part-bed powder as it fuses the powder particles together. The laser speed for most part-builds is very fast e.g. between 1m/s to 5m/s, and so, cross-sections of a large fabricated part can be scanned in seconds (Kai & Fai, 1997; Pham & Dimov, 2000). Laser speed depends on other parameters such as laser-power and scan-spacing to produce parts with a superior energy density, as shown in Equations 2-3, leading to low porosity, good surface finish and good mechanical properties.

2.2.5.1.3 Laser beam offset

Laser beam-offset is an important parameter affecting the accuracy of SLS parts. Beam-offset comprises laser-spot diameter, the area of the powder surface affected by heat and the deflection angle through the laser scan. The dimensions of the laser-spot diameter change at different points on the surface of the powder, depending on the deflection angle of the laser beam from the scanning mirror (Wang, 1999; Jamal, 2001). As shown in Figure 2.7, when $\alpha = 0$, the laser-spot has the smallest diameter *(D)*, and therefore the laser-spot can focus most effectively on the scan surface. When $\alpha > 0$, the diameter of the laser-spot on the scan surface is $D' = D/\cos\alpha$. A difference of D' and D is articulated as:

$$\delta = D\left(\frac{1}{\cos\alpha} - 1\right) \qquad \text{(Eq.2.2)}$$

D, however, increases in direct proportion to α but the increase in diameter is not expected to be significant (approximately 5.4% at the maximum value of α 19˚ and D = 0.42mm). The effect of this increase is therefore usually ignored.

2.2.5.1.4 Scan-spacing

Scan-spacing is described in Figure 2.8, where laser-path movement during scanning is shown. Scan-spacing is the distance between two neighbouring, parallel, scanned vectors. The scan-spacing distance must be smaller than the effective diameter of the

laser beam during scanning, otherwise adjacent scanned paths may not be bonded properly together and the part will be very fragile. By contrast, if the scan-spacing distance is too small, the surface of the part may be uneven (Ilkgun, 2005).

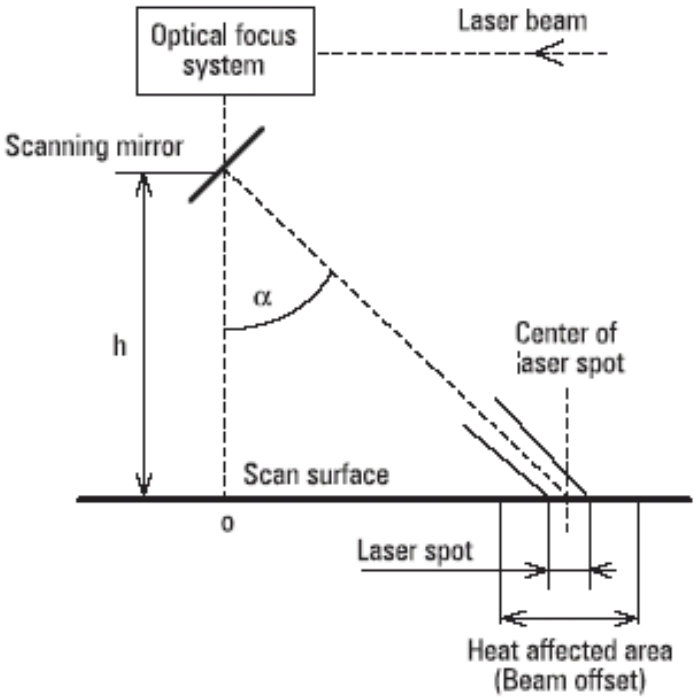

Figure 2.7: Changes in Laser-Spot Diameter (Wang, 1999).

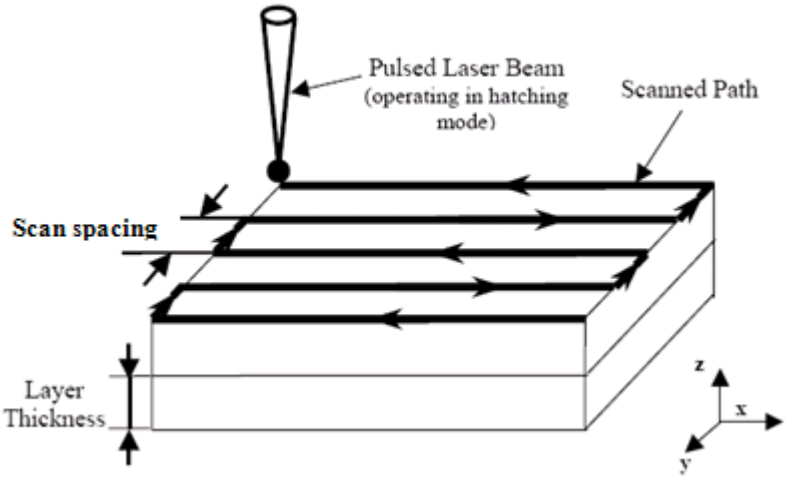

Figure 2.8: Scan-Spacing (Ilkgun, 2005).

2.2.5.1.5 Scanning strategy

The scanning strategy of the laser beam for building a layer is controlled by a machine operator which may be 'fill-only' - a strategy which can produce the part faster but less accurately, or a strategy which both 'fills and outlines' to produce a part more slowly but with greater accuracy. These two strategies are shown in Figure 2.9. The laser scan proceeds through a 'fill' or a 'fill and outline' procedure, depending on the slice (layer) geometry obtained from the STL file (Ilkgun, 2005).

2.2.5.1.6 Energy density

Energy density is energy transferred to the surface of the part-bed. Laser power, scan-spacing and laser-scanning speed are considered to be relatively more effective here as regards energy density, than they are in other processes. To produce high-quality functional SLS parts, it is important that the powder on the surface of the part-bed receives a sufficient amount of energy density through the laser sintering process. Energy density can be calculated using the following equation:

$$ED = \frac{P}{LS * SCSP} \qquad \text{(Eq.2.3)}$$

Here, *P* represents the level of laser power during scanning exposure, *SCSP* refers to the scan-spacing and *LS,* to laser speed during scanning exposure. The high energy density of a laser beam, however, results in better fusion of polymer particles, consequently resulting in decreased porosity and enabling a more compact structure to be built. Excessively high energy density will produce degradation of the polymer, hard part-cake, difficulty in taking parts out of the build, rough texture, and a light brown colour on the surface of the part due to overheating. On the other hand, at low energy density levels, the part is likely to have insufficient bonding between powder particles and subsequently higher porosity resulting in weakness (Caulfield et al., 2007).

2.2.5.1.7 Slice thickness

Slice thickness is the powder thickness of each layer in the part-cylinder, determined by the depth to which the part piston lowers for each layer and the level at which the roller-counter rotates from one of the feed-cartridges onto the part-bed. Slice thickness is considered to be an important factor, influencing both the building time of the SLS process and surface roughness. The production of parts using thinner slices can decrease surface roughness but the build takes more time. Although thicker slices can save time, however, they may reduce the dimensional accuracy of fabricated parts with a stair-step effect, as shown schematically in Figure 2.10. In the Sinterstation 2000 process, slice thicknesses range from 0.07mm to 0.5mm and the default setting is 0.1mm (Gibson & Shi, 1997; Jamal, 2001). Roller-counter rotations

may affect slice-thickness i.e. high rotation speeds may result in powder being pushed in front of the roller. Setting roller speeds too low, however, increases processing time.

During SLS, the greatest slice thickness is limited by the penetration depth (*Dp*) of the powder. Consequently, penetration depth (*Dp*) depends on laser power, energy density, particle size, powder density, specific heat and thermal conductivity. A suitable slice thickness of the powder should therefore be set to balance the requirements of the application.

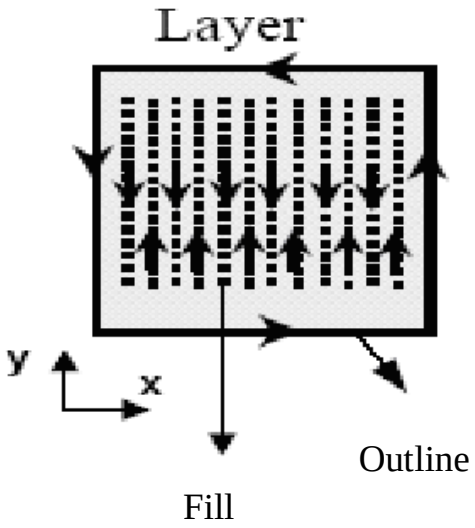

Figure 2.9: Scanning Strategy (Ilkgun, 2005).

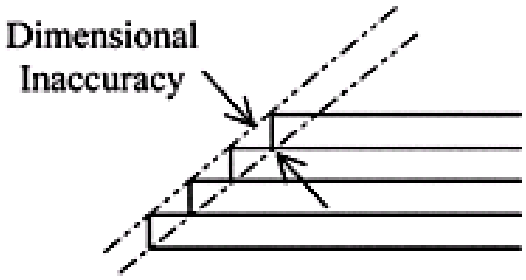

Figure 2.10: Stair-Step (Jamal, 2001).

2.2.5.1.8 Heater control

Before exposure to and sintering by the laser beam, powder in the SLS machine is heated by a specific device to a temperature just below the melting point of the material in order to decrease heat stress to the lowest possible degree. Three such heaters are used in the DTM SLS system to maintain and control the temperature of the powder during this process. The heaters are located above the part-bed and two feed-cartridges. The part-heater controls the powder part-bed area and the right and left heaters control the right and left powder feed-cartridges respectively. The heaters are automatically adjusted by an IR sensor which monitors temperature at the surface. Certain kinds of DTM SLS systems, such as Sinterstation 2000, have one IR sensor which only monitors the temperature at the top surface of the part-bed, while both the right and left heaters are adjusted by thermocouples (DTM, 1997). In general, the SLS system material build-process is made up of three stages:

A. Warm-up stage

This stage focuses on the first step in the heat process, which stabilises the temperature in the process chamber, part-build area and feed-cartridges to set points (see Figures 2.11 and 2.12). These fixed temperature points are adjusted for part and feed conditions by the SLS machine operator, according to the material used. This stage takes approximately 2 hours, during which the roller does not initially move to

spread the powder and the part-bed piston guides downwards while the roller delivers 25.4 mm of powder from the right and left feed-cartridges to the part-cylinder.

During this stage, part-bed powder temperatures slowly increase from 10ºC to 12˚C below the material's melting point to reach the set points. The set part-bed heater temperature points determine when the surface powder in the part-bed begins to glaze. The temperature of the feed-powder is also slowly increased to its highest possible level and reaches set temperatures at which it can still flow freely. The feed-heater temperatures set determine when surface powder in the feed-bed begins to crack. Small cracks are acceptable. If the cracks are excessive, then the temperature should be reduced in increments of 1˚C until only small cracks are visible. This limits the degree of thermal shock, or cooling, from the feed-cartridge powder on the part-bed (DTM, 1997; Yusoff, 2007).

B. Build stage

This stage maintains the temperature of the powder in the part-bed and feed-cartridges (see Figures 2.11 and 2.12). Part-bed powder temperatures are usually close to melting-point, and so relatively low laser power is used to melt the powder in each successive layer during the construction of parts. Excessive laser power will affect powder outside the part boundary and cause growth. Conversely, insufficient laser power will not completely fuse powder particles, resulting in porous, weak parts. As the build-platform is lowered, the fabricated part is covered by the feed-

powder which then cools it to the part-bed temperature. The cooling rate is influenced by the part's geometry and its position in the build. Variation in density of the part also influences the cooling rate. A piston heater heats the top of the part-bed piston, which helps to slow the cooling rate of the first set of parts built and subsequently reduces the thermal gradient and prevents distortion. If the cooling rate is too slow, it may cause growth, whilst if the cooling rate is too high, warping and curling can occur (DTM, 1996; DTM, 1997). .

C. Cool-down stage

This stage is the final process which allows the sintered parts to cool sufficiently so that the fabricated parts and un-sintered powder may be removed from the part-bed cylinder, as shown in Figures 2.11 and 2.12. The fabricated parts may be removed from un-sintered powder only after their temperature falls below that of the glass transition of the material, otherwise they could curl and warp, or deform. The duration of this stage depends on the building volume and the degree of cylinder and piston heat. A longer cool-down stage will affect the properties and usability of the material, so un-sintered powder which has been exposed to a long period of cool-down needs to be refreshed with a sufficient amount of new powder in order to produce good quality parts (DTM, 1997).

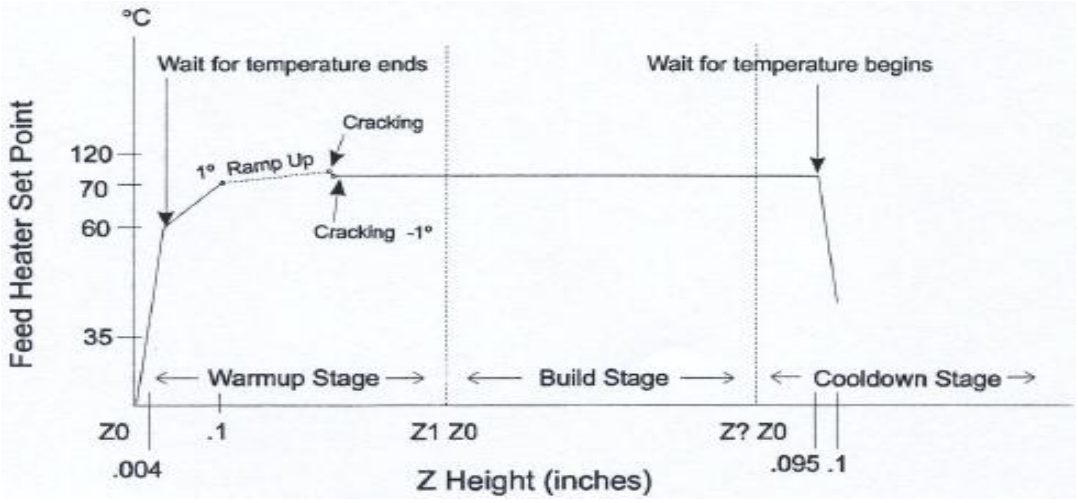

Figure 2.11: Feed-Heater Set Point (DTM, 1997).

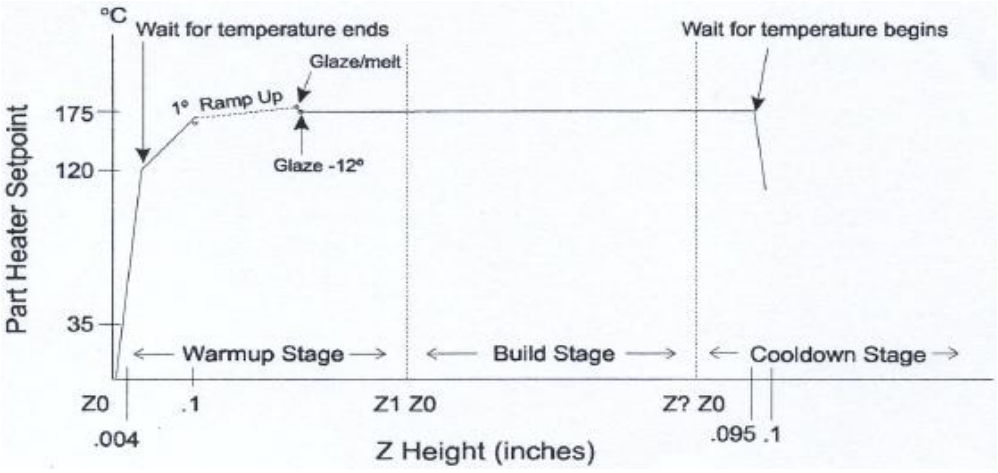

Figure 2.12: Part-Heater Set Point (DTM, 1997).

2.2.5.2 Materials used in SLS and their applications

Compared with other RP methods, one of the main advantages of the SLS process is its capacity for manufacturing parts using diverse, non-toxic multiple materials, as essentially any material that can be pulverised may be used, e.g. thermoplastics, metals, ceramics and composites through direct sintering, or indirectly by using a low melting-point binder (Hon & Gill 2003). In general, the SLS process uses a finer particle size to produce a thinner layer, better resolution, smoother surface texture and less shrinkage (Kurth et al., 2003). A wide range of materials with varied properties have been developed to meet the demands of different applications. Materials commonly used in the LS process are presented here (Kai & Fai, 1997; Pham & Dimov, 2000; Cooper, 2001).

2.2.5.2.1 Polyamide 12

Polyamide 12 is the material most commonly used in SLS. It is semi-crystalline and has low processing temperatures, melting flow control and ease of production in the SLS process. In addition, the semi-crystalline polymers have a 3%-4% proportion of shrinkage and this is due to the fact that the SLS process involves a thermal stage (Pham et al., 2000; Jamal, 2001; Kurth et al., 2003). The particle shape of the Polyamide 12 is spherical and irregular to a considerable degree, with an average size of 60 micrometres and good physical properties, such as a high melting temperature due to strong hydrogen bonding. Polyamide 12 is used in SLS to create models and

prototypes that can perform in a demanding environment and which also deliver good long-term stability, offering resistance to most chemicals. Furthermore it is harmless to the environment and safe to use with foodstuffs. Moreover, the parts produced are durable and offer considerable heat-resistance. The fine particle size produces parts with improved detail and edge definition, which becomes apparent when complex parts are fabricated.

2.2.5.2.2 Metal

The metal family of steel, aluminium, alloys and composites can also be used in the SLS process. The SLS of metals is divided into indirect and direct methods. Indirect SLS involves the metal powder being mixed with a thermoplastic binder to produce a 'green part'. The green part is not completely dense, and so may be infiltrated with copper or bronze to obtain a completely dense part. The direct SLS (DSLS) process use metal powder blends without any binder. Preprocessing and post processing stages are eliminated by using DSLS. In general, metal is used with a rapid tool process in the SLS system to create a mold cavity and core inserts for prototype tooling. It reveals superior material properties, so the metal is strong enough to produce more than 50000 parts when used for rapid tool moulds. Metal is characterised by very good corrosion resistance and mechanical properties and is widely used in a variety of engineering applications (Kai & Fai, 1997; Dewidar & Dalgarno, 2001; Cooper, 2001; Bertrand, 2007).

2.2.5.2.3 Polystyrene / CastForm

Polystyrene is considered to be an amorphous polymer and has been extensively used in the SLS process. CastForm is 'investment-caster' friendly powder that gives low ash content and is compatible with standard foundry practices. Processing CastForm involves two main stages: a green part produced by SLS, and wax infiltration. The green part is 45% so the part is very brittle, due to its specific material properties. The part is completed by dipping into molten red foundry wax. CastForm material patterns require few modifications to standard foundry practices, and are quickly and easily removed. Low density polystyrene and high quality foundry wax ensure a clean pattern. In addition, CastForm enables a fast track route to metal castings, such as titanium, aluminium, magnesium, and zinc. In contrast CastForm has some disadvantages in that it is very difficult and risky to clean away loose powder, as the part strength is very low at this stage and some features could deform and break (Gubbels, et al., 1994; Pham, et al., 2003; Dotchev & Soe, 2006; 3T RPD, 2008; Paramount, 2009).

2.2.5.2.4 Polycarbonate (PC)

Polycarbonate is an amorphous thermoplastic which has been used quite extensively in the SLS process. The polycarbonate powder is supplied by 3D systems and has a broad size distribution and irregularly shaped particles with a mean diameter of 90 micrometers. Polycarbonates reveal good thermal stability characteristics and can

produce parts with very good dimensional accuracy, feature resolution and surface finish. The parts produced have moderate strength and durability caused by the porous structure, so they are only useful for applications that do not require part strength and durability. If it is necessary to improve mechanical properties, parts can be infiltrated with an epoxy resin. Polycarbonate is commonly considered as a polymer to be used for sacrificial patterns in investment casting, as the porous structure of the polycarbonate parts prevents them from expanding to the point of ceramic shell cracking (Nelson et al., 1993; Jamal, 2001; Kruth, et al., 2003; Fan et al., 2005; Berzins et al., 2007).

2.2.5.3 Common problems related to the SLS process

SLS part quality depends on SLS process parameters which are set differently according to powder properties and the requirements of the application. Optimising process parameters can eliminate many problems, reduce geometrical inaccuracies and improve fabricated part properties by monitoring part-build, therefore process parameters can be established to suit the application. Changes in some process parameters, however, may affect other parameters and require adjustment. For these reasons, SLS manufacturers have specified default values for all process parameters, based on the materials used. Common problems relating to the SLS process, together with a brief description, as well as the causes, results and corrective action are presented in the following section (DTM, 1997; Yusoff, 2007; Jamal, 2001).

2.2.5.3.1 Powder fluff

Powder fluff is a phenomenon identified when the powder has a higher packing density at the bottom of the feed-powder cartridges than it has on the top (see Figure 2.13). It occurs when powder is not uniformly consolidated during the loading process as a result of short feeds during the initial part of the build, thus leading to low quality parts. As a corrective measure, it has been recommended to minimise powder fluff by compressing the powder using a flat plastic or heavy cardboard plate, the same size and shape as the feed-cartridge. This is pressed down onto the cartridge (DTM, 1997; Boivie, 2000; Zhou, 2009).

2.2.5.3.2 Cracking of part-bed and feed-cartridge

The surfaces of the part-bed and feed-cartridge can crack open as the roller moves across them (see Figure 2.14). This occurs due to an excessive heating rate from the part-bed and feed-heaters, causing partial melting of powder on the part-bed and feed surfaces. As a result, the part cracks if it is built over the seam area that is cracking. To avoid this problem it has been suggested that the part-bed and feed-heaters' set points are decreased in increments of 2°C until the crack disappears (DTM, 1997).

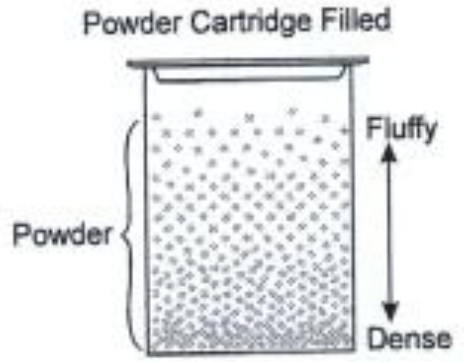

Figure 2.13: Schematic View of Powder Fluff (DTM, 1997).

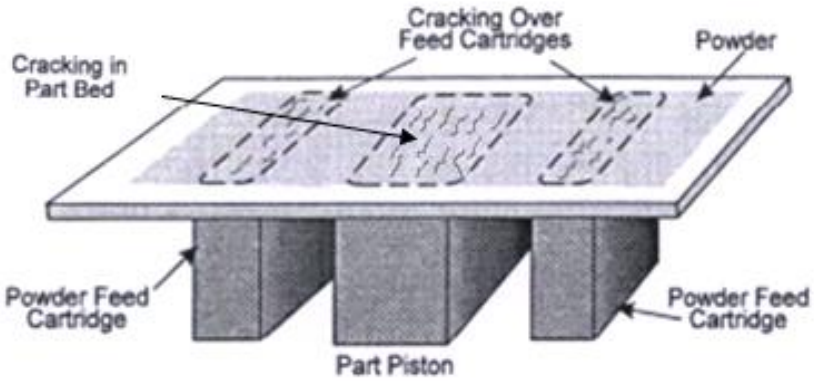

Figure 2.14: Cracking Appears in Part-Bed and Feed-Cartridge (DTM, 1997).

2.2.5.3.3 Clumping

Clumping is a term which refers to agglomerated powder on the powder-bed surface, in front of the roller as it moves across the part-bed. This results in streaks or cracks of powder part-bed surface appearing behind the roller (see Figure 2.15). Agglomerated powder builds up because of moisture, recycled powder, overheated powder in the feed-cartridges and inadequate sifting. It results in streaks appearing behind the roller, and uneven powder thickness, which may cause growth or insufficient melting and poor quality parts. To correct this, it has been suggested that the set temperature points for the left and right feed-heaters are reduced and that recycled powder is systematically sifted before use (DTM, 1997; Abid, 2009).

2.2.5.3.4 Crystals and condensation

Crystals and condensation manifest in small amounts of volatile material which vaporise during SLS processing (see Figure 2.16). This phenomenon occurs due to extreme part-bed temperatures and can result in crystals or condensation forming on the lens of the IR sensor, which may then cause incorrect part-bed temperature readings, with an extremely difficult or impossible break out and melting of the part-bed. Crystals or condensation on the laser window can also reduce the amount of laser power delivered to the part-bed surface, resulting in weak or curled parts. As a corrective measure, DTM recommends cleaning the IR sensor and laser window before, but not during, each build. No corrective measures are taken, however, once the build has started (DTM, 1997).

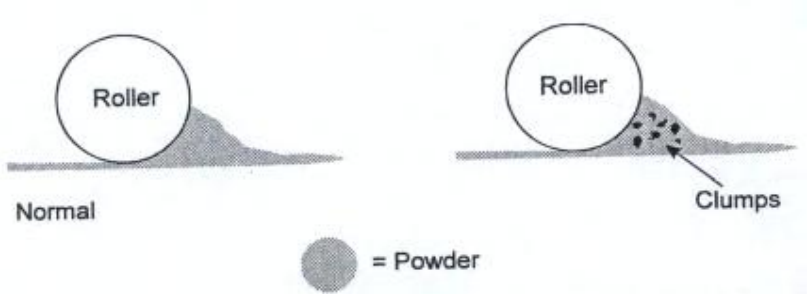

Figure 2.15: Schematic View of Clumping (DTM, 1997).

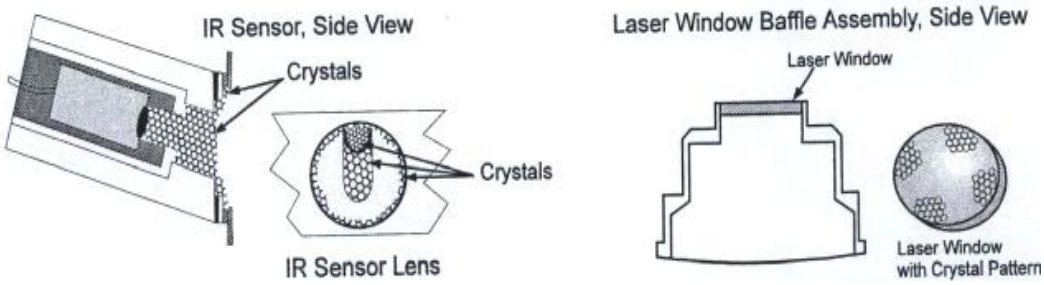

Figure 2.16: Crystals and Condensation on the Lens of the IR and Laser Window (DTM, 1997).

2.2.5.3.5 Bonus Z

Bonus Z is a phenomenon identified when the laser melts a part beyond the specified depth [usually 0.004 inch (0.1 mm)] during the first few scans and causes vertical growth in the Z axis. The difference between growth and bonus Z is that growth may occur on any part edge, while bonus Z occurs only on downward-facing surfaces (see Figure 2.17). This phenomenon occurs due to the laser penetrating the un-sintered powder below the part boundary, resulting in a part dimension outside the tolerance range of the Z axis. To solve this problem, the possibility of bonus Z should be minimised by reducing the temperature time relative to the powder bed and the fill-laser power for the first few layers (between the first and fourth layers). Constant offset in the Z dimensions of the STL file is applied using the DTM offset. The Z offset affects only downward-facing surfaces by moving them upward, in accordance with the specified distance (DTM, 1997; Ho et al., 2002; Dewidar et al., 2003).

2.2.5.3.6 Curling "in-build"

Curling is a phenomenon identified when the edges or corners of the part rise above the powder part-bed surface. The parts may get thinner in the Z axis, as shown in Figure 2.18. This phenomenon occurs due to temperature difference and the part temperature dipping too low after the feed-powder is added. Curl can also occur if the part-bed temperature is too low (Jamal, 2001; Min Hur et al., 2001). As a result, parts are not flat, especially where large surface-area cross-sections are concerned and the

part may move in the part-bed when the roller passes over if the curling is severe. As a corrective measure, it has been recommended to increase the set point values for the left and right feed heaters to the highest possible temperature at which the powder can still flow freely. Increasing the powder-bed temperature may also reduce heat transfer from the build to the powder part-bed. Furthermore, reducing left and right feed distances may also cut down on curling 'in-build' (DTM, 1997).

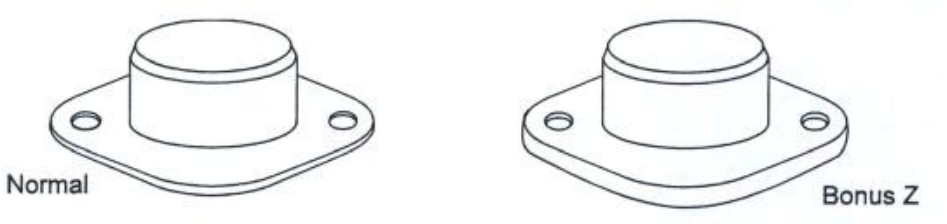

Figure 2.17: Schematic View of Bonus Z (DTM, 1997).

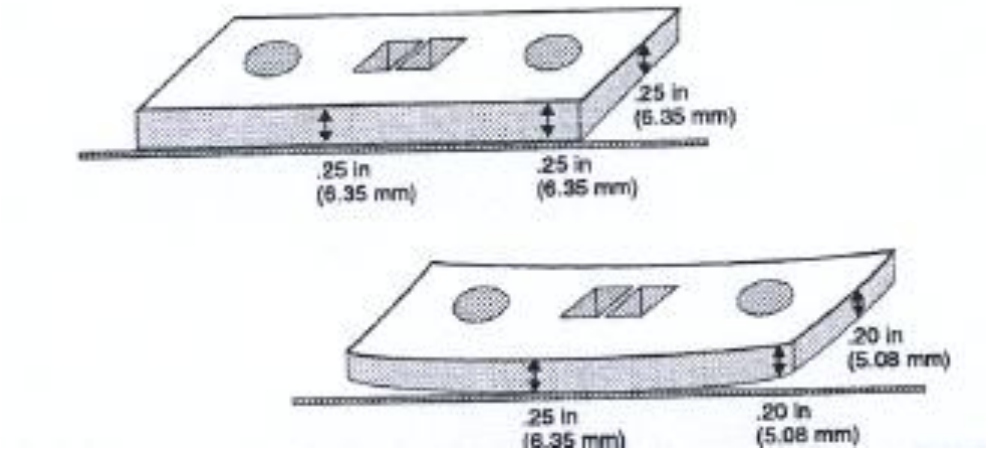

Figure 2.18: Schematic View of Curling "In-Build" (DTM, 1997).

2.2.5.3.7 Curling "post-build"

Curling "post-build" is identified when the final product is not flat, but the Z dimensions are still correct. These cases are therefore different from curling "in-build" (see Figure 2.19). Here, curling occurs due to excessive cooling rates when the heater temperature decreases rapidly and the part is prematurely removed from the process chamber. As a result, parts are not flat, especially where cross-sections with a large surface area corresponding to the correct Z dimensions are concerned. Recommended corrective measures advise increasing the temperature of the powder-bed and left and right feeds. The part-cake should be allowed to cool for longer inside the SLS machine and then left to cool completely outside the machine before parts are removed (DTM, 1997; Jamal, 2001).

2.2.5.3.8 Growth

Growth is a phenomenon identified when extra powder sinters on the part, changing its dimensions. Growth is particularly evident in fine detail or small apertures. The difference between growth and bonus Z is that growth may occur on any part edge, while bonus Z occurs exclusively on downward-facing surfaces (see Figure 2.20). Growth occurs due to excessive laser power and part-bed temperatures, thus leading to heat diffusion beyond part boundaries and resulting in oversized parts and parts which may be difficult or even impossible to break out. To avoid this problem, reducing part-bed temperature and fill-laser power is recommended (DTM, 1997; Shi et al., 2007).

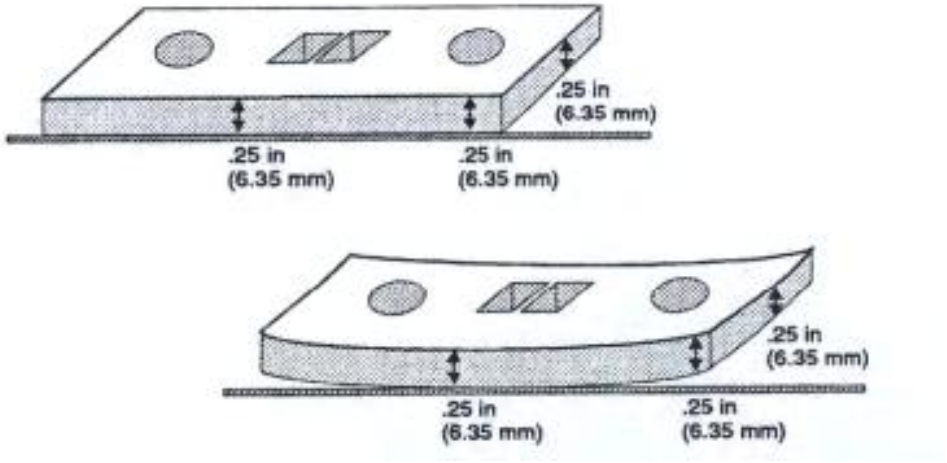

Figure 2.19: Schematic View of Curling "Post-Build" (DTM, 1997).

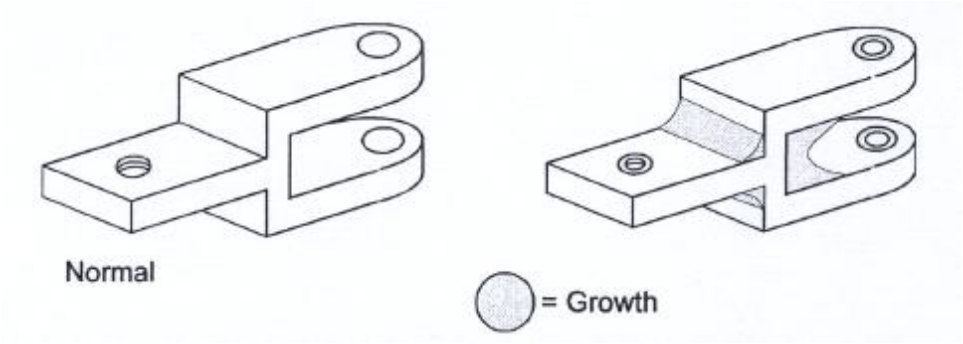

Figure 2.20: Schematic View of 'Growth' (DTM, 1997).

2.2.5.3.9 Missed-scan

A missed-scan is identified when the laser beam does not completely scan the fill area of a part (see Figure 2.21). Missed-scans occur when an error in the STL file received from the CAD model does not contain properly connected surface patches. This problem is not material-related, but will result in incorrect part geometry and perhaps poor part properties. As a corrective measure, it has been recommended to verify that the STL and CAD files are correct, or else to create new files (DTM, 1997; Chen, et al,. 2001; Dimov, et al,. 2005).

2.2.5.3.10 Weak parts/porosity

This problem is identified when parts appear porous and solid, which means that the part will then be brittle and low density (see Figure 2.22). These cases arise when the laser window is obscured by crystals and laser power is therefore insufficient. They also occur when laser speed very high. The result is low strength and density in the parts fabricated. Corrective performance consists of cleaning the laser window, increasing fill-laser power during the build, raising part-bed temperature and decreasing the laser speed (DTM, 1997; Hon, 2003; Schmidt, 2007).

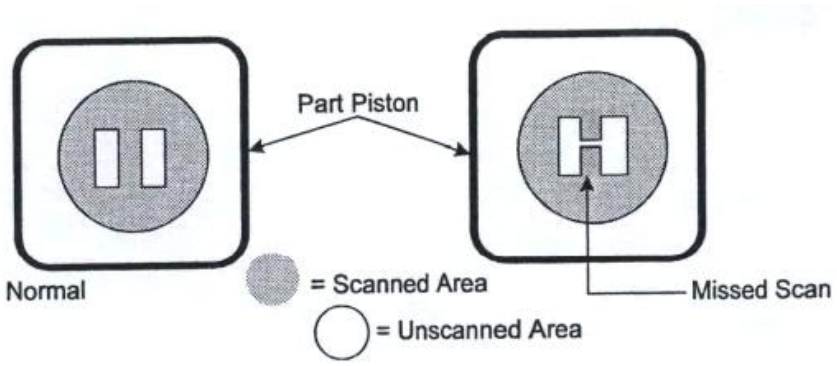

Figure 2.21: Schematic View of a 'Missed-Scan' (DTM, 1997).

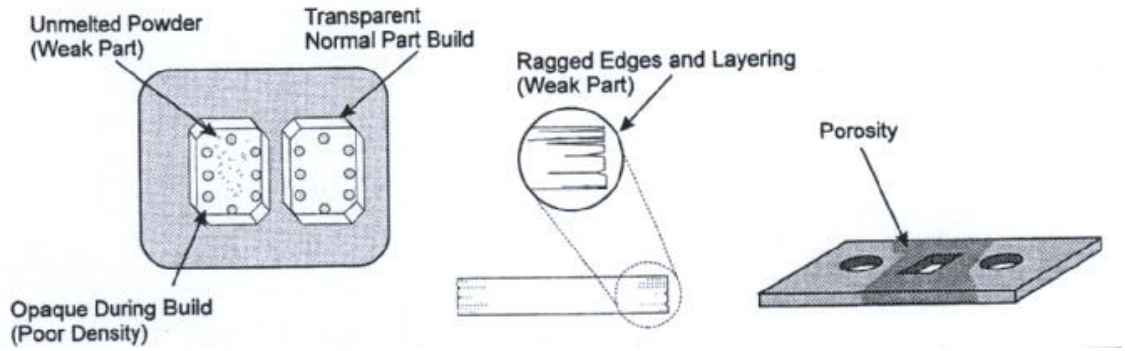

Figure 2.22: Schematic View of 'Weak Parts/Porosity' (DTM, 1997).

2.2.5.4 Previous studies of composite material used in SLS

2.2.5.4.1 Glass-filled polyamide 3200

PA 3200 GF is a composite material made from glass bead and polyamide. The glass bead consists of particles of regular shape and an average size of about 50 micrometres with a high melting-point. However Polyamide 12 is presented in this composite as a binder and the glass particles as a structural material. When the PA 3200 GF composite is sintered through SLS, the Polyamide 12 particles are fully molten, and the glass particles remain solid. Glass-filled polyamide differs from Polyamide 12 in that it has greater mechanical properties, such as rigidity and flexural qualities. Using glass bead is thought to reinforce the Polyamide 12, consequently increasing strength, dimensional stability, rigidity and heat resistance. The glass-filled blend is perfect when prototyping rigid parts intended for production in advanced, engineered thermoplastics, and is the right choice for functional testing (Childs & Tontowi, 2001; Cooper, 2001; Mazzoli, et al,. 2006 ; Abid, 2009). In contrast, one of the drawbacks of PA 3200 GF supplied by EOS is that it is more expensive than Polyamide 12, which is also supplied by EOS.

2.2.5.4.2 Aluminium-filled polyamide (Alumide™)

Alumide is a new composite material made by EOS GmbH, consisting of two materials: polymer and aluminium filler. The aluminium has an average particle size

of 45 µm and the particle size distribution (90% volume distribution) is in the range 26–75 µm with a high melting-point of around 660 ºC (EOS, 2008 ; Mazzoli, et al,. 2006). Polymer particles are used as binder because they have a low melting point. Alumide™ has a high dimensional accuracy, can stand high temperatures and has excellent mechanical properties, such as tensile and flexural modulus. In addition, Alumide™ promises a greater surface finish and better finishing properties for many functional prototypes. Mazzoli, (2006) mentions that aluminium-filled polyamide powder was developed because of the need to manufacture models with excellent dimensional accuracy and resistance to mechanical stress, especially bending strength and the ability to stand high temperatures. A typical application for Alumide™ is the production of stiff parts, with a metallic appearance, for applications in the automobile industry (e.g. wind tunnel tests), tool inserts for injecting and moulding small production runs, education, and high accuracy medical models. Moreover, the surface of Alumide parts can be finished by grinding, polishing, or coating. An additional advantage is that low tool-wear machining is possible (e.g. milling and drilling) (Subramanian, et al,. 1995; Mazzoli, et al,. 2006).

2.2.5.4.3 CarbonMide®-Carbon fibre-filled polyamide

CarbonMide is a new composite material introduced into the commercial market by EOS. It is based on two materials: a carbon-fill and polyamide to produce black parts. CarbonMide has another commercial name, Windform XT, which has almost the same characteristics. The parts manufactured through the SLS process using

CarbonMide have exceptional mechanical properties characterised by high stiffness levels, high tensile strength and tensile modulus. Moreover, they have low density, electrical conductivity, a smooth finish and a sparkling appearance. A typical application for CarbonMide is the production of fully functional prototypes with high-end finish for applications in the automobile industry, such as wind tunnel tests or other aerodynamic applications. Blocher, the managing director of FKM (2008) has explained that CarbonMide has a great deal of potential in the production of large, mechanically loaded parts for racing and sports cars (Jain et al., 2006; EOS, 2008).

2.2.5.4.4 Silicon carbide/polyamide

Sic/Polyamide composite has been developed for use with SLS. It consists of two materials, polyamide and silicon carbide filler as rigid particles. The silicon carbide has an average particle size of 44.5 μm and is angular in shape when compared to the polyamide, with a high melting-point of around 2700 ºC. The polyamide powder is therefore used as a binder because of its low melting point (Gill & Hon, 2004). Simple and complex shapes are easily produced with this material by using optimised parameters. Sic/Polyamide composite can be infused with metal by using an infiltration process to produce both metal matrix and ceramic matrix composites, such as by infiltrating aluminium matrices into SiC in a nitrogen atmosphere at 750-850º C, where the polymer was thermally removed. Silicon Carbide loadings near 45 vol.% are typically achieved. At this maximum vol.% of Silicon Carbide, moduli of

about 180 GPa and a 4-point bending strength of about 275 MPa are obtained. Its advantages include the ability to form complex geometries that are not achieved by a casting process with shrinkage of less than 1%, and minimum machining after infiltration (Vail, et al., 1993; Beaman et al., 1997; Gill & Hon, 2004).

2.2.5.4.5 Copper polyamide (CuPA)

Copper polyamide is a metal-plastic composite of a copper powder and polyamide blend introduced by DTM in May 1998 to use in the SLS process (Pham & Dimov, 2000). Tooling inserts are produced with a layer thickness of 75 µm and it is necessary to finish the tools before their integration in the tool base. Unfinished tool inserts can be produced in a day and no furnace cycle is required. CuPA is produced to create tooling for short production runs of equivalent plastic parts with conformal cooling, good thermal conductivity, heat resistance and durability. CuPA can be built into mould tool inserts in the SLS machine in the same way as other PA materials (e.g. PA2200). In addition, the advantages of using CuPA are both numerous, significant and suitable for injection moulded inserts for several hundred parts (100–400 parts) from common plastics such as polyethylene (PE), polypropylene (PP), polystyrene, ABS, PC/ABS. Moreover, the surface of parts made of CuPA can be easy to machine and finish. In contrast, one of the drawbacks of copper polyamide is that it is very expensive (Pham & Dimov, 2000; Levy & Schindel, 2002; King & Tansey, 2002).

2.3 Summary

This chapter presents a brief description of common rapid prototyping processes with the focus on SLS technology for 3D Systems. These are considered one of the most popular rapid prototyping techniques. In the SLS process, the main fabrication parameters which influence the quality of sintered parts are described. Some of the common materials employed to produce RM and RP parts by SLS are presented. The main problems with using PA12 powder produced through SLS are highlighted, followed by a description of previous studies of composite material used in SLS.

Chapter 3

Experimental techniques

3.1 Preliminaries

This chapter presents the equipment, methodologies and experimental procedures used to characterise the behaviour of composite material of cement additives with Polyamide 12 as powder and sintered specimens. In addition, it describes the composite material used in this research. A better understanding of material properties is an enormous help in obtaining more appropriate data to input into the SLS process, in order to get new SLS material and excellent quality sintered specimens.

3.2 Material Preparation

The material used in this research consists of composite material made from polyamide with cement additive. The polyamide used is the Polyamide 12-based powder, supplied by EOS. This is an ultrafine powder of Polyamide 12, with a narrow particle size distribution and nearly round particle shape. Polyamide 12 is a kind of viscoelastic thermoplastic material with mechanical properties that reflect the characteristics of both viscous liquids and elastic solids. This means that when the material is stressed, it responds with viscous flow, which dissipates energy, and with elastic displacement, which stores energy (Crawford, 1987). The cement used is Portland cement, defined as an adhesive material capable of joining fragments or masses of solid substance to a compact whole. The raw materials commonly used to make Portland cement are limestone or chalk and clay or shale. Limestone and chalk usually contain significant quantities of components of CaO, which represent the main constituent of Portland cement clinker. Clay and shale normally contain large quantities of the compounds SiO_2, Al_2O_3 and Fe_2O_3. The widespread availability of limestone and shale keep the cost of Portland cement low (Lea, 1970; Barnes, 1983; Shirley, 1986). The material specifications for both PA12 and Portland cement are listed in Table 3.1, while Figure (3.1) shows scanning electron microscopy (SEM) micrographs of both types of powder. It can be observed that Portland cement is more angular in shape when compared to PA12.

Composite of cement and PA12 was prepared in the Manufacturing Engineering Centre Laboratory (MEC LAB) at Cardiff University. Both materials were sifted through an intensive shaking procedure, using a VORTI-SIV sifter to avoid agglomerates of powder. Following this, composite powder was mechanically mixed to a determinate formulation (see Table 3.2), in a high-speed mixer for 20 minutes in order to obtain homogeneous powder mixtures of uniform colour, so that maximum dispersion of particles was ensured. However, care in mixing was checked by scanning electron microscopy (SEM), as shown in Figure 3.2.

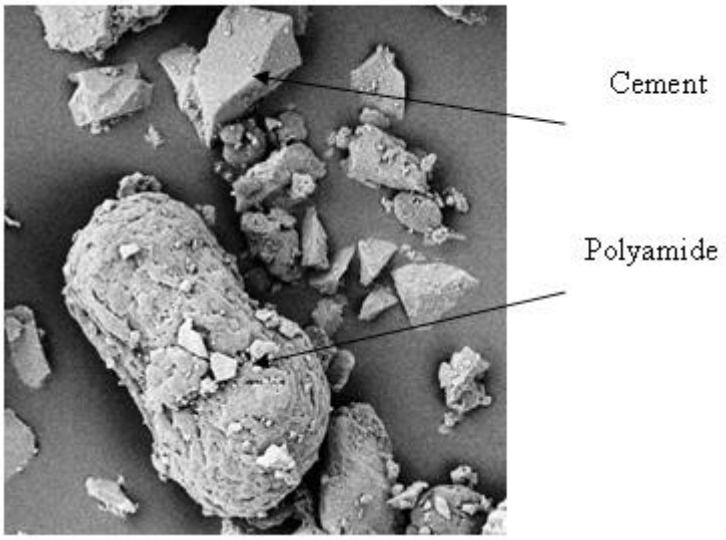

Figure 3.1: (SEM) Electron micrograph scans of PA12 and cement.

Table 3.1: Material specifications.

Powder properties	Portland cement	Polyamide 12
Average grain size (μm)	15	58
Bulk density (g/cm³)	1.04	0.59
Particle shape	Irregular	Irregular
Melting temperature (°C)	1400	185

Table 3.2: Cement/PA12 mixture powder formulation.

Cement (g)	PA (g)	Proportion
30	581	5:95
63	571	10:90
98	558	15:85
136	544	20:80
175	526	25:75
217	507	30:70
261	485	35:65
308	462	40:60

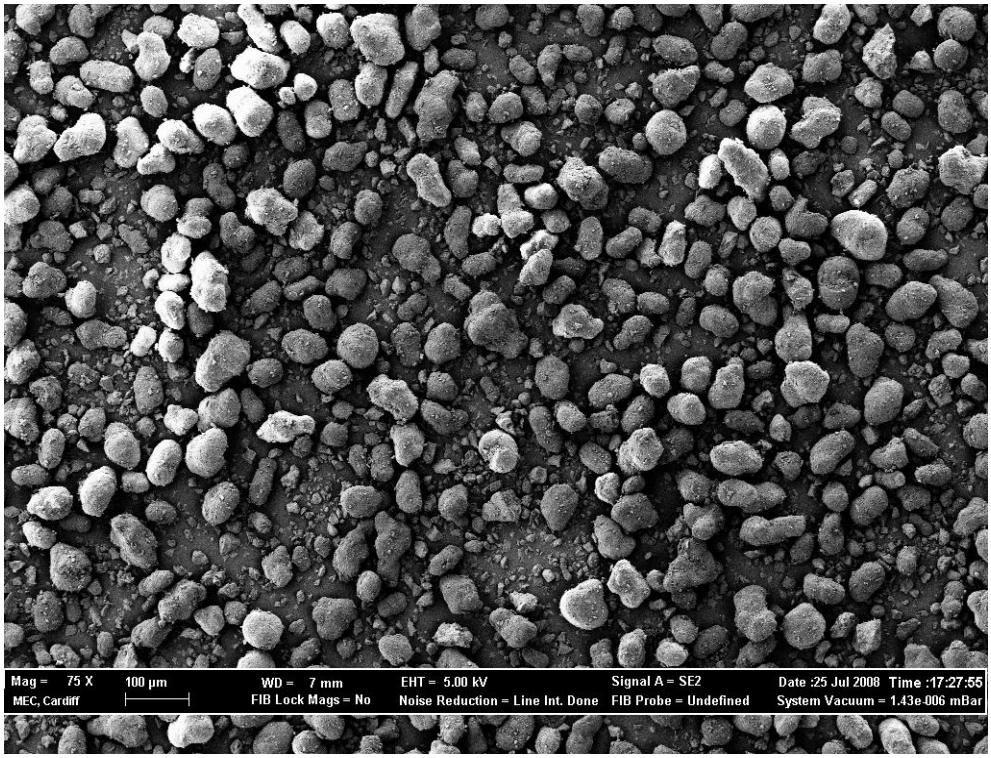

Figure 3.2: (SEM) Electron micrograph scans of PA12 and cement.

3.3 Equipment used for the preparation and production of specimens

Cement and PA12 were mechanically mixed in a drum mixer, BS 125, with a capacity of 150 L and mixing speed of 30 r.p.m. (see Figure 3.3). Composite powder was sifted in an intensive shaking procedure, using the VORTI-SIV pilot, RBF-15 (see Figure 3.4). The size of the particles was computed with an optical microscope using OmniMet software, from the image analysis of a two dimensional projection of the particles. The image analysis system consists of the optical microscope named above, fitted with a camera for obtaining the image as a pixel representation and a high-resolution monitor screen for displaying the image. OmniMet software was used to obtain the average particle size (see Figure 3.5). Agar Auto Sputter Coater was used to coat the specimens in gold, in order to make the sintered samples conductive (see Figure 3.6). The topographical information on the surface features of specimens, their texture and shape, size and arrangement of the particles, were studied using the Scanning Electron Microscope (SEM), at a voltage of 2-5 kV, and a ZEIZZ 1540 XB, with 0.000000001 mm resolution and 1000,000X magnification. The SEM images were obtained with a very small electron probe (or electron spot), scanned over the surface of the specimens, and by mapping the electron signals detected from each specimen pixel onto the corresponding pixel of the Cathode Ray Tube (CRT), or Charge Coupled Device (CCD), i.e. the screen (see Figure 3.7).

All sintered parts were built on a DTM Sinterstation 2000 machine using composite material of PA12-cement. Directions in the build chamber of the SLS machine are *x*-

axis parallel to the front of the machine, while the *y*- axis is perpendicular to the *x*-axis. The top plane of the powder bed is then the *x*–*y*-plane of the build chamber and the *z*-axis is perpendicular to the *x*–*y*-plane, as shown in Figure 3.8. In order to simulate the conditions of the SLS process and produce the mechanical properties of SLS specimens, while understanding the effects of the temperature and heating time on the deterioration of composite material of cement/PA12, the samples were set in an Oven Heraeus Instruments Vacutherm, Type 6060M, at 220 ºC in an optimal nitrogen atmosphere, in order to prevent the powders from oxidising (see Figure 3.9). All cast specimens were produced in an aluminium die and the die was machined using the AGIE AGIECUT EXCELLENCE wire cutter (see Figure 3.10). To meet the British Standard Specification for cast specimens, all parts were post-machined using the XYZ MACHINE TOOLS LIMITED EDGE 3000 (see Figure 3.11).

Figure 3.3: Drum mixer BS 125.

Figure 3.4: VORTI-SIV pilot RBF-15sifter

Figure 3.5: Optical microscope.

Figure 3.6: Agar Auto Sputter Coater.

Figure 3.7: Scanning Electron Microscope (SEM).

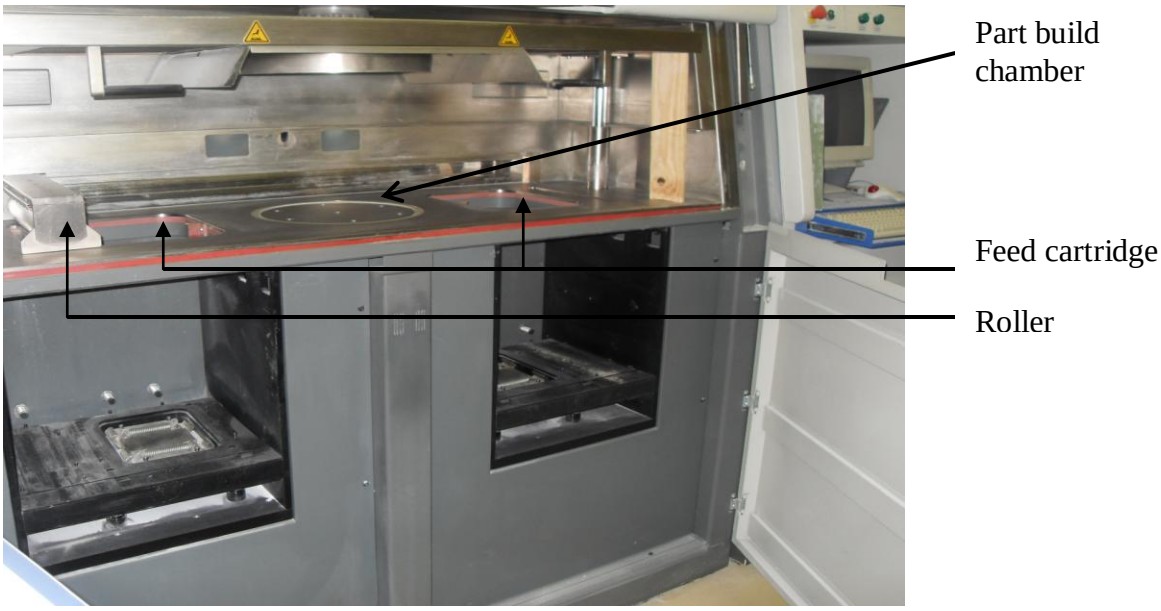

Figure 3.8: DTM Sinterstation 2000 machine.

Figure 3.9: Oven Heraeus Instruments.

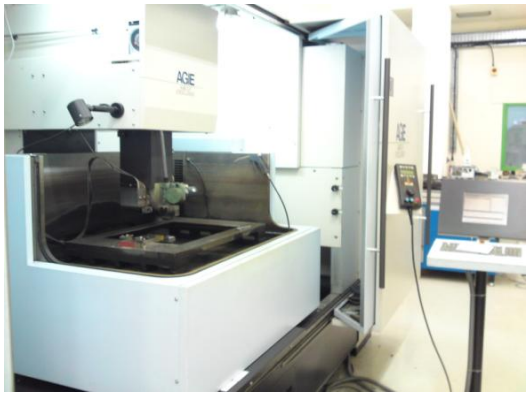

Figure 3.10: AGIECUT EXCELLENCE.

Figure 3.11: XYZ MACHINE TOOLS LIMITED.

3.4 Equipment used for measurements of powder properties

3.4.1 Melt Flow Rate (MFR)

The melt flow rate is used to accurately measure the melt flow characteristics of polymers when extruded through a capillary die of specified length and diameter at specific temperatures, load and piston positions in the barrel, while a timed measurement is made (see Figure 3.12) (Crawford, 1990). The MFR process begins by adding a small amount of material (4-8 grams) to the measurement cylinder at 235ºC. To guarantee a homogenous rope is extruded through the small die, the sample should be manually compressed several times during the filling procedure. The latter should take no longer than 1 minute. The measurement piston remains in place for a waiting period of 5 minutes, or until the heating of the sample is finished. After that, weights of 1.835 kg are added to the measurement piston to a total of 2.16 kg, and the rope is cut at a pre-determined distance between the two markers of the measurement piston at measured intervals. In this study, 6 MFR measurements were taken for each sample (ThermoHaake, 2000; ISO1133, 2005). Two ways to determine the MFR and its results are indicated in g/10min. One is via a PC, which shows the value automatically. The second is calculated manually from the determined size of the sample mass and the duration of the measurement corresponding to the following equation:

$$\mathrm{MFR}(T, m_{\mathrm{nom}}) = \frac{600m}{t} \qquad \text{(Eq.3.1)}$$

Here, T is the test temperature in degrees Celsius, ^{m}nom is the nominal load in kilograms, m is the average mass, in grams, of the cut-offs, t is the cut-off time-interval in seconds, and 600 is the factor used to convert grams per second into grams per 10 min (600 s).

Understanding the melt flow rate of polymers is a key indicator for producers, processors and converters of plastic materials in the manufacture of consistently quality products. The chemical structure of polymer affects its melt flow, so polymer with a high molecular weight has a greater flow resistance than polymer with low molecular weight (ISO1133, 2005; Yusoff, 2007).

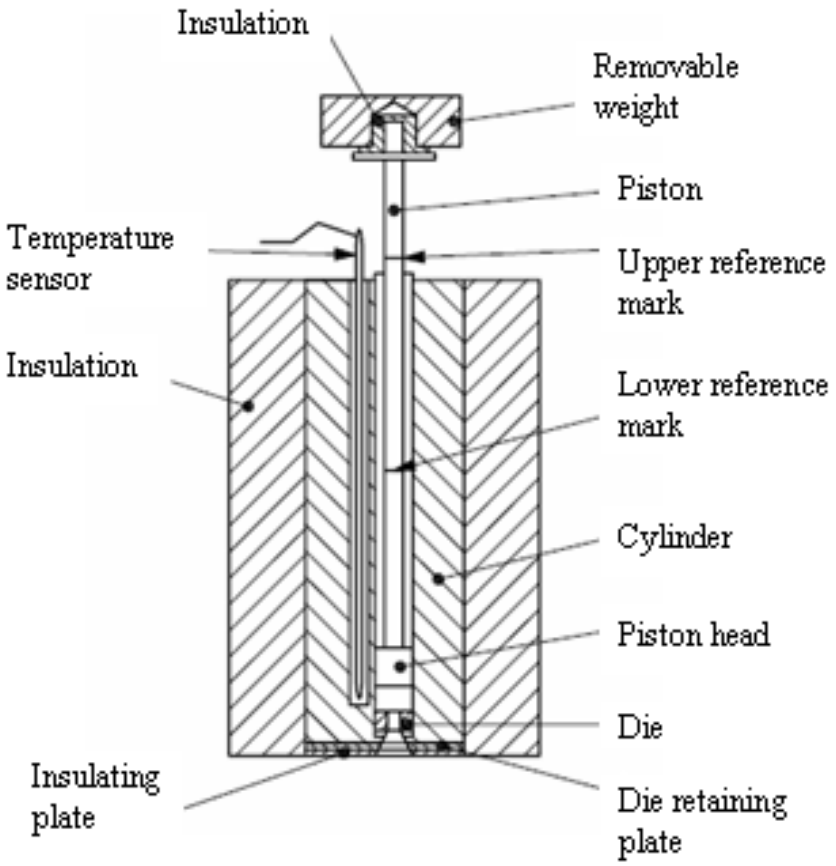

Figure 3.12: Melt flow rate indexer (MFR) equipment (ISO1133, 2005).

3.4.2 Differential Scanning Calorimetry (DSC)

Differential scanning calorimetry is a technique used to investigate the changes (thermal transitions) that take place in polymer when exposed to various temperatures (DSC, 2005). The most important thermal transitions that occur in polymer are melting temperature, *Tm* (endothermic transition), crystallisation temperature, *Tc* (exothermic transition), and glass transition temperature, *Tg.* The DSC instrument has two crucibles made of aluminium. One of the crucibles contains the sample of polymer and the other is the reference (an empty pan). The sample and reference are provided with separate heaters connected to a computer which controls them as illustrated in Figure 3.13. The computer turns on the heaters and starts to heat the two crucibles at a specific rate, typically 10 °C/min. Feedback loops control the feed of heat to the sample and reference so the temperature programme is closely followed. The output of a DSC is a plot of the temperature difference on the *x*-axis and the heat flow difference between a sample and an inert reference on the *y*-axis (Gibson & Shi, 1996; Sichina, 2000; ISO11357, 2008). DSC as part of the Mettler Toledo Thermal Analysis was used in this research to study the thermal transition of composite material of cement and PA12. The temperature accuracy of DSC is +/- 0.2K and the heat flow accuracy is +/- 2% (MettlerToledo).

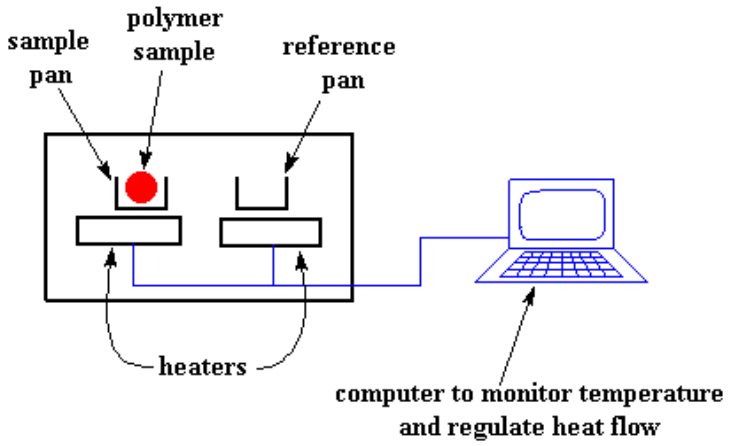

Figure 3.13: DSC instrument (DSC, 2005).

3.4.3 Gel Permeation Chromatography (GPC)

GPC is a technique for determining the average molecular mass and the molecular mass distribution of polymers by separating polymer samples into fractions, according to their molecular size, using a non-ionic stationary phase of packed spheres. The average molecular mass and the molecular mass distribution are calculated from a calibration curve constructed using polymer standards (Cowie, 1973; ISO16014, 2003). In this experiment, a single solution of each sample was prepared by adding 5 ml of solvent to 10 mg of sample and leaving it overnight to dissolve. The solutions were well mixed and filtered through a 0.45 μm PTFE filter. The data was collected and analysed using polymer laboratory 'Cirrus' software. The chromatographic conditions during the GPC analysis are summarised in Table 3.3.

Table 3.3: Chromatographic conditions.

Sample	Composite material of cement and Polyamide12
Instrument	GPC and polymer laboratory 'Cirrus' software
Columns	PL HFIP gel guard plus two 300x7.7mm, 9µm
Solvent	1,1,1,3,3,3-hexafluoro-2-propanol with 25 mM NaTFAc
Flow-rate	0.8 mL/min (nominal)
Temperature	40º C
Detector	Refractive index

3.5 Equipment used for measurements of mechanical properties

The tests for the mechanical properties of the SLS specimens were carried out using a Testomeric M500 machine, with a load range of 0 to 25 KN, accuracy +/- 0.5% and speed range of 0.001 to 1000 mm/min. The machine was connected with the controller system to choose the test type, to adjust the test speed and enter the dimensions of the sample. In addition, the readout screen showed real time test curves of calculated results. The Young's modulus was tested using an extensometer capable of measuring strain or elongation for certain materials when they are subjected to loading in a tensile testing machine. The tensile specimens were dog-bone shaped and the test speed was 5mm/min, according to ISO 527.2. The dimensions of the flexural specimens were 80mm x 10mm x 4 mm thick, the span was 60 mm and the test speed used was 2mm/min, consistent with ISO 178. The dimensions of the compression specimens were 10mm x 10mm x 4mm thick and the test speed was 5mm/min, in agreement with ISO 604. All tests were conducted at room temperature. The Izod impact specimens were tested using a Pendulum impact W&T AVERY machine, and determined with reference to ISO 180. The dimensions of the cross-sectional area (CSA) value of the specimens were obtained using a micrometer.

3.6 Summary

This chapter describes the materials Portland cement and Polyamide 12, used in this research as composite material, in addition to explaining the equipment and experimental procedures used for the preparation and production of all specimens employed in this research. The equipment and experimental procedures used for obtaining of the thermal and physical properties of composite material as powder were described. Devices for measuring powder particles and sintered specimens, and the equipment used for measuring the mechanical properties of composite material as sintered components were also presented.

Chapter 4

Thermal Properties of Cement and Polyamide 12 Composite in the Selective Laser Sintering Process

4.1 Preliminaries

SLS employs powder-processing in the construction of parts and SLS parameters, depending on the thermal properties of the powder. An average of 80% to 90% of the powder in the build chamber is not sintered during the SLS process and could be reused in relation to its properties. However, the properties of un-sintered powder deteriorate due to exposure to various temperatures for extended periods of time during the SLS system material build-process.

This takes place in three stages, starting from the warm up stage, the build stage, where the powder is exposed to just below the melting point of the material, and the cool-down stage. This chapter discusses the properties of cement and Polyamide 12 composite, as well as the thermal behaviour, melt flow rate, and molecular weight of this material. The influence of temperature and time on these properties is investigated.

The main purpose of this research is to develop a methodology for controlling the SLS parameters by studying the thermal properties of different proportions of composite material of cement and PA12 of the virgin powder, together with the input material properties from un-sintered powder, in order to obtain consistent and good quality fabricated SLS specimens.

4.2 Characterisation of composite material of cement and Polyamide 12 powder

One of the factors which make thermoplastics attractive for applications in engineering is the possibility of improving properties through reinforcement. Composites have therefore enabled thermoplastics to become acceptable in the demanding aerospace and automobile industries (Crawford, 1987). As mentioned before, the cement used is Portland cement, defined as an adhesive material capable of joining fragments or masses of solid substance to a compact whole. The raw materials commonly used to make Portland cement are limestone or chalk and clay or shale. Limestone and chalk usually contain significant quantities of component CaO which represents most of the composition of Portland cement clinker. Clay and shale, however, normally contain major quantities of compounds of SiO2, Al2O3, Fe2O3. Portland cement is a fine powder with tiny particle size and irregular shape. Widespread availability of limestone and shale suppresses the cost of Portland cement (Lea, 1970; Barnes, 1983; Shirley, 1986).

The polyamide used, Polyamide 12, is a thermoplastic that is derived from polymers. Polyamide 12 consists of 12 carbon atoms and an amide group (-CONH-) as a recurring part of the chain. Most polyamides are partially crystalline polymers and usually described in terms of having two parts: amorphous and crystalline components in a spherulitic microstructure. In an amorphous state, the distribution of polymer chains is completely random, while in the crystalline state, the chains are in a regular order, so that polymers do not form 100% crystalline structures in the same way as metals and ceramics (see Figure 4.1) (Mangonon, 1999). They display their most useful properties in the range between glass transition temperature *Tg* and melting temperature, *Tm*. Furthermore, they are designed so that the temperature of operation comes within this range (Young, 1981). Consequently, semi-crystalline polymers have distinct melting points and solidify when cooled down. Furthermore, Polyamide 12 is an ultrafine powder with a narrow particle size distribution and nearly round particle shape (Kohan, 1995).

As mentioned before, the material specifications for both PA12 and Portland cement are listed in Table 3.1 while Figure 3.1 shows scanning electron microscopy (SEM) micrographs of both types of powder to demonstrate irregularity. It can also be seen that Portland cement is more angular in shape when compared to PA12.

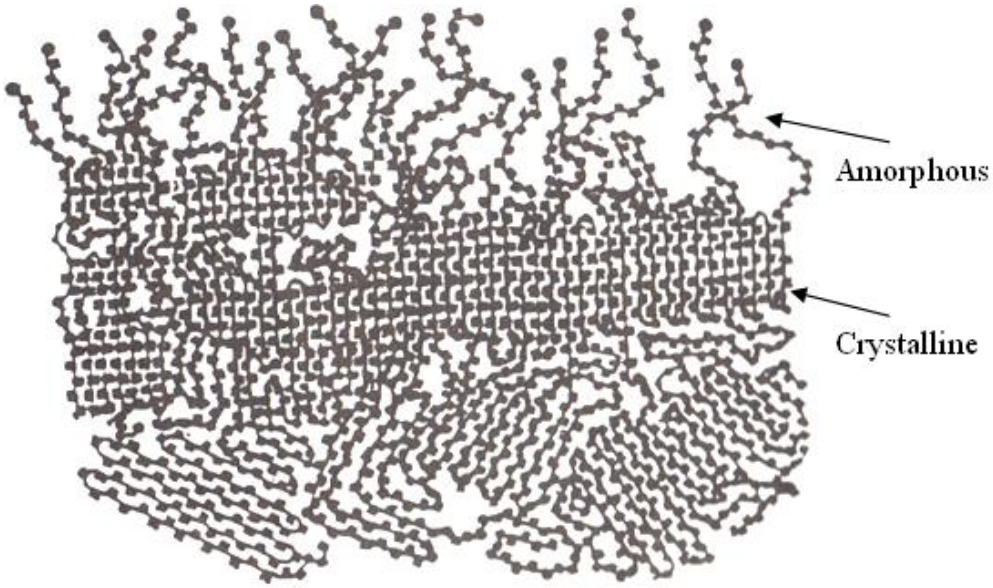

Figure 4.1: The molecular structure of a semi-crystalline polymer (Mangonon, 1999).

Most SLS technologies can be classified according to the binding mechanisms involved. The SLS of material-reinforced polymers can be seen as liquid phase sintering of composite powder particles, where the polymer is a binder and the material-reinforced particles represent structural material. The polymer does not just act as binder material but constitutes the main phase of the structural material, and basically a structural material that is fully molten, while the material reinforced particles remain solid (Kruth et al., 2005).

4.3 Thermal properties of the powder

In the SLS process, where the fabrication parameters involve using composite powder as a reinforced-polymer powder, the polymer acts as a binder within the reinforced powder, so the fabrication parameters are mainly dependent on the properties of polymers. As shown in Figure 4.2, the most important characteristics determining the application of thermoplastic polymers constitute glass transition temperature *Tg*, melting temperature *Tm* and crystallisation temperature *Tc* (Cowie, 1973; Gibson & Shi, 1996).

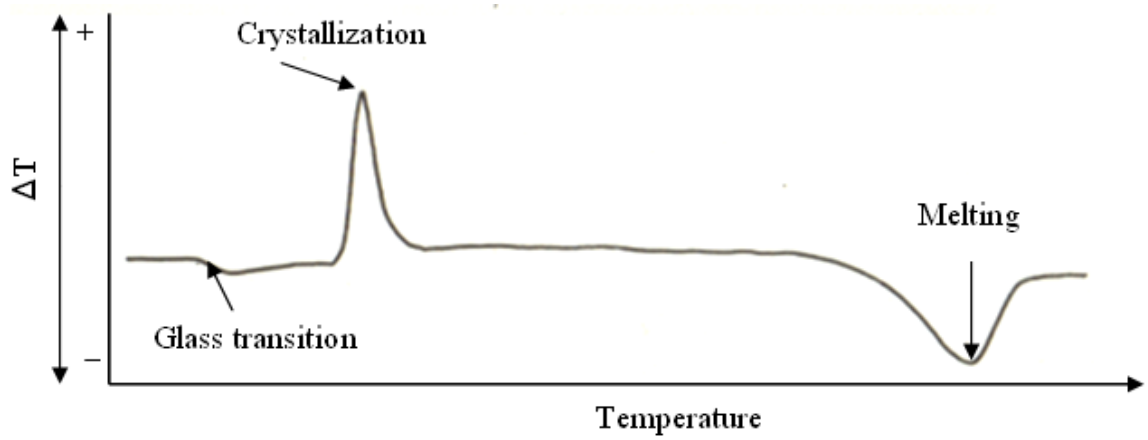

Figure 4.2: Characteristics that determine the application of thermoplastic polymers (Cowie, 1973).

4.3.1 Glass transition temperature *Tg*

The glass transition temperature, *Tg*, is the temperature where a rapid decrease in elastic modulus occurs. It varies with different polymers and takes place in an amorphous region of the semi-crystalline polymers. At ambient temperature, the amorphous regions are solid and the polymer is in a glassy state which causes it to be very hard and brittle. *Tg* occurs due to an increase in motion of large segments of molecular chains caused by heating from below *Tg*. When a certain amount of heat is applied, there is a point where the behaviour of the polymer rapidly changes due to breaks in the van der Waal bonds. At this point, the mechanical behaviour of the polymer changes from being glassy and brittle and becomes less rigid and more rubbery. However the crystalline regions are maintained, due to stronger covalence bonds, so melting does not occur until a higher temperature is applied (Cowie, 1973; Crawford, 1990; Gibson & Shi, 1996; Mangonon, 1999).

There are a number of structural features which have a bearing on the value of glass transition temperature. As *Tg* depends largely on the amount of thermal energy required to keep the polymer chains moving, a number of factors influence *Tg*, including chain flexibility, molecular structure, molecular weight, branching and cross-linking. Flexible chains have a low *Tg* whereas a rigid chain has a high *Tg*. Molecular structure and the size of the group attached to the main chain carbon atom can influence the glass transition point. In this case, the steric factor affects the flexibility of the chain and these arise when bulky pendant groups hinder the rotation

around the backbone and cause *Tg* to increase. The molecular weight of a polymer will have some effect on the *Tg*, so an increase in molecular weight causes an increase in the glass transition temperature. Cross-links will also have an impact on the *Tg* when they are introduced into a polymer. The density of the sample is increased proportionally and this leads to a restriction of the molecular motion in the sample and a rise in *Tg* (Cowie, 1973; Kohan, 1995).

4.3.2 Melting temperature *Tm*

The melting temperature is the temperature where the polymers eventually obtain sufficient thermal energy as the temperature rises to enable their chains to move freely enough and to behave like a viscous liquid. The melting temperature is typically in the order of 100ºC above the glass transition temperature, *Tg*, or 50ºC above crystalline temperature, *Tc*. This varies for different polymers (Cowie, 1973). When the temperature rises from *Tg* to about 30K above *Tg*, the molecular motion starts to increase and this causes the modulus of elasticity to go down, with continuance in temperature rising to just above *Tm*. Here, the polymer becomes liquid and the chains are all tangled up with their neighbours (Gibson & Shi, 1996). The viscosity of the molten polymer depends significantly on the temperature; as the temperature increases, the viscosity of the polymer decreases considerably and can be expressed in its form (Cowie, 1973; Beamam et al., 1997; Brydson, 1999):

$$\eta_0 = A\exp^{(\Delta E / RT)} \qquad \text{(Eq. 4.1)}$$

where ΔE is the activation energy for viscous flow, η_0 is the viscosity; A, a constant specific to molecule mobility; R, the gas constant, and T, the absolute temperature.

As the melting temperature, *Tm*, depends largely on the amount of thermal energy required to keep the polymer chains moving, a number of factors influence *Tm*, i.e. symmetry, intermolecular bonding, branching and molar mass. The symmetry of the chain shape influences the *Tm*. More thermal energy is required for polymers that are sufficiently symmetrical to be considered as smooth, stiff cylindrical rods and this leads to raised *Tm*. Intermolecular bonding will affect the melting temperature, so any interaction between chains in the crystal lattice will help to hold the structure together more firmly and raise the melting temperature. The branching in the side group tends to stiffen the chain and raise the melting temperature. The last factor is molar mass which can change *Tm*. This is where, if the molar mass in the sample increases, the melting temperature will rise (Cowie, 1973; Young, 1981; Kohan, 1995; Brydson, 1999).

4.3.3 Crystallisation Temperature *Tc*

Crystallisation temperature occurs between melting temperature *Tm* and glass transition temperature *Tg*. Usually, the rate of crystallisation is seen between 10K below melting point and 30K above glass transition temperature (Cowie, 1973). At temperatures close to melting point, the crystallisation rate is low and large crystal sizes can be obtained, while at temperatures far below melting point and near *Tg*, the

melt is so viscous that molecular motion is extremely slow, thus leading to a faster crystallisation rate.

The maximum rate of crystallisation takes place at *Tc* (see Figure 4.3) (Young, 1981) and this is influenced by molecular mass. The sample with the lower molecular mass crystallises faster. In addition to this, the presence of homogeneous or heterogeneous nuclei affects the overall crystallisation rate by facilitating the initial nucleation step. The reason for this is that even in the melts, some hydrogen bonds remain fixed and result in effective nucleation sites on cooling. The thermal history should therefore be erased and all homogeneous nuclei destroyed by holding the product for a sufficient time in the melt before crystallisation kinetics can take place (Cowie, 1973; Young, 1981; Kohan, 1995).

The growth of a crystal nucleus can take shape in one, two or three dimensions with the crystals in the form of rods, discs or spheres, respectively. The crystal growth rate is strongly dependent upon the crystallisation temperature. When the crystallisation temperature *Tc* remains just below the melting temperature of the polymer, the growth rate is relatively low. As mentioned early in Equation 1, when the temperature is reduced, there will be an increase in viscosity and transport of material to the growth point will be more difficult. Growth rate therefore peaks, and as the temperature decreases to close to glass transition temperature, the growth rate decreases. The growth rate also depends upon the molar mass, M. As M is reduced, the growth rate increases (see Figure 4.3) (Young, 1981).

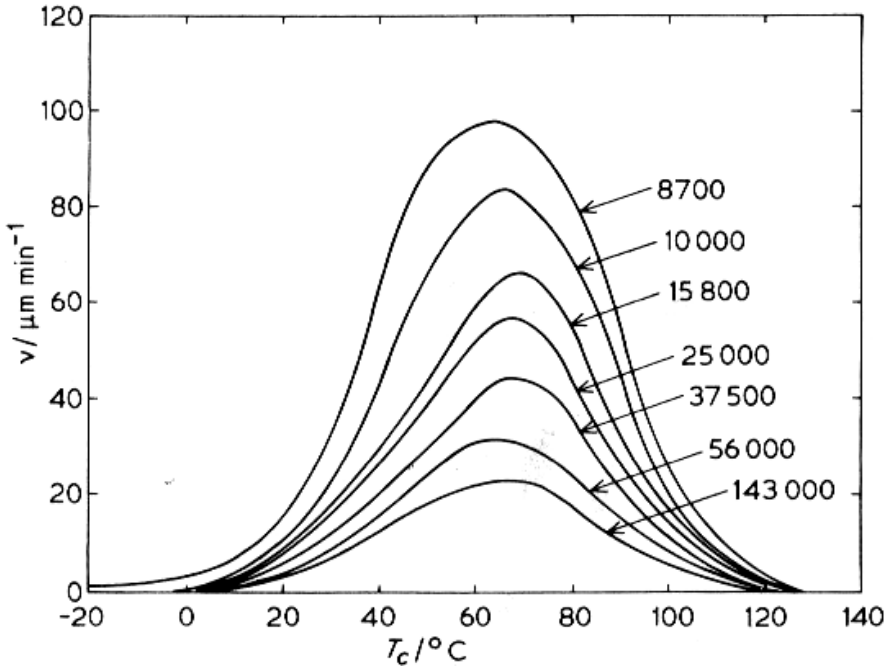

Figure 4.3: Crystallisation temperature *Tc* with crystal growth rate ν for different molar mass in g mol^{-1} (Young, 1981).

4.4 Molecular weight

The most important property for describing the characteristics of polymers is molecular weight, which influences the thermal properties of polymers through the melting viscosity. This is due to the fact that high molecular weight can lead to difficulties in forming the material, given the high viscosities involved. The common effects of molecular weight which affect viscosity largely are caused by the amount of entanglement between the molecules. Consequently an increase in the entanglement, increases viscosity. Viscosity is directly proportional to the average molecular weight when the molecular weights fall below a critical molecular weight value *Mc* from 5000-1500, but beyond this point viscosity depends on greater power (see Figure 4.4) (Cowie, 1973; Beamam et al., 1997; Brydson, 1999). It has been found that melting viscosity varies greatly with changes in the molecular weight for many polymers, as shown in the equation:

$$\eta_0 = K\,(M_w)^n \qquad \text{(Eq.4.2)}$$

where η_0 is viscosity and Mw is molecular weight, K is a constant that depends upon the type of polymer and exponent n=3.4-3.5.

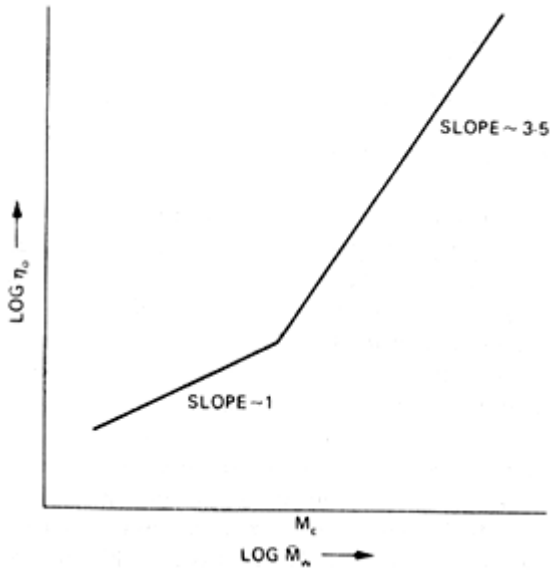

Figure 4.4: Relationship between molecular weight, Mw and viscosity, η_0 (Brydson, 1999).

4.5 Additives

Additives are commonly used in nylon and these include reinforcements, such as ceramic and glass fibres. Reinforcements play an essential role in composite material. They can produce a number of attractive effects in the mechanical properties of specimens, such as increased flexural strength, compression, stiffness, improvement in fracture toughness, creep resistance and, in some cases, tensile strength. To be a candidate for reinforcing nylon, a product must have a melting point above that of nylon (Kohan, 1995; Gill & Hon, 2004). Additives of filler to polyamide directly affect viscosity. As the fillers increase, the viscosity of the composite material increases proportionally (see Figure 4.5). The Einstein equation declares that the filler increases viscosity in a consistent manner:

$$\eta_c/\eta_0 = 1 + 2.5\phi \qquad \text{(Eq.4.3)}$$

while the Guth equation declares a simple extension of Einstein's relationship to higher concentration (Kohan, 1995):

$$\eta_c/\eta_0 = 1 + 2.5\phi + 14.1\phi^2 \qquad \text{(Eq.4.4)}$$

Here, η_c represents the viscosity of the filled polymer at the volume concentration, ϕ, and η_0 consists of the zero shear rate melt viscosity of the unfilled polymer.

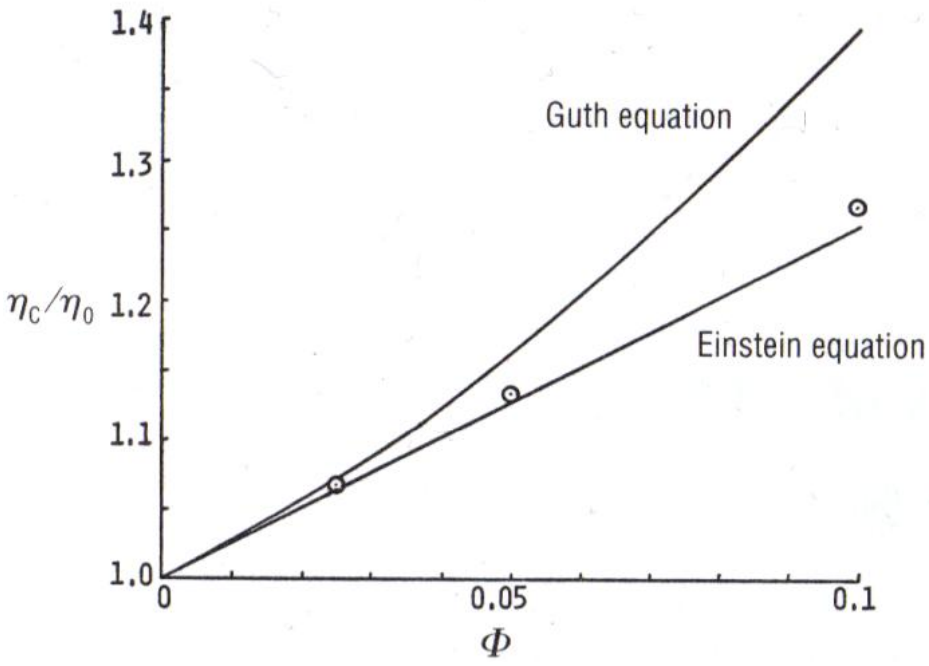

Figure 4.5: Relative viscosity with volume fraction filler (Kohan, 1995).

4.6 Experimental work

4.6.1 Methodology

In order to simulate the conditions of the SLS process, the samples were set in the Oven Heraeus Instruments Vacutherm, Type 6060M, in an optimal nitrogen atmosphere to prevent the powders from oxidising (yellowing), and heated at a specified temperature for varying periods. The samples were heated at temperatures 100ºC and 180ºC, the reason being that 100ºC is considered the minimum degree to which the powder in the left and right cartridges can be exposed through the SLS process, while 180ºC is considered the maximum degree to which the powder may be exposed through the SLS process while located in the bed part. The samples were kept for 20, 40, 60, 80, and 100 hours at each temperature. They were heated using two methods, continuous heating and cyclic heating. The first method was used to simulate the SLS process for one build and the second method for simulating the SLS process for a number of builds by taking out the samples from the oven to cool down to room temperature before returning them to the oven. Samples of new and recycled grade powder were tested, and the results analysed to investigate the effect of the temperature, time and number of builds on the powder properties.

4.6.2 Results and discussion

4.6.2.1 Effect of the cement proportion on viscosity, melt flow rate, thermal behaviour and molecular weight of Polyamide 12

Graphs relating to viscosity, melt flow rate, thermal behaviour and molecular weight values of cement/PA12 composite in relation to various proportions of cement are shown in Figures 4.6 to 4.9. As mentioned earlier in Section 4.5, and Equations 3 and 4, the direct addition of filler to Polyamide 12 theoretically affects viscosity. As the fillers increase, the viscosity of the composite material increases proportionally. In this experiment, viscosity and melt flow rate of cement/PA12 composite is affected via different proportions of cement added to Polyamide 12. Figures 4.6 and 4.7 show that average, minimum and maximum results were tested using the Melt Flow Rate Indexer. From Figure 4.6, the relationship between the viscosity of the composite and weight fraction (wt%) of the cement can be observed. It can be seen that the viscosity increases gradually with an increase in the weight fraction (wt%) of the cement. From the results obtained, this suggests that cement particles can affect the melt viscosity of the composite. This means that the addition of rigid particles such as cement to Polyamide 12 can increase viscosity due to the decrease in melted Polyamide 12 and the fact that the gap between the cement particles becomes narrower. This leads to stickier extruded material.

Figure 4.7 demonstrates a melt flow rate which has decreased at the same time the weight fraction (wt%) of the cement has increased. Therefore, it is clear from an examination of the data presented, that the weight fraction (wt%) of the cement used has had an influence on the MFR value, and this is due to an increase in the viscosity of the composite as the filler increases. As mentioned earlier in Section 3.4.1, the MFR depends on the mass and time-interval cut-off of the extruded material. Therefore, when the viscosity increases, this leads to an influence on mass and the time frame of the extruded material, ultimately causing the MFR of the composite to decrease.

Figures 4.8 and 4.9 show the results were tested using Gel Permeation Chromatography (GPC) and DSC analysis, respectively. These figures illustrate the relationship between the molecular weight and *Tm*, *Tg* and *Tc* of the composite in relation to various proportions of cement. In this experiment, the molecular weight and *Tm*, *Tg* and *Tc* of cement/PA12 composite are not affected via different proportions of cement added to the Polyamide 12. As the *Tg* and *Tm* are used to calculate the part bed temperature, the results obtained suggest that the part bed temperature is fixed by different proportions of cement added to the Polyamide 12.

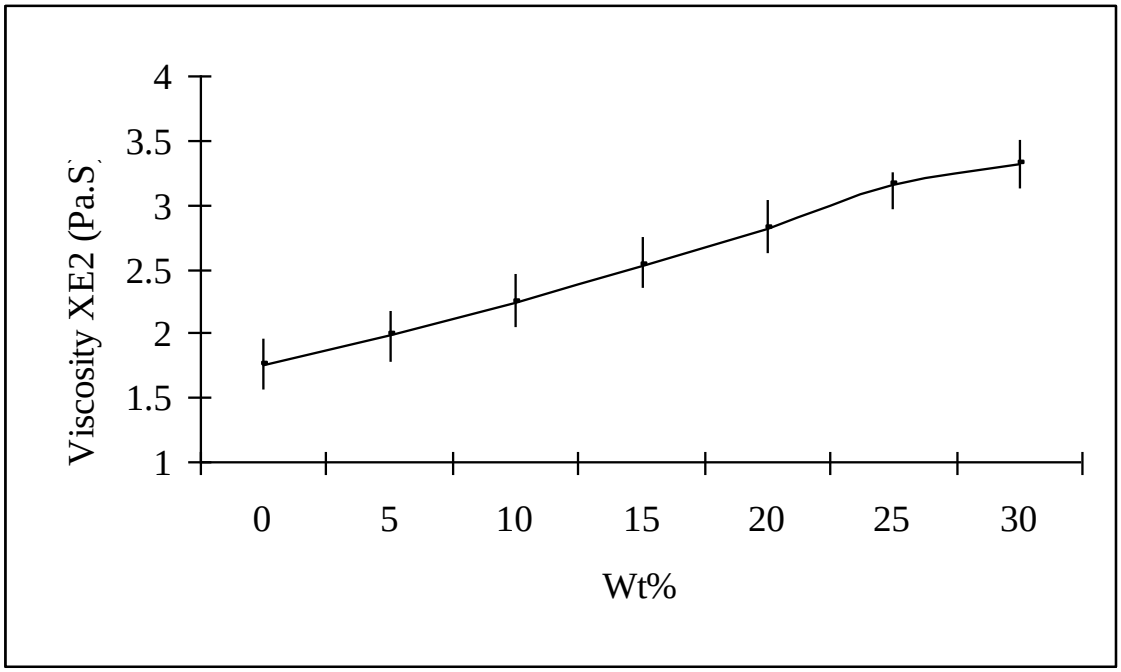

Figure 4.6: Variation of viscosity with cement content added to Polyamide 12.

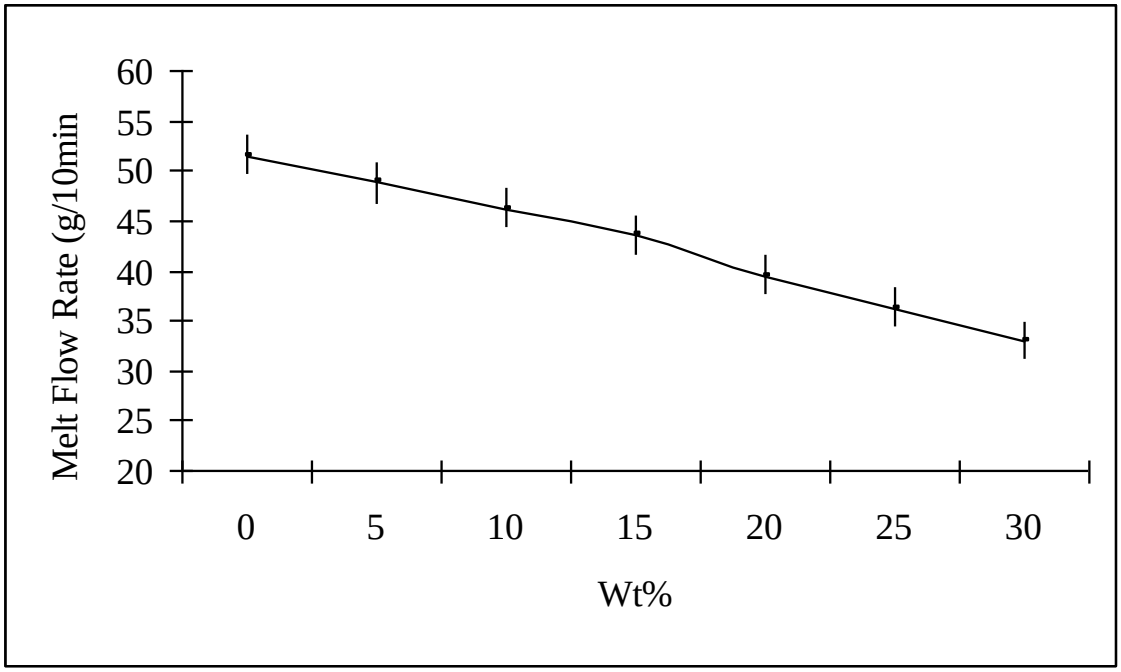

Figure 4.7: Variation of MFR with cement content added to Polyamide 12.

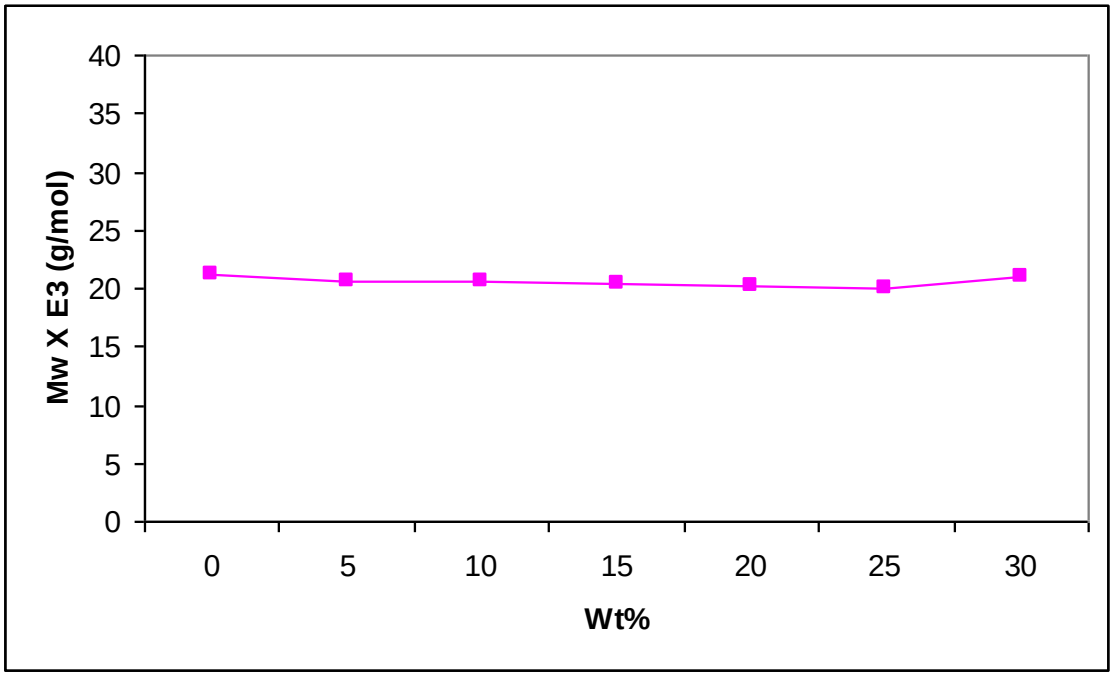

Figure 4.8:Variation of molecular weight with cement content added to Polyamide12.

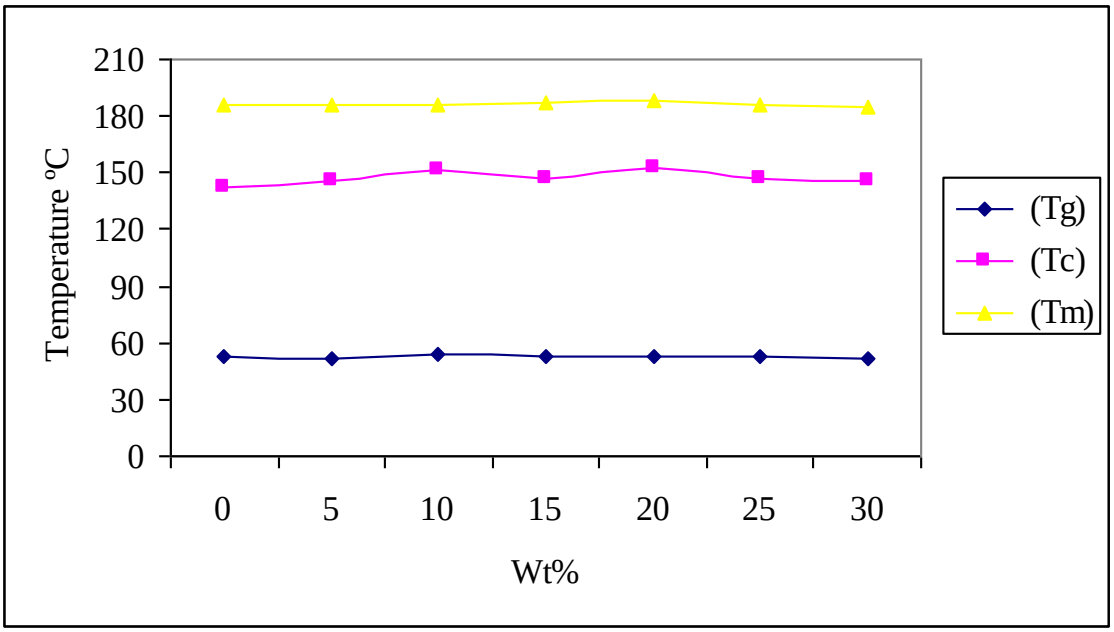

Figure 4.9: Variation of *Tg*, *Tm* and *Tc* with cement content added to Polyamide 12.

4.6.2.2 Effect of temperature and time on molecular weight

In this experiment, composite material of cement/PA12 was exposed to 100ºC and 180ºC temperatures in an oven with a nitrogen atmosphere. The purpose was to simulate the deterioration of the composite powder during the SLS process and after that, arrive at the maximum proportion of used powder that can be re-used in the SLS process.

Figure 4.10 show the results were tested using Gel Permeation Chromatography (GPC). This figure illustrates the relationship between the molecular weight (Mw) and the heating period. It can be seen from the figure that the powder heated to 100ºC (considered to be the minimum degree the powder is exposed to during the SLS process) has a lower molecular weight and experiences a leisurely increase compared to the powder heated at 180ºC. For instance, the fastest change in molecular weight takes place at 180ºC. Temperature plays an essential role in the Mw, as shown in Figure 4.10. Mw at the high temperature of 180ºC increases rapidly for the first 25 hours from 20 E3 g/mol to 141 E3 g/mol. After a 25 hour heating period, the increase in Mw is slower. From this Figure, it can be seen that temperature has a more significant influence on the Mw of the powder than SLS time. It is therefore Mw which affects the quality of SLS parts.

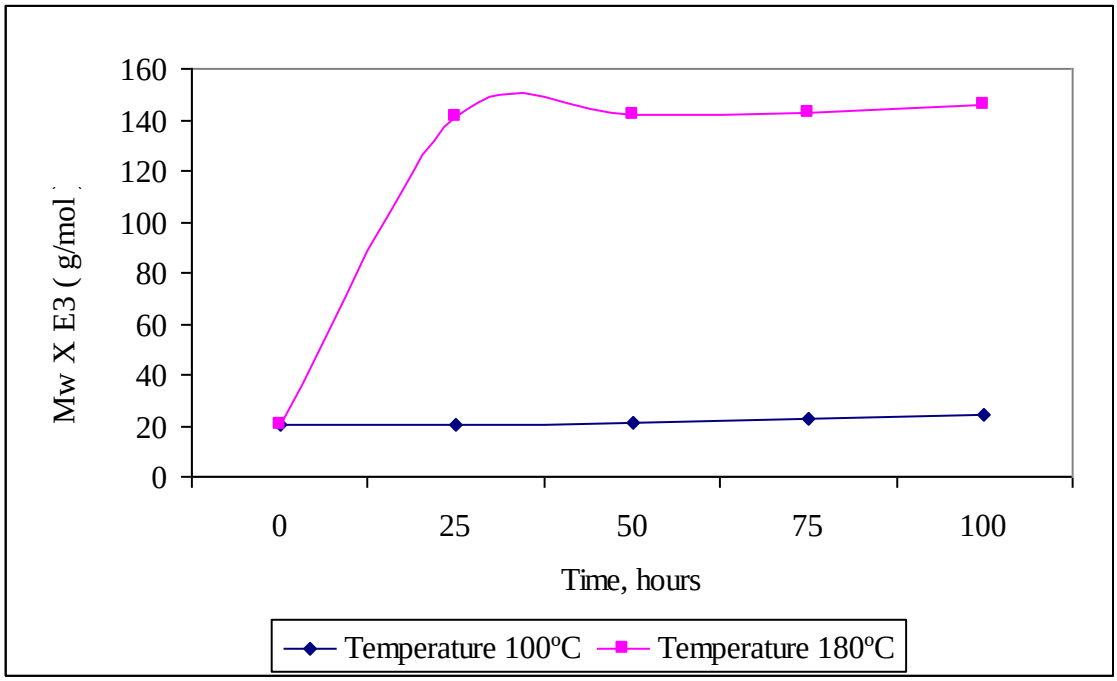

Figure 4.10: Variation of molecular weight (Mw) of composite of cement/Polyamide 12 powder with different temperatures and timings.

4.6.2.3 Effect of temperature and time on the viscosity and melt flow rate

As mentioned earlier in Section 4.4, Equation 2 theoretically demonstrates that the viscosity of polyamide is affected by molecular weight. As molecular weight depends on the exposure of the powder to various temperatures, the viscosity of the powder directly increases (see Figure 4.11). In this experiment, the composite material of cement/PA12 has been exposed to temperatures as described in Section 4.6.2.2 and the results are presented in Figures 4.12 and 4.13.

Figures 4.12 and 4.13 demonstrate the results of viscosity and MFR, respectively, of the composite material of cement/PA12. These have been through varying temperatures and timings, and were tested using the Melt Flow Rate Indexer. From these Figures, it is clear that temperature and heating time play an essential role in the viscosity and MFR of the composite material. The largest increase in viscosity appears to be at 180ºC in the first 25 hours, so it is clear from Figure 4.12 there is a rapid increase in viscosity at 180ºC during the first 25 hours, and then a gradual increase after that period. In contrast, at the same temperature of 180ºC and during the same time period, the largest decrease in MFR occurs (see Figure 4.13). This has been attributed to increased molecular weight, thus leading to an increase in viscosity, followed by decreasing MFR. New powder unexposed to temperature has the lowest viscosity and highest MFR, while powder exposed to the highest temperatures and longest time periods has the highest viscosity and lowest MFR.

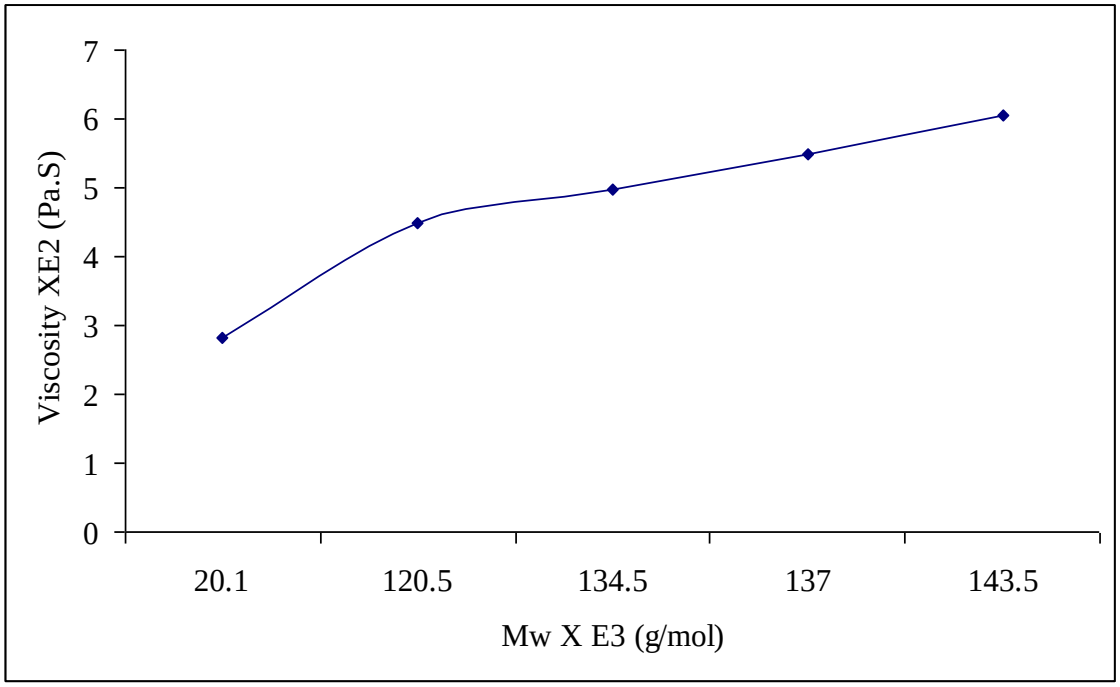

Figure 4.11: Relationship between molecular weight Mw and viscosity $\eta_{0.}$

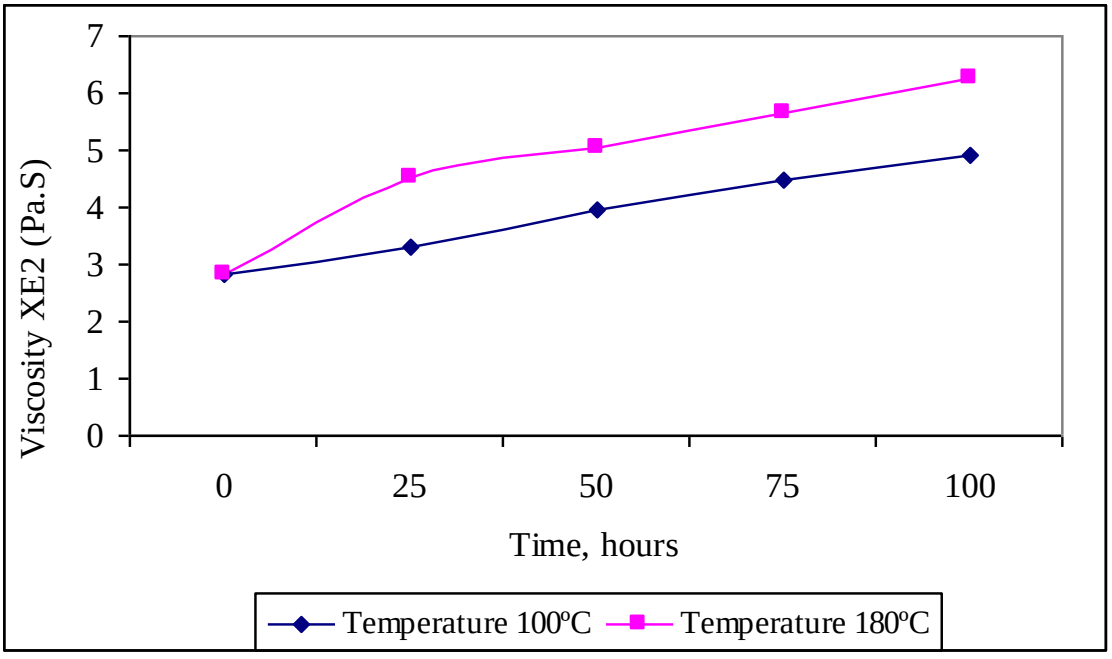

Figure 4.12: Variation of viscosity of composite of cement/Polyamide 12 powder with different temperatures and timings.

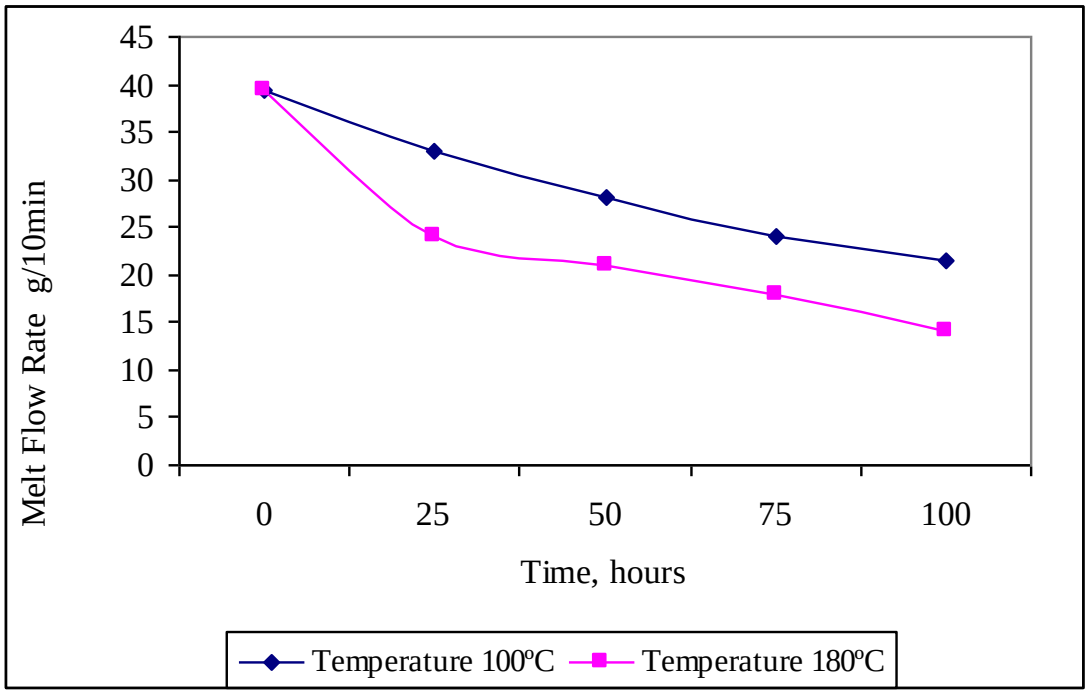

Figure 4.13: Variation of MFR of composite of cement/Polyamide 12 powder with different temperatures and timings.

4.6.2.4 Effect of continuous and cyclic heat on MFR and molecular weight

In the following experiments, the samples of composite material of cement/PA12 were exposed to a temperature of 180ºC in an oven with a nitrogen atmosphere, and a heating method referred to as 'continuous' and 'cyclic' heating. In the cyclic heating method, the powder samples were placed in the oven at a temperature of 180ºC and heated for 25 hours. They were then taken out and cooled to room temperature. After a small amount of the powder was taken to measure and record MFR and molecular weight, they were returned to the oven for another 25 hours. This procedure was repeated in 25 hour periods for up to 100 hours in total. The results of these experiments are shown in a bar chart format in Figures 4.14 and 4.15. The purpose is to explore whether cyclic heating would have a different effect on composite powder deterioration from SLS time alone.

Figure 4.14 and 4.15 show the molecular weight and MFR, respectively, of composite material of cement/PA12, obtained through two methods of heating, continuous and cyclic. These results show a clear trend of slightly faster deterioration of the samples subjected to continuous heating, compared with those subjected to cyclic heating. Generally, the difference between these methods does not have as significant an effect on molecular weight and MFR as the influence of temperature and heating period do on material deterioration.

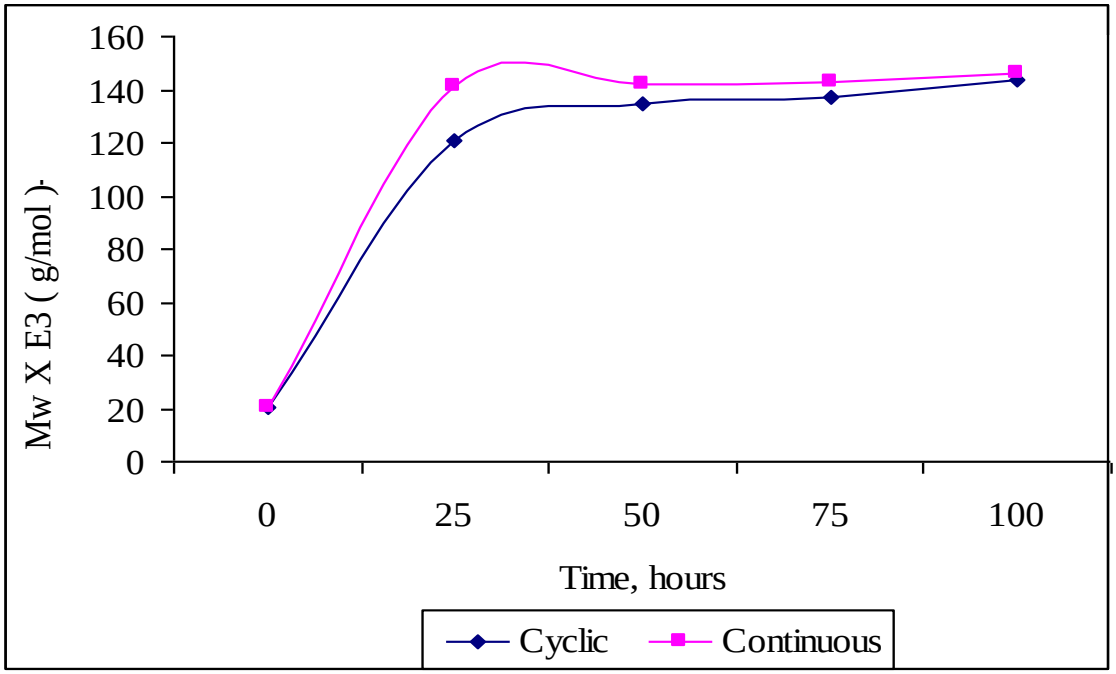

Figure 4.14: Effect of continuous and cyclic heat on Mw of composite of cement/Polyamide 12 powder.

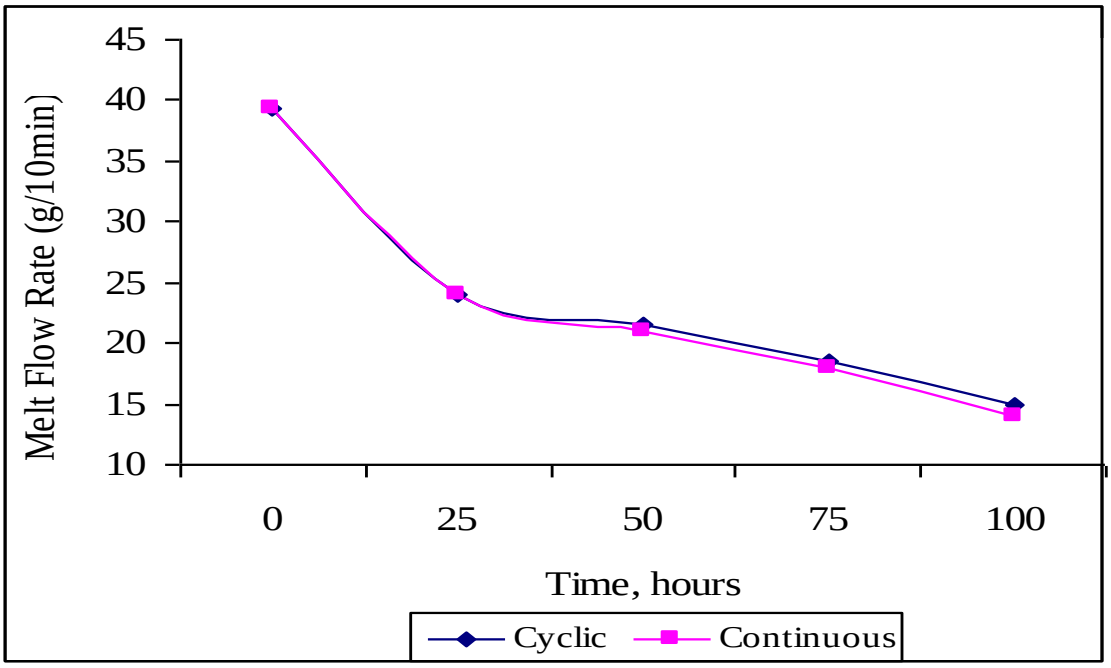

Figure 4.15: Effect of continuous and cyclic heat on MFR of composite of cement/Polyamide 12 powder.

4.6.2.5 Effect of temperature and time on *Tg*, *Tm* and *Tc*

Figures 4.16 to 4.18 show that the results were tested using DSC analysis. These Figures illustrate the relationship between *Tg*, *Tm* and *Tc* of the composite material of cement/PA12, various temperatures, and heating period. In this experiment, the samples of composite material were exposed to the temperatures described in Section 4.6.2.2. As mentioned earlier in Section 4.3, the common factor affecting the three transition temperatures *Tg*, *Tm* and *Tc* is, theoretically speaking, molecular weight. As the molecular weight increases, the *Tg* and *Tm* of the material increase, while the *Tc* of the material decreases.

Figures 4.16 and 4.17 demonstrate that powder heated to a temperature of 100ºC, which is considered to be the minimum degree to which the powder is exposed during the SLS process, has lower *Tg* and *Tm* and experiences a leisurely increase compared to the powder heated at 180ºC. For instance, the fastest change in *Tm* takes place at 180ºC, so temperature clearly plays an essential role in the effect on thermal properties of composite material. As shown in Figures 4.16 and 4.17, the *Tg* and *Tm* at the highest temperature of 180ºC increase approximately by 5ºC to 7ºC within 100 hours. However, the *Tg* and *Tm* of the samples heated at the lowest temperature of 100ºC increase by just 1ºC to 3ºC for the same period. In contrast, with regard to *Tc*, as mentioned above, when the molecular weight increases, the *Tc* of the composite material decreases. It can be seen from Figure 4.18 that the largest decrease in *Tc* occurs at 180ºC and it is clear from the same Figure, there is a rapid decrease in *Tc* at

180ºC and 100ºC within the first 25 hours, and then a gradual decrease after that period. From these results, the *Tg*, *Tm* and *Tc* are used to calculate the part bed temperature and thermal properties of the selected samples and these indicate that the thermal properties of the composite material of cement/PA12 change with reprocessing, thus affecting the properties of SLS parts.

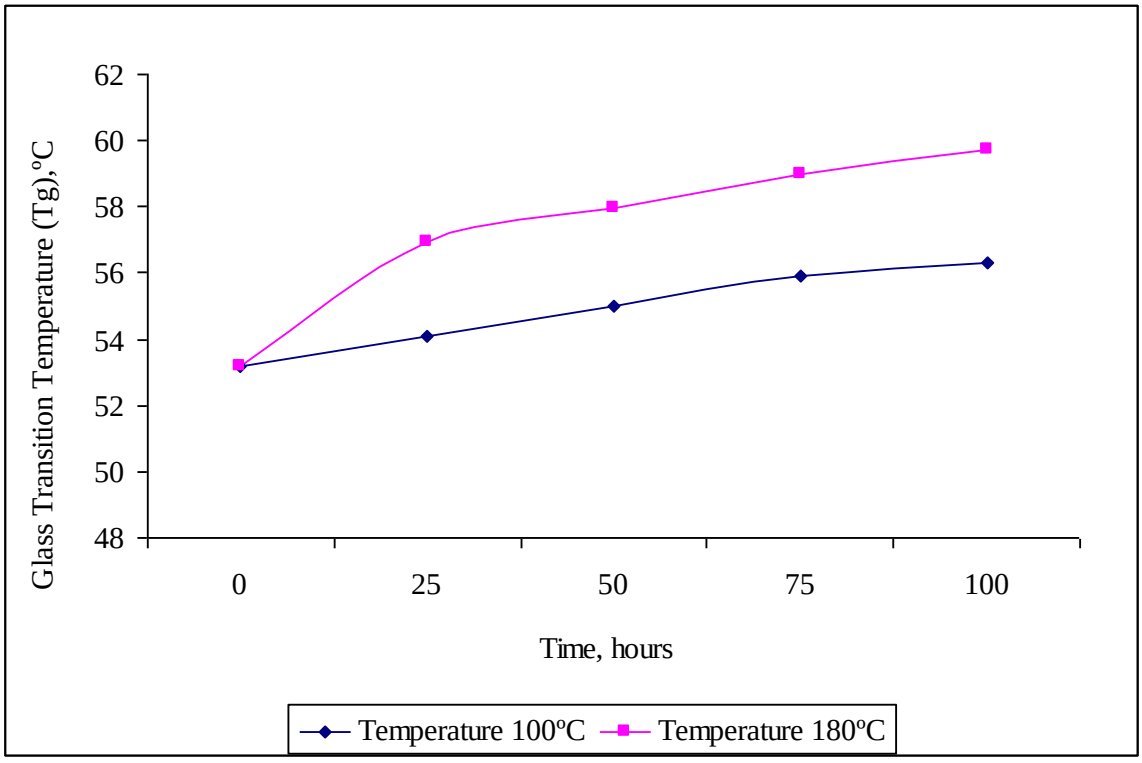

Figure 4.16: Effect of temperature and time on *Tg* of composite of cement/Polyamide 12 powder.

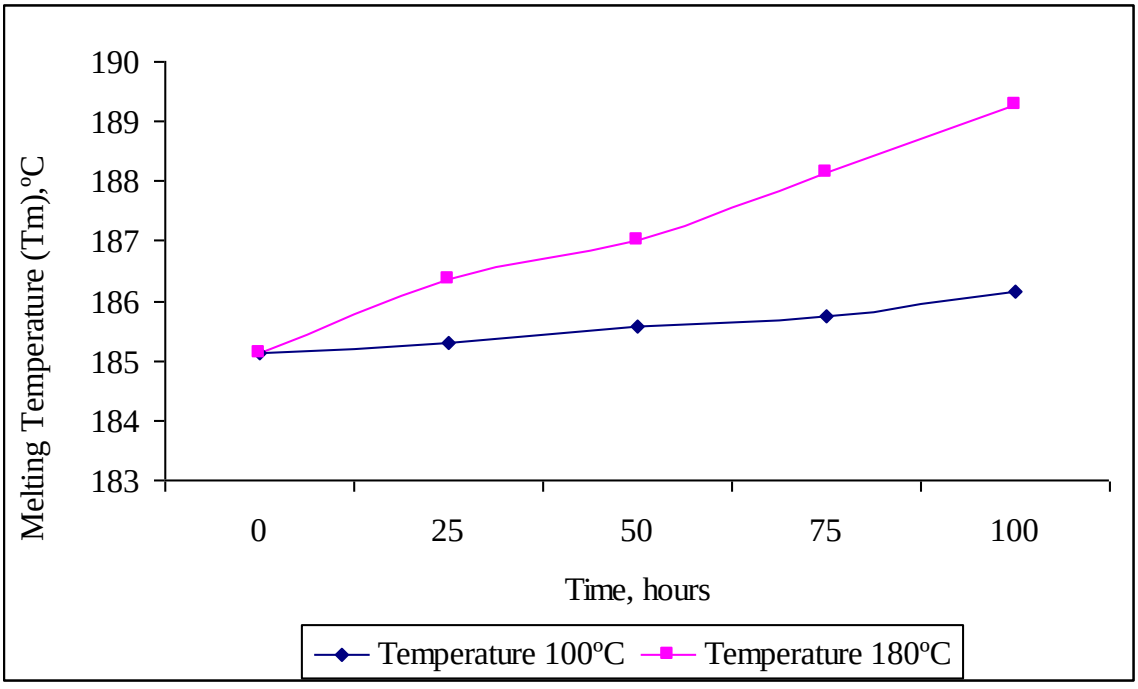

Figure 4.17: Effect of temperature and time on *Tm* of composite of cement/Polyamide 12 powder.

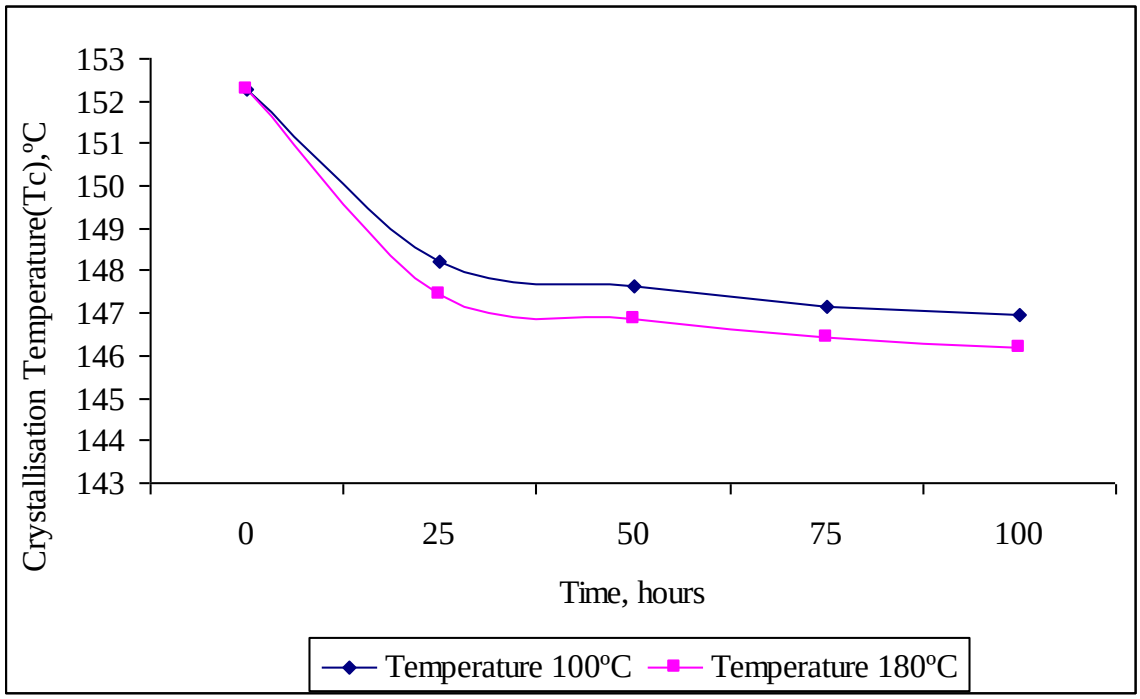

Figure 4.18: Effect of temperature and time on *Tc* of composite of cement/Polyamide 12 powder.

4.7 Discussion

A better understanding of the thermal properties of composite material of cement and PA12 of both virgin powder, and used, un-sintered powder, is an enormous help in controlling SLS parameters and maintaining consistent quality of the fabricated SLS specimens.

The combined indications of the differential scanning calorimeter suggest that the different proportions of cement added to the Polyamide 12 are not change the glass transition temperature *Tg*, melting temperature *Tm* or crystallisation temperature, *Tc*. This can lead to fixing the part bed temperature with different proportions of cement added to the Polyamide 12, while the melt flow rate index test proposes that the addition of cement particles to Polyamide 12 affects the melt flow rate of the composite. As the proportion of cement increases, so does its viscosity, due to the decrease in melted Polyamide 12 and the fact that the gap between the cement particles becomes narrower. This leads to the extruded material becoming stickier, which is a sign of a decrease in the MFR index. It ultimately affects the quality and surface finish of the fabricated SLS specimens.

Huge amounts of powder left un-sintered during SLS could be reused depending on their properties. However, the properties of un-sintered powder deteriorate due to exposure to high temperatures, e.g. just below the melting point of the composite material for an extended period of time during SLS building and the cool-down stage.

The temperature and heating time to which the un-sintered powder are exposed are the most significant parameters for powder aging and the deterioration of material properties.

The melt flow rate index tests indicate that the temperature to which the un-sintered composite powder was exposed and the duration of this exposure affect the melt flow rate of the composite. MFR of composite material decreases by 18-25 g/10min with powder usage and this was attributed to increased molecular weight, leading to greater viscosity and then decreased MFR. The powder left unexposed to such temperatures has the lowest viscosity and highest MFR, while the powder exposed to the highest temperature and longest heating period has the highest viscosity and lowest MFR. The molecular weight and melt flow rate of the samples subjected to continuous and cyclic heating are less significant than the temperature and heating time of the SLS process on material deterioration.

The differential scanning calorimeter DSC suggests that the temperature and heating time to which the un-sintered powder was exposed affect the glass transition temperature *Tg*, melting temperature *Tm* and crystallisation temperature *Tc*. This leads to changes in part bed temperature with different grades of powder. The melting temperature of the composite material increases by 0.5-1 ºC with each build or cycle until it reaches 4ºC with the longest possible powder exposure period. The fabrication parameters in the SLS process are mainly dependent on the properties of powder

used, so changing the fabrication parameters as the powder aged, gives consistently and high quality fabricated SLS specimens.

As the powder degrades due to exposure to high temperatures for an extended period in the SLS system, the quality and surface finish of the fabricated SLS specimens become poorer. Therefore the amount of virgin power to be added to achieve the target melt index range appears too vary from 25% to 42% depending on the length of time the powder was exposed to the respective temperature. The melt flow rate index has therefore proved to be a good indicator of powder fitness.

4.8 Summary

This chapter focuses on understanding the thermal properties of different proportions of composite material of cement/PA12 to determine the optimum parameters of the SLS process. In addition, it examines the thermal and physical properties of used or un-sintered powder in order to develop a methodology for controlling SLS parameters, and so, in turn, to obtain consistent, good quality fabricated SLS specimens. The most significant factors affecting the aging or deterioration of composite material of cement/PA12 are the temperatures and heating times to which the un-sintered powder was exposed.

Chapter 5

Mechanical Properties of Selective Laser Sintered Cement and Polyamide 12 Composite

5.1 Preliminaries

In the work reported in this chapter, selective laser sintering is used to produce mechanical specimens of composite material made up of cement and Polyamide 12. The chapter discusses the interactions between cement and Polyamide 12 particles and between Polyamide 12 themselves. It describes an experimental investigation of tensile, Young's modulus, flexural, compression, impact strengths and density, to determine the effects of varying the energy density (ED) generated by the laser and the proportion of cement additive to Polyamide 12 on the physical and mechanical properties of sintered specimens.

The effect of using un-sintered powder on MFR and mechanical properties is investigated to determine the usability of the powder. In addition, the mechanical properties of actual parts produced using SLS are compared with data-sheet values for PA12 material, in order to generate confidence in its mechanical properties. The effects of varying ED on composite material properties is explained by examining the

physical construction of the specimens. The optimum ED for producing parts with maximum density, strength and stiffness has been determined.

5.2 Interaction between cement and Polyamide 12 particles and Polyamide 12 particles

5.2.1 Interaction between cement and Polyamide 12 particles

PA12 is a crystalline polymer with low melted viscosity. In their initial state during the sintering process, the Portland cement particles are homogeneously distributed throughout the larger Polyamide 12 grains. In the first stage of the SLS process (see Figure 5.1 A), the composite cement with Polyamide 12 powder mixture is exposed to CO2 laser radiation. The PA12 material subsequently absorbs the laser energy and melts. The low melted viscosity is positive for PA12 flowing in the sintering layer, and so, in the second stage of the SLS process, the cement particles are surrounded by the melted PA12. During this local melting process, the small cement particles enter the Polyamide 12 grain (see Figure 5.1 B), while melting additional regions of the Polyamide 12. This is a possible explanation for the observation that cement particles can barely be detected by SEM at the surface and fracture surface of sintered parts (see Figure 5.2).

In the third stage, as a result of the complete melting of the Polyamide 12, the formation of ‘sintering necks’ from one polymer particle to another is initiated (see

Figure 5.1 C) and this causes viscous flow to occur (Ajoku et al., 2006). Viscous sintering was first explored by Frenkel (German, 1996; Beaman et al., 1997). Frenkel uses a model for viscous sintering to describe the neck growth between two particles:

$$\left(\frac{x}{r}\right)^2 = \frac{3}{2}\left(\frac{\sigma t}{r\eta}\right) \qquad \text{(Eq.5.1)}$$

where x is half the thickness of the neck formed between contiguous particles, r is the radius of the particle, t represents the time needed for sintering, and ηo represents the melt viscosity.

In the last stage (see Figure 5.1 D), the laser power has left one region for another and the Polyamide 12 starts to cool down. Following this, the crystallisation process starts.

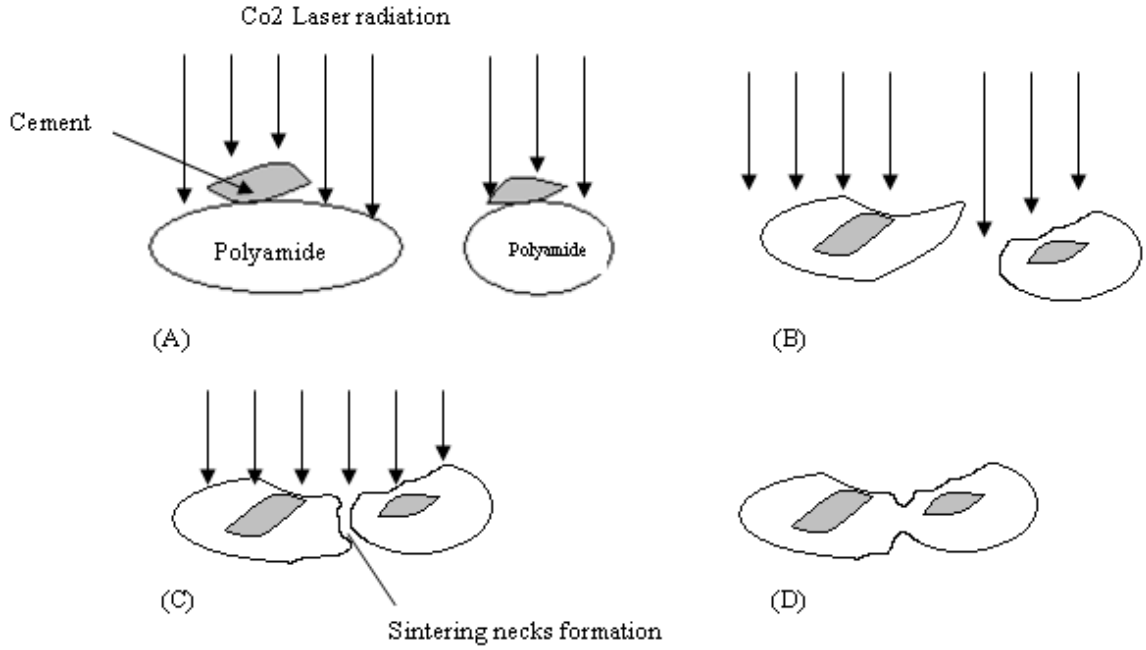

Figure 5.1 illustrates the various states of the sintering process for SLS.
(A) State one: laser energy absorption by PA12 particles; (B) State two: cement particles are surrounded by the PA12 melt; (C) State three: the PA12 particles are completely melted and sintering necks start to form; (D) Final state: laser exposure is carried out and the sintered layer has begun to form.

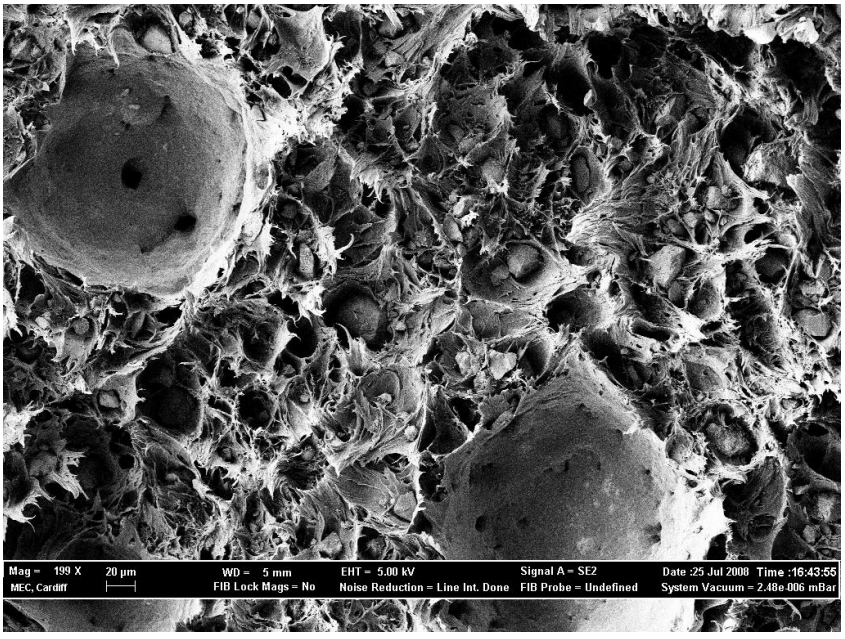

Figure 5.2: Electron micrograph scans of the fracture surface of the PA12 and cement specimen.

5.2.2 Interaction between Polyamide 12 particles themselves

During the SLS process, the higher ED leads to an increase in neck radius between sintered particles, reducing porosity and consequently promoting greater bonding between the particles as well as increased density. The sintering process is considered to be a thermal treatment for bonding particles which often takes place on an atomic scale (German, 1996; Ajoku et al., 2006).

The bond between the particles forms in three directions, X, Y and Z. During the first stage, after they have been exposed to a laser beam, the particles bond together with a neck which begins in the X axis (see Figure 5.3 A). After that, the laser beam moves in the Y axis to scan the next vector and the particles bond together with a neck which starts in the Y axis (see Figure 5.3 B). A new layer of powder is spread when the first layer has been sintered completely and particles bond together with a neck which starts in the Z axis (see Figure 5.3 C). The bond strength between the particles depends totally on the temperature, and consequently the size of the neck radius in the X axis is considered to be the maximum size, while the smallest neck radius is found on the Z axis because the particles in the previous layer have cooled and led to a reduction in the neck radius between sintered particles. The thickness of the neck formed between contiguous particles in the Y axis is less than in the X axis due to the fact that particles in the vector along the X axis are of a higher temperature than the particles between vectors in the Y axis (see Figure 5.3 B).

A high-quality SLS part requires careful control of parameters that determine particle fusion. The major build parameters in the SLS process are laser power, scan-spacing, laser scanning speed, bed temperature, layer thickness and part-build orientation. ED equals energy transferred to the surface of the part bed and can be calculated from the laser power, scan-spacing and laser scanning speed, which are considered to have relatively greater effect on ED than other factors. To produce high-quality functional SLS parts, it is important that the powder on the surface of the part-bed receives a sufficient amount of ED through the laser sintering process. This can be calculated by using the following equation:

$$ED = \frac{P}{LS * SCSP} \qquad \text{(Eq.5.2)}$$

where P is the laser power during scanning exposure, $SCSP$ is the scan-spacing and LS is the laser speed during scanning exposure. However, the high ED of a laser beam results in better fusion of the Polyamide 12 particles, consequently leading to a decrease in porosity and enabling a more compact structure to be built. Excessively high ED will cause degradation of the Polyamide 12, hard part cake, difficulty in taking parts out of the build, roughness, and a part surface which is light brown due to overheating. On the other hand, at low ED levels, the part is likely to have insufficient bonding between powder particles, thus leading to higher porosity and a weak part (Caulfield et al., 2007).

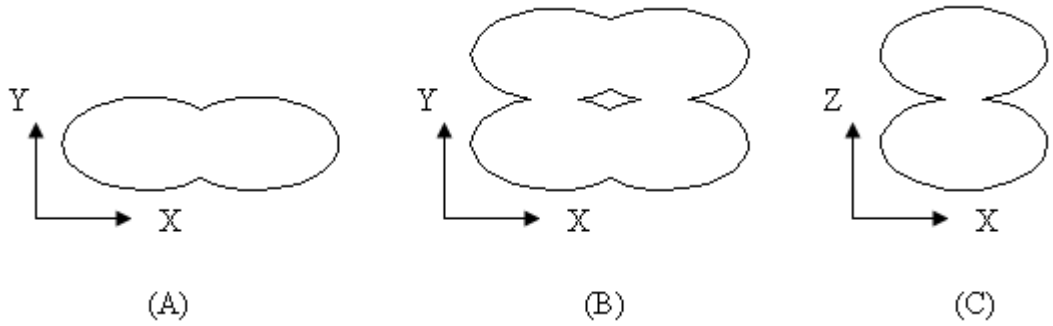

Figure 5.3: Schematic of bond between the particles occurs in X, Y and Z directions.

5.3 Experimentation

5.3.1 Sample preparation

Composite of cement and PA12 was sifted by an intensive shaking procedure using a VORTI-SIV sifter to avoid agglomerates of powder. After this, composite powder was mechanically mixed in a determinate formulation (see Table 5.1) using a high-speed mixer for 20 minutes to obtain homogeneous powder mixtures of uniform colour. The blended powder is then transferred onto the Sinterstation 2000 into two feed cartridges. The sintering condition is adjusted by changing the applied laser power between 4.5 and 8 Watts, with a laser scanning speed of 914 mm/s, scan-spacing of 0.15 mm, layer thickness of 0.1 mm and a part bed temperature of 177-178° C. When the parts have been sintered, they are removed from the parts cake and manually cleaned using a brush, before being sandblasted and passed under pressurised air to remove remnants of the powder on the surface of part. The EDs applied to the SLS parts are calculated using Eq. (2) and this is indicated in Table 5.2. The sintered parts are then observed using an SEM. As the samples are not made of conductive material, gold coating is needed to improve electron conductivity before capturing images with the Cam Scan.

Table 5.1: Cement/PA12 mixture powder formulation

Cement (g)	PA (g)	Proportion
30	581	5:95
63	571	10:90
98	558	15:85
136	544	20:80
175	526	25:75
217	507	30:70
261	485	35:65
308	462	40:60

Table 5.2: Sintering parameters of the cement/PA12

Scan- spacing (mm)	0.15							
Laser power (W)	4.5	5	5.5	6	6.5	7	7.5	8
Energy density (J/mm^2)	0.0328	0.0364	0.04	0.043	0.047	0.051	0.054	0.058

5.3.2 Measurement and test specimens

The tensile, flexural and compression specimens were tested using a Testomeric M500 machine and were determined with reference to ISO 527.2, ISO 178 and ISO 604, respectively. The tensile specimens were dog-bone shaped (see Figure 5.4) and the test speed was 5mm/min.; the flexural specimens were 80-10-4 mm; the span, 60 mm and the test speed, 2mm/min. Finally, the compression specimens were 10-10-4 mm and test speed, 5mm/min. The Izod impact specimens were tested using a Pendulum impact W&T AVERY machine and determined with reference to ISO 180. The density of the material was assessed by building density specimens. The density specimens were 30-10-4 mm determined with reference to ISO 1183-3. The dimensions of the specimens were obtained using a micrometer, with each dimension being measured three times and an average dimension connected with each part. Once the density specimens were measured and weighed, the salient density was calculated through dividing mass by volume. The cross-sectional area (CSA) value was developed from the average part thickness and width per ED. The CSA of the part is therefore important as it is required in calculating the tensile and flexural specimens. The intended CSA for all the parts was 40mm^2.

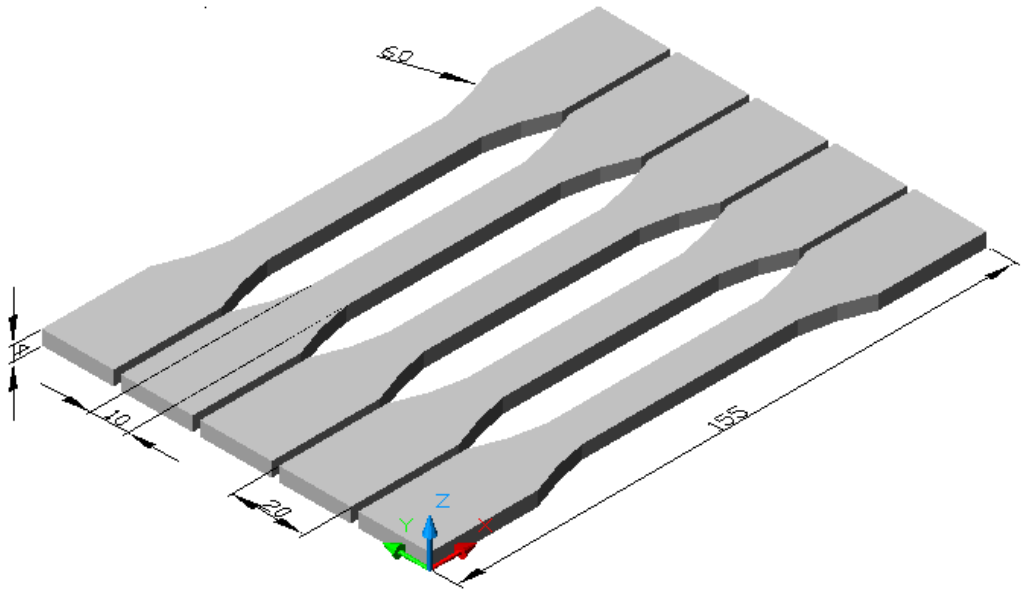

Figure 5.4: Building and dimensions of tensile test specimen.

5.4 Results and discussion

5.4.1 Sintering part dimensions and density

Figures 5.5 to 5.7 show the part length, width, thickness and density results obtained, as opposed to their ED. To investigate the effect of the ED on the dimensions and density of the test specimens, three different measurements of the specimens were taken: length, width and thickness. Figure 5.5 shows the part length increased by raising ED. All parts were somewhat smaller than the intended part length of 30 mm except when the highest ED level, 0.058 J/mm², was exceeded. As shown in Figure 5.6, the required width of 10mm was reached and exceeded by the ED > 0.043 J/mm², and in a similar way, part widths increased with rising ED. Figure 5.7 shows the part thickness on the verge of reaching the intended target of 4mm but discontinued at a maximum value with 0.051 J/mm² of ED, consequently initiating a decrease relative to increased ED. Figure 5.8 displays variations in density amongst the samples, correlating to ED. When ED < 0.051 J/mm², the density of the composite increased with rising ED, and then gradually decreased with increasing ED.

From the results, it can be concluded that ED has an effect on the dimensions and density of the SLS parts of composite material. The parts' dimensions increased relative to increased ED. The parts' thickness yielded values closer to the desired thickness of 4 mm. However, the desired thickness was not reached due to shrinkage of the sintering part during cooling. In addition, the thickness dimensions were

controlled by the height of the powder layer. While the parts' length and width were unlike the part thickness, the length and width values reached and exceeded their desired values due to the laser, which controlled the length and width dimensions. In general, the increase in part dimensions as a result of ED may be explained by the increase in ED leading to growth in the amount of conduction through the powder, thus causing excess powder particles to melt and fuse, resulting in extra length, width and, to some extent, thickness.

Where the density of the parts was concerned, their dimensions increased through raised ED, which to some extent causes density to increase at optimum ED and then decrease with raised ED. At ED levels in excess of the optimum, the binder in the composite material degrades and evaporates due to excess heat from the laser power, or longer heating time.

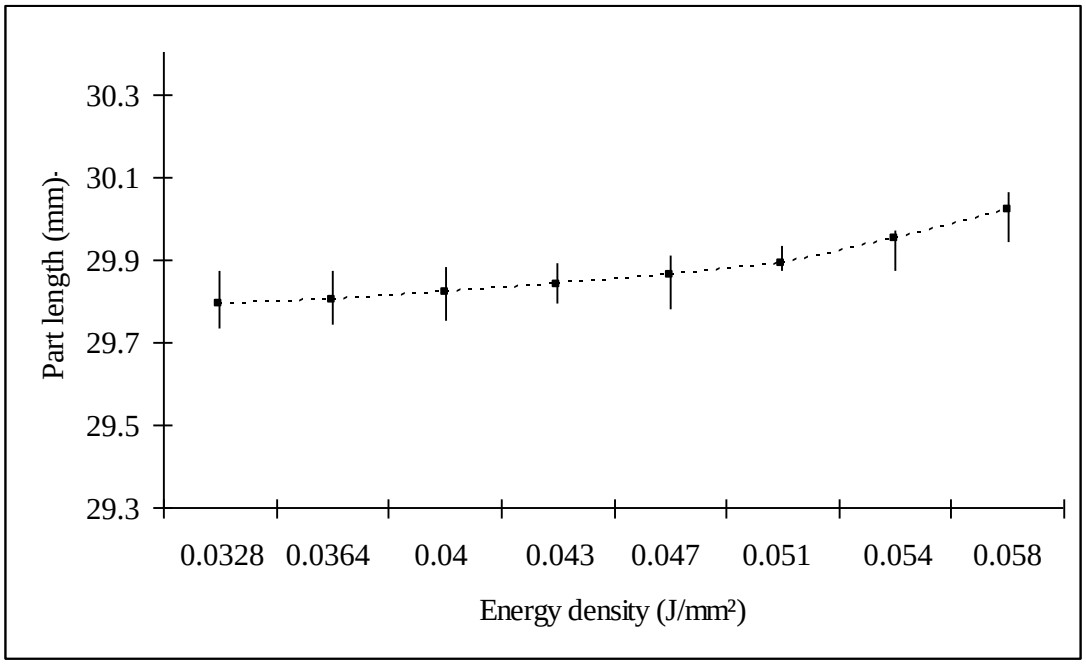

Figure 5.5: Variation of length with energy density.

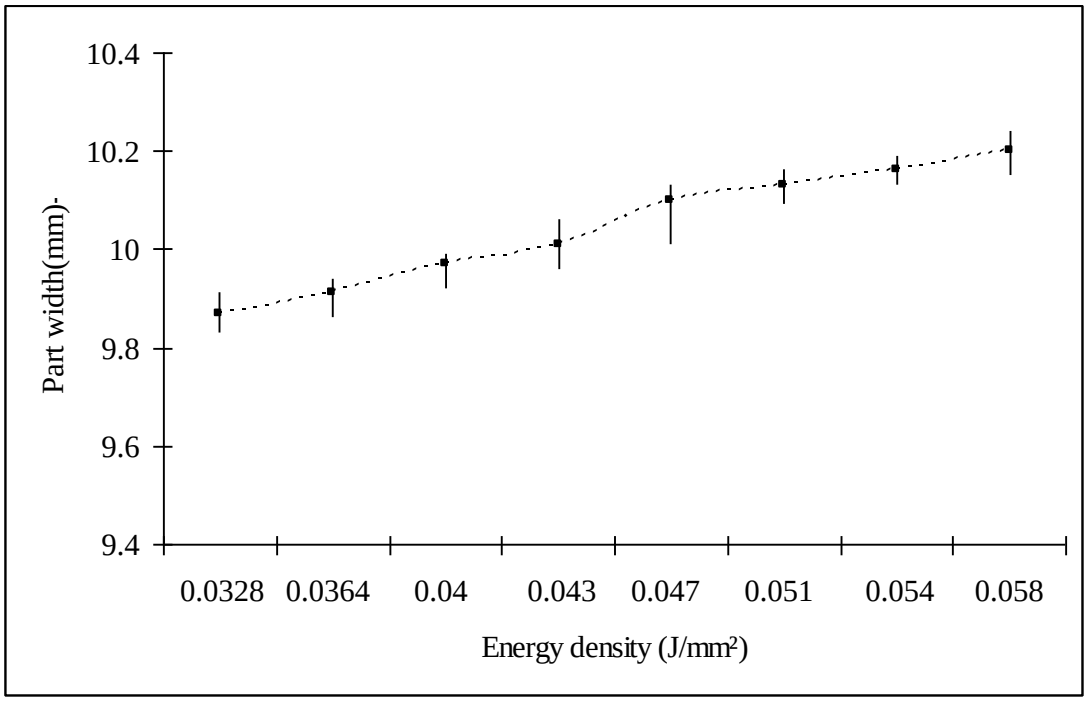

Figure 5.6: Variation of width with energy density.

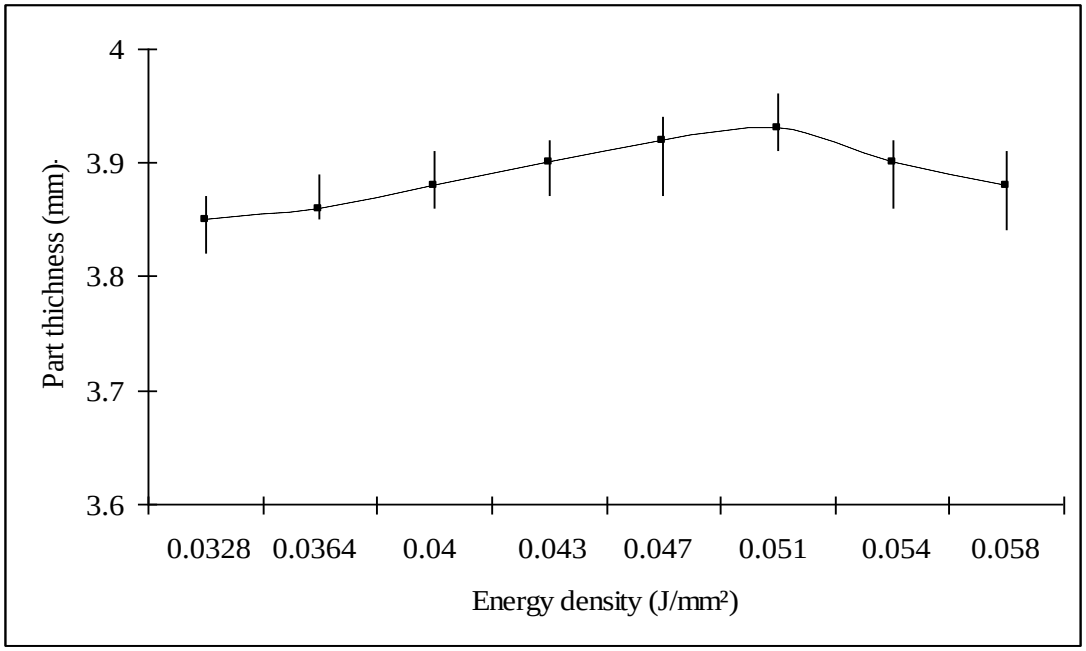

Figure 5.7: Variation of thickness with energy density.

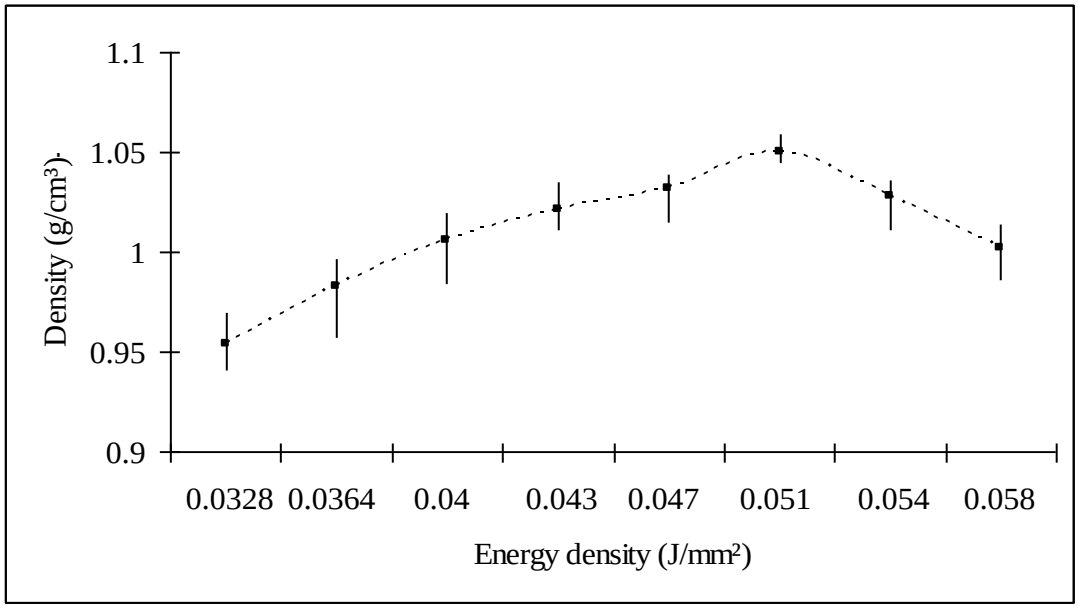

Figure 5.8: Variation of density with energy density.

5.4.2 Mechanical properties

The effects of various EDs and proportions of cement on the mechanical properties of SLS parts are shown in Tables 5.3 and 5.4, respectively. These show the average results in terms of ultimate tensile strength (UTS), elongation at break, flexural modulus, flexural yield strength, compressive strength, impact strength and Young's modulus from 5 test parts built in the SLS machine (five tensile, five flexural, five impact and five compression). A massive amount of the powder remained un-sintered during the SLS process and could be reused, depending on its properties.

The effect of using un-sintered powder on the MFR and mechanical properties is examined and shown in Figures 5.23 to 5.25. A comparison of the mechanical properties of actual parts produced using SLS, along with data-sheet values for PA12 material, is shown in Table 5.5.

Table 5.3: The mechanical properties of SLS parts according to various energy densities.

Mechanical Properties	ED 0.0328	ED 0.0364	ED 0.04	ED 0.043	ED 0.047	ED 0.051	ED 0.054	ED 0.058
Tensile Strength, Ultimate(MPa)	36.4	38.05	41.15	44.72	49.01	50.58	49.52	48.9
Young's Modulus (Mpa)	1830	1895	1990	2115	2240	2350	2260	2125
Elongation at break (%)	2.16	3.4	4.98	6	6.96	7.8	7.68	7.5
Flexural Modulus (GPa)	1.52	1.59	1.65	1.73	1.85	2.07	1.88	1.75
Flexural Yield Strength (MPa)	39.4	44.28	45.33	47.75	48.71	52.56	48.91	48.05
Compression Strength (MPa)	30.15	34.48	42.16	47.44	51.93	54.44	52.67	51.31
Notched impact strength (KJ/m²)	10.56	11.12	11.83	12.62	13.12	13.71	12.63	11.64

Table 5.4: The mechanical properties of SLS parts with various proportions of cement.

Mechanical Properties	PA12	PA12-cement (5wt%	PA12-cement (10wt%	PA12-cement (15wt%	PA12-cement (20wt%	PA12-cement (25wt%	PA12-cement (30wt%	PA12-cement (35wt%	PA12-cement (40wt%
Tensile Strength, Ultimate(MPa)	49.49	49.9	50.6	49.1	48.36	47.95	47.26	46.56	45.94
Young's Modulus (Mpa)	1975	2205	2350	2480	2575	2670	2760	2790	2810
Elongation at break (%)	9.6	8.6	7.8	5.4	3	2	1.8	1.5	1.1
Flexural Modulus (GPa)	1.71	1.92	2.07	2.24	2.32	2.34	2.38	2.42	2.44
Flexural Yield Strength (MPa)	46.72	50.06	52.56	55.48	57.26	57.85	58.1	58.44	58.77
Compression Strength (MPa)	47	52.15	54.44	56.03	57.87	58.35	58.84	59.26	59.55
Notched impact strength (KJ/m²)	15.33	14.67	13.71	12.65	11.57	10.39	9.28	8.1	6.9

5.4.2.1 Tensile properties

Figures 5.9 and 5.10 show the ultimate tensile strength (UTS) and results obtained in relation to various EDs and proportions of filler. From Figure 5.9, it is clear that UTS increases rapidly with an increase in ED, except at the highest ED level when the tensile strength decreases steadily. Judging from the results obtained, the UTS is directly influenced by part-density, which is in turn affected by ED. Density and tensile strength are in direct proportion to each other. Therefore, as the part-density increases, so does the tensile strength, resulting in enhanced fusion of Polyamide 12 particles and a decrease in porosity to produce a more compact structure and consequently greater tensile strength. With degradation of the Polyamide 12 particles due to excessively high ED, the tensile strength declines directly.

Figure 5.10 illustrates the dependence of the UTS in the samples on the weight fraction (wt%) of the cement. When wt% is < 10%, the UTS of the composite increases steadily with the addition of wt%, and then decreases gradually with increasing wt%. This suggests that the cement particles can enhance the ultimate tensile strength to some extent and continue to do so as the filler is increased. This is explained by He & Jaing who have presented the percolation theory, which states that a matrix zone around each particle of filler is affected by stress concentration. Consequently, if the particles are fine, well distributed and the distance between them is small enough, it leads to the merging of zones, which increases strength (Mareri,

1998; Unal, 2004). When the filler increases by more than 10%, the gap between the Polyamide 12 particles increases, and so the adhesion between the particles will decrease, leading to a reduction in UTS.

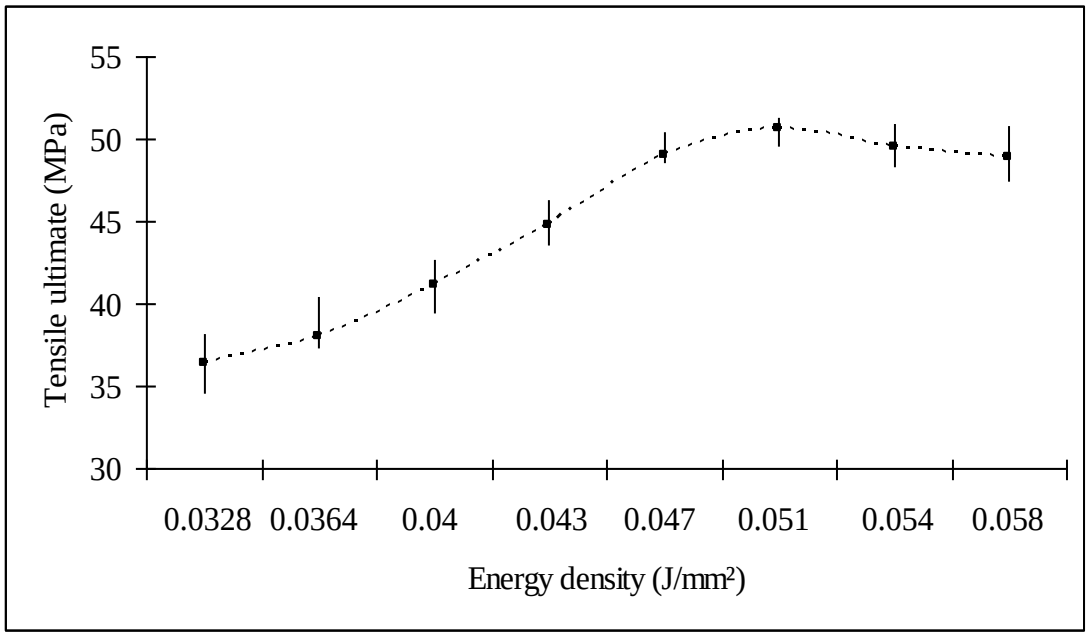

Figure 5.9: Variation of tensile ultimate with energy density.

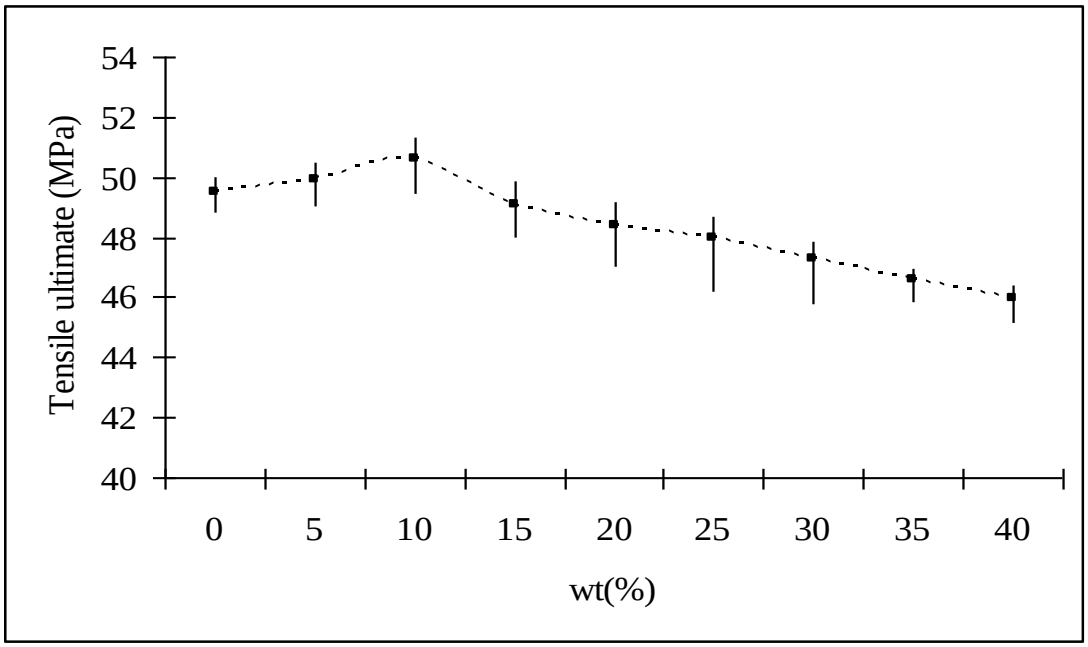

Figure 5.10: Variation of tensile ultimate with cement content.

5.4.2.2 Young's modulus

The resulting stress-strain curve is obtained using an extensometer to find the corresponding Young's modulus. Figures 5.11 and 5.12 demonstrate the Young's modulus results plotted against the ED level used to create the specimens and proportions of filler. From Figure 5.11, it can be seen from an examination of data that the ED level used to create the parts has a strong influence on the resultant Young's modulus value. When sintering at higher ED levels, the bonds between the powder particles become stronger, which leads to greater ductile behaviour with large plastic regions in the stress-strain curves. This can be seen in the relationship between the modulus and density of the parts. As the density of the part increases, so does Young's modulus. There is, therefore, a strong connection between the shape of the curves in Figure 5.11 and the density curves shown in Figure 5.8. The stiffness of the composite beyond the optimum level of the ED starts to decline due to the degradation of Polyamide 12 particles binder.

Figure 5.12 displays the influence of various weight fractions (wt%) of cement on the Young's modulus of the composite specimen. As shown in the Figure, the modulus of composite elasticity increases in relation to increased wt% of filler, namely from 1722 MPa at 0% of filler to 2810 MPa at 40%, where the influence is significant. This result confirms that the addition of rigid particles to Polyamide 12 enhances the stiffness of the composite, and that due to the interfacial adhesion between the filler and matrix, it is good and strong. With the addition of rigid particles to the

Polyamide12 and the difference in modulus between the particles, some physical cross-linking points might be generated and the movement of the molecular chains of the matrix is to some extent blocked, leading to improved stiffness of the composite. In addition, the stiffness of the composite depends on adequate dispersion of the particles in the matrix and the interfacial bonding between the matrix and the filler (Gill & Hon, 2004; Liang, 2005). On the other hand, in the tensile process, there will be stress concentration which causes the matrix to form shells around the filler particles. If the distance between the particles is small enough, there will be shear stress between the nearest neighbouring particles, thus causing them to connect to each other and form percolation pathways. As the volume fraction of particles increase, the distance between shells around the filler decreases, leading to an increase in the number of percolation pathways, thus ultimately raising the elasticity modulus (He & Jiang, 1993).

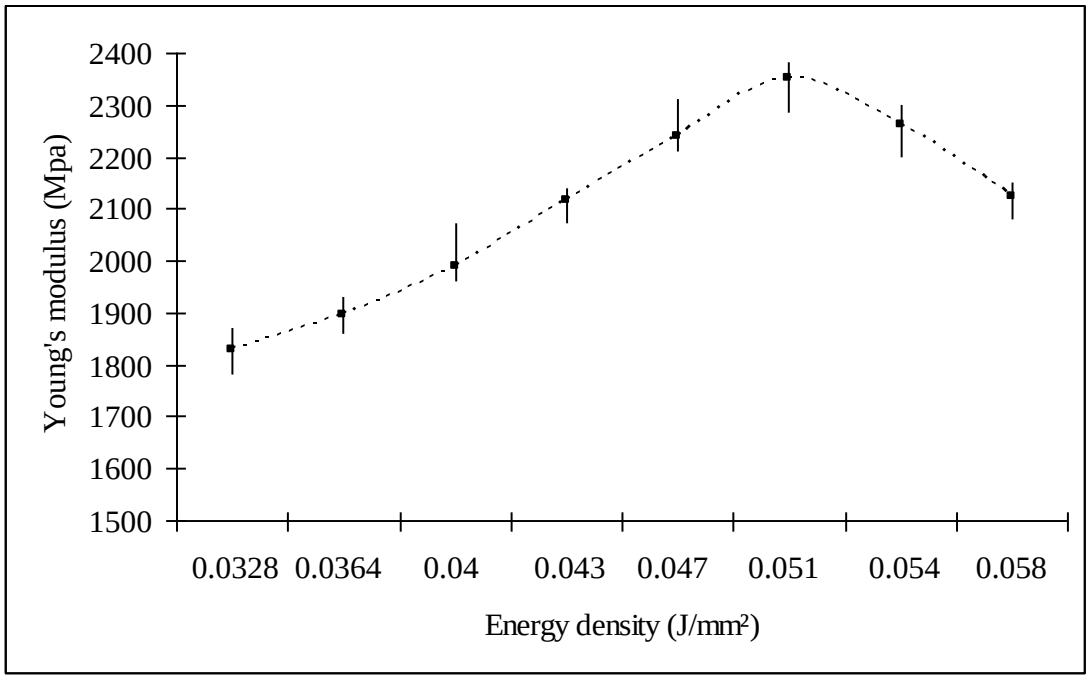

Figure 5.11: Variation of Young's modulus with energy density.

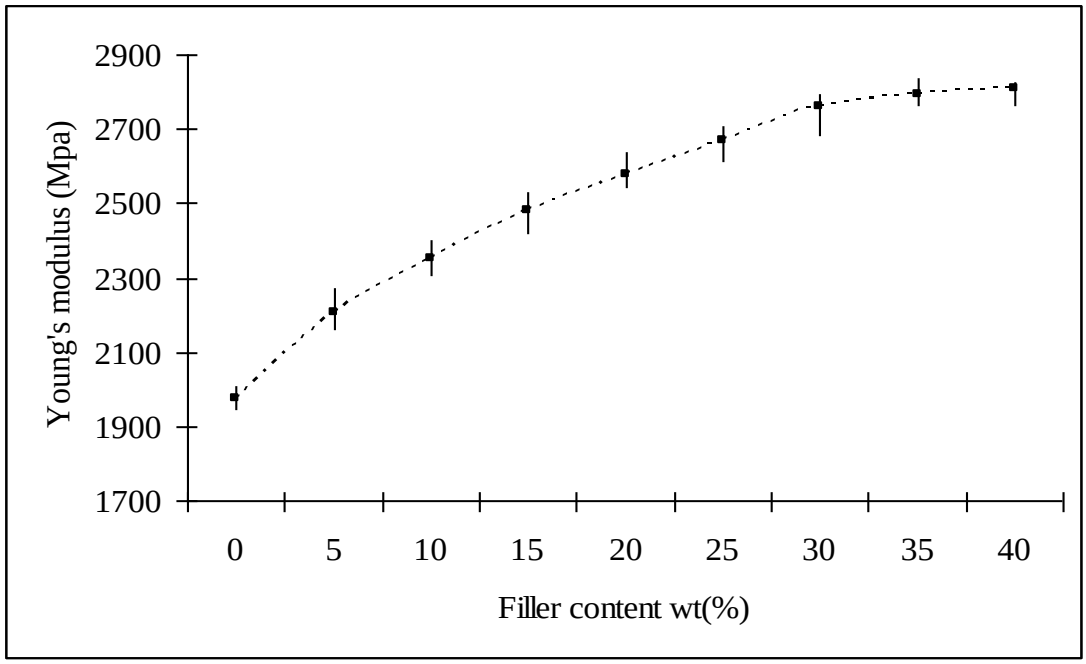

Figure 5.12: Variation of Young's modulus with cement content.

5.4.2.3 Elongation at break

Figures 5.13 and 5.14 show elongation at break and the results obtained in relation to various ED, and proportions of filler. Elongation at break is an important factor for the characterisation of the tensile fracture toughness of materials. From Figure 5.13, it is clear that elongation at break increases significantly with increasing ED, except for the highest ED level. From the results obtained, it becomes clear that the increase in elongation in relation to increased ED levels can again be attributed to the increase in part density and particle fusion. Enhanced material integrity and greater adhesion of particles to each other clearly results in a reduction in material brittleness. As the ED is increased beyond the optimum level, the elongation at break begins to decrease and this can be attributed to the powder particle of binder becoming damaged or burnt by excess heat from the laser.

In Figure 5.14, the elongation at break curve shows a considerable influence from various weight fractions (wt%) of the cement filler. It decreases at a leisurely rate with an increase in wt% of up to 10%, then continues more rapidly than before up to 25%, before gradually persisting. From the results obtained, this suggests that the addition of cement particles to Polyamide 12 diminishes the elongation of the composite. This is due to the immobilisation of macromolecular chains by the filler, which increases the brittleness of the composite.

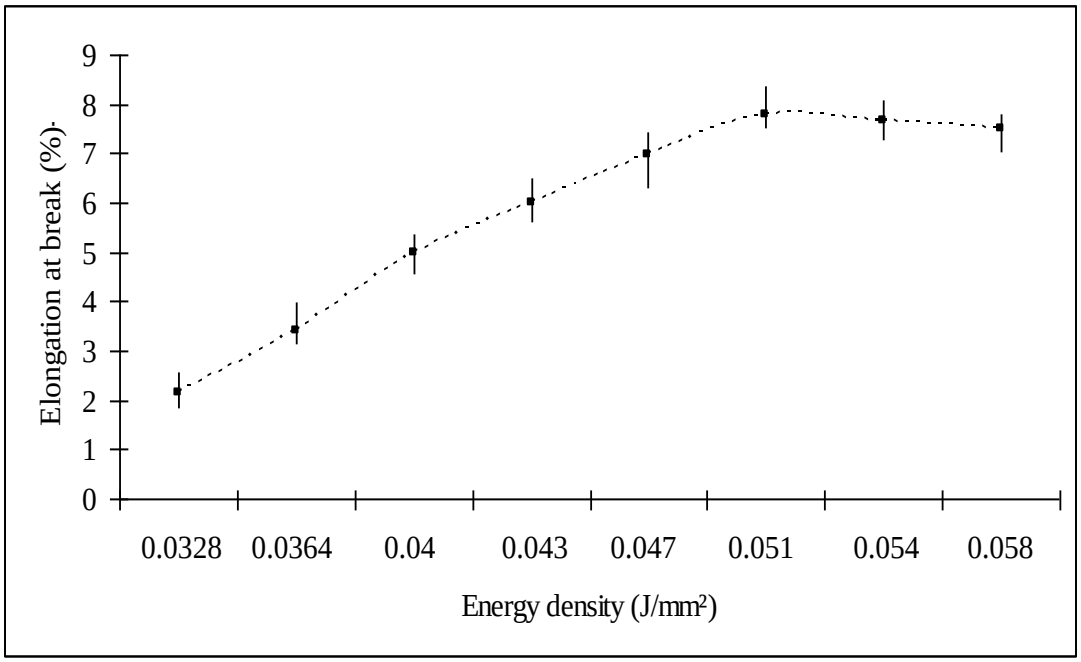

Figure 5.13: Variation of elongation at break in relation to energy density.

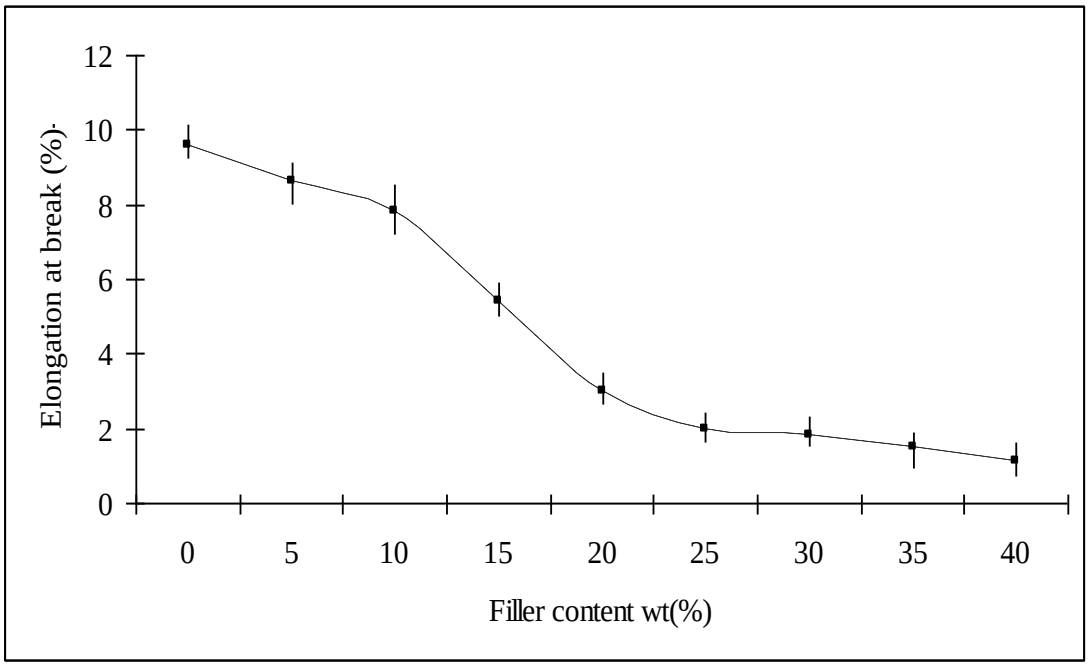

Figure 5.14: Variation of elongation at break in relation to cement content.

5.4.2.4 Flexural properties

Graphs of the flexural modulus and flexural yield strength values in relation to various EDs and proportions of filler are shown in Figures 5.15 to 5.18. The flexural modulus and flexural yield strength values are effectively dependent on the ED, so Figures 5.15 and 5.16 demonstrate flexural modulus and flexural strength respectively, which have increased rapidly, more or less in relation to ED, and then decreased in inverse proportion to increases in ED. Therefore, it is clear from an examination of the data presented, that the ED level used to produce the parts has had a physically powerful influence on the resultant flexural modulus and flexural strength values, which can be related back to their density. As the density of the part increases, the flexural properties increase; if the density of the part decreases, the flexural properties also decrease in direct proportion. As a matter of fact, there is a substantial similarity between the figures for flexural and density curves shown in Figure 5.8.

From the results obtained, it would appear that both the flexural modulus and flexural yield strength have been influenced directly by the part-density, which is itself affected by ED. As ED increases, therefore, there is greater fusion of the Polyamide 12 particles, causing higher density and enabling a more compact structure, with consequently greater flexural properties. When the ED is increased beyond the optimum level as a consequence of binder degradation, however, this leads to a decline in strength.

Figures 5.17 and 5.18 display the relationship between the flexural modulus and flexural strength, respectively, alongside the weight fraction (wt%) of the cement. It can be seen that flexural modulus and flexural strength increase speedily with the increase of wt% when wt% is < 15%, and then rises gradually. From the results obtained, this suggests that the cement particles can enhance both flexural modulus and flexural strength. The addition of rigid particles, such as cement to polyamide, can increase the stiffness (Gill & Hon, 2004). This means that for the flexural modulus, the flexural strength not only depends on the adhesion of particles to each other, but also on the strength of the particles. Flexural modulus and flexural strength would therefore seem to increase with a rise in the proportion of cement (wt%).

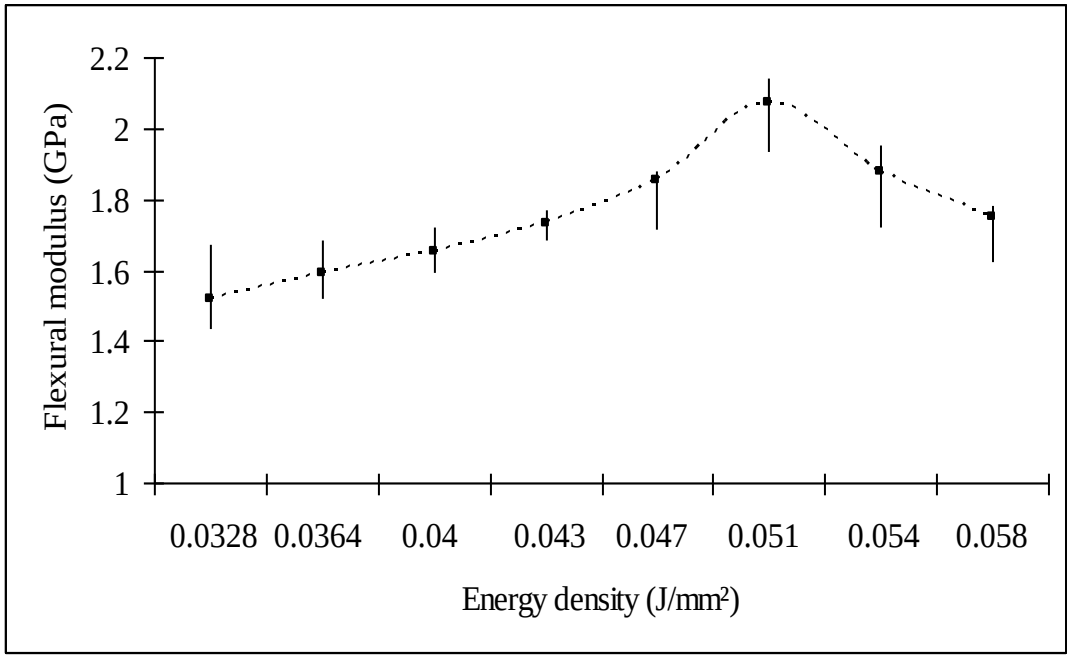

Figure 5.15: Variation of flexural modulus with energy density.

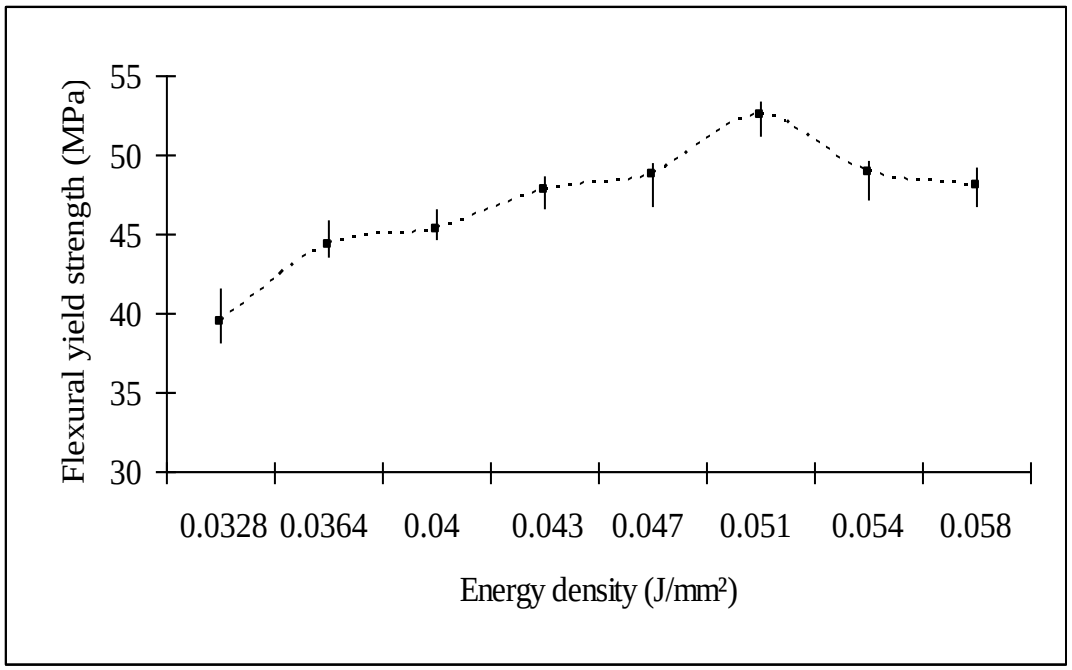

Figure 5.16: Variation of flexural yield strength with energy density.

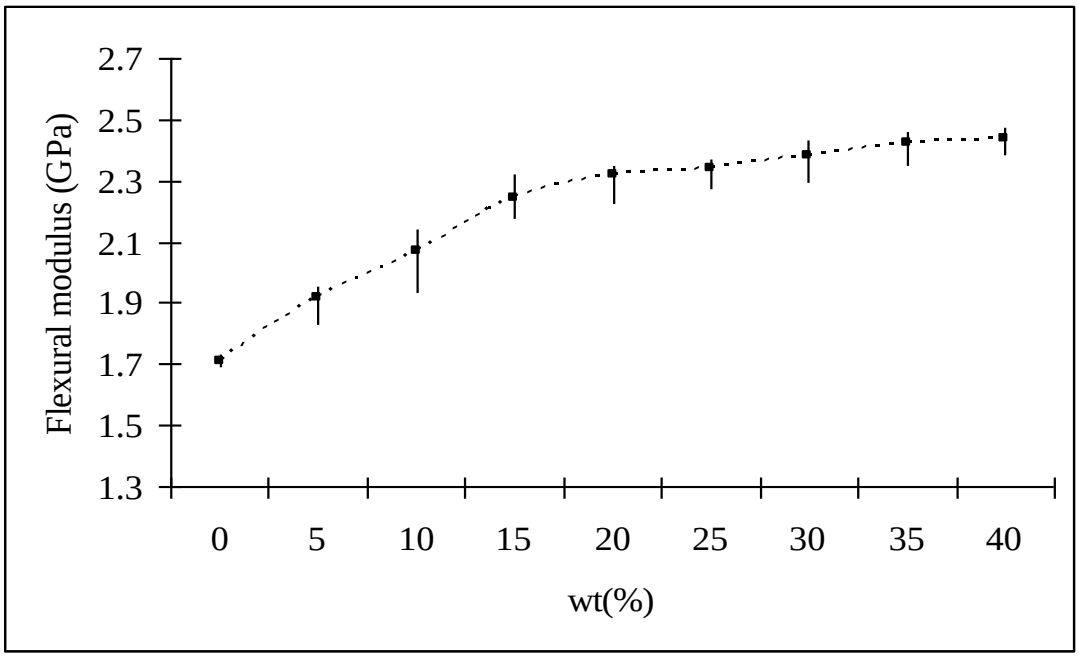

Figure 5.17: Variation of flexural modulus with cement content.

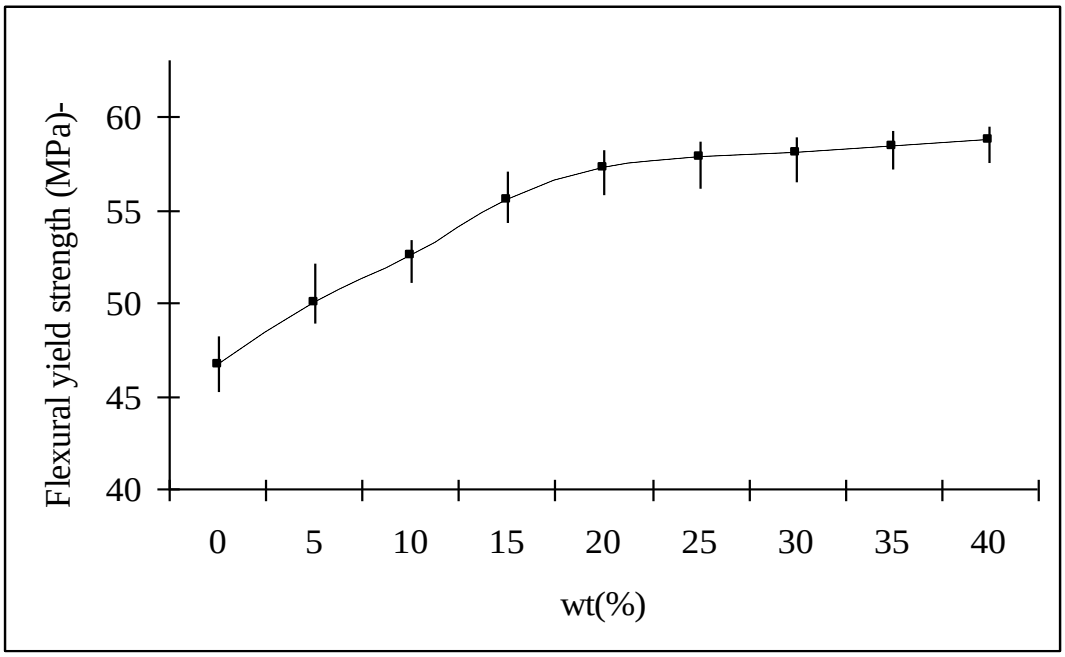

Figure 5.18: Variation of flexural yield strength with cement content.

5.4.2.5 Compression properties

The compression test results are presented in Figures 5.19 and 5.20. Figure 5.19 is a chart of compressive yield strength values obtained against various EDs, where ED is shown to have an effect on the compressive yield strength. It can be seen that the compressive strength quickly increases with an increase in ED when ED is < 0.051, and then decreases slowly. This demonstrates the strength of the relationship between compressive yield strength and density. As the density of the part increases, so does the compressive yield strength, due to more binder particles melting, subsequent to a certain degree of increase in ED. The compressive yield strength then starts to decrease as ED is increased because of the degradation of binder.

In Figure 5.20, the compressive yield strength curve shows considerable influence from various weight fractions (wt%) of the cement. The compressive strength initially increases rapidly with an increase in wt% of up to 5% and then continues more gradually than before. This result confirms that the addition of rigid particles to Polyamide 12 enhances rigidity as stated earlier. Consequently, as the (wt%) of the cement increases, so does the compressive yield strength.

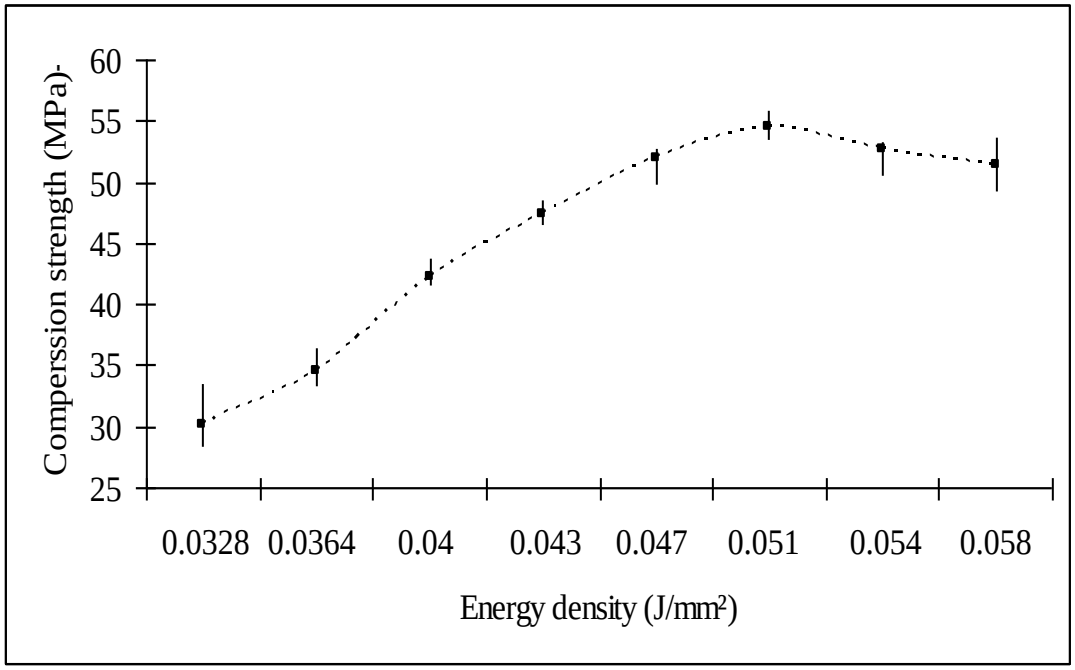

Figure 5.19: Variation of compression strength with energy density.

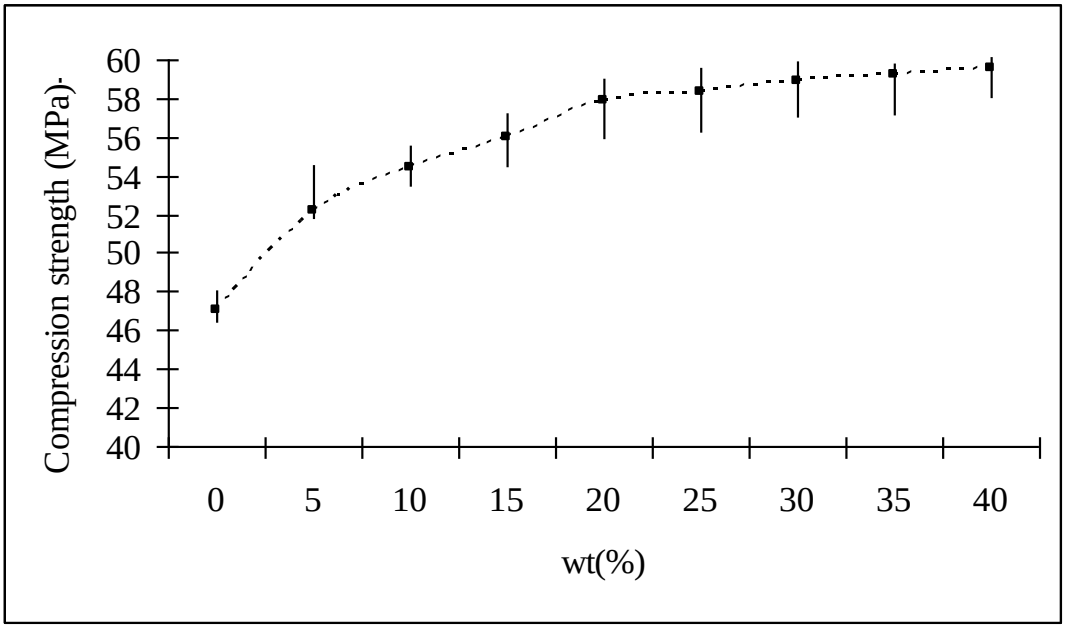

Figure 5.20: Variation of compression strength with cement content.

5.4.2.6 Impact properties

Figures 5.21 and 5.22 show the impact strength and results obtained in relation to various ED and proportions of filler. Impact strength is an important factor for the description of the ductile of materials. From Figure 5.21, it is clear that impact strength increases significantly with an increasing ED, except at the highest ED level. From the results obtained, it can be seen that the increase in impact strength with increased ED level can again be attributed to an increase in part density and particle fusion which results in an enhanced material ductile. As the ED is increased beyond 0.051 J/mm², the impact strength begins to decrease as a result of the degradation of binder.

In Figure 5.22, the impact strength curve shows considerable influence from the addition of various weight fractions (wt%) of cement to Polyamide 12. It is clear from the graph that the impact strength decreases at a leisurely rate, with an increase in filler wt%. From the results obtained, this suggests that the addition of cement particles to Polyamide 12 weakens the impact of the composite. The deterioration in impact properties can be attributed to the immobilisation of macromolecular chains by the filler, which limits their ability to deform freely and leads the composite to be less ductile.

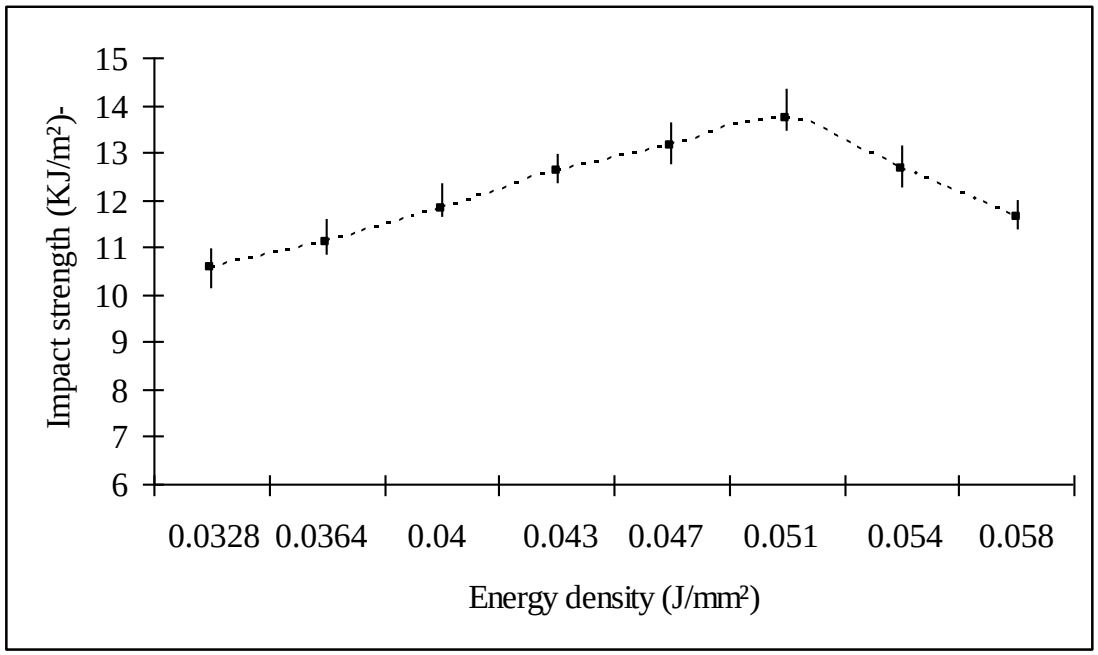

Figure 5.21: Variation of impact strength with energy density.

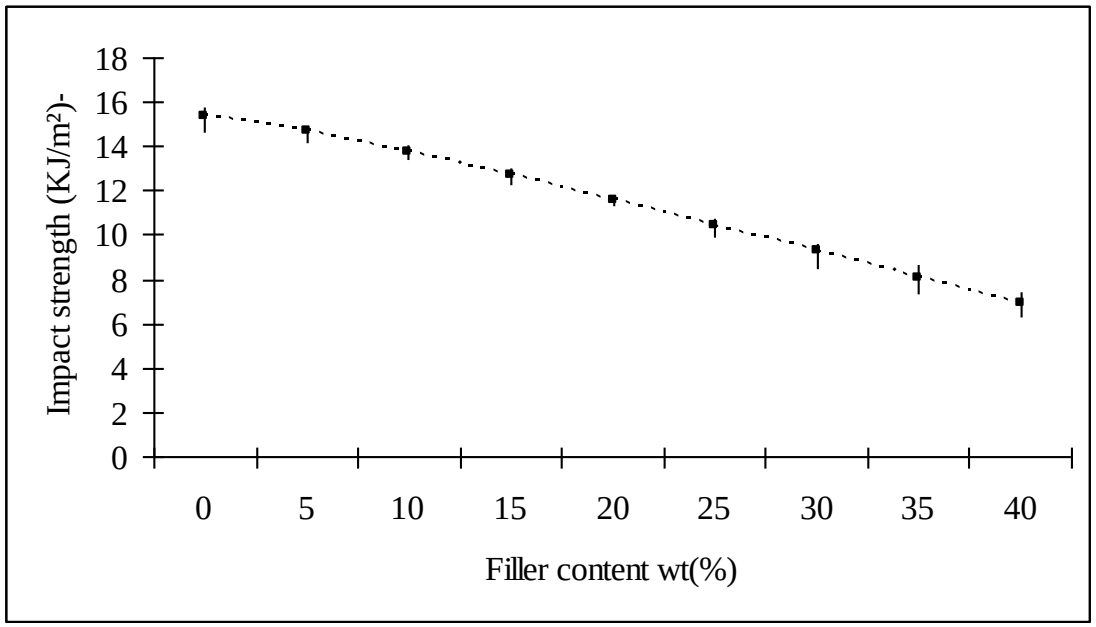

Figure 5.22: Variation of impact strength with cement content.

5.4.2.7 Effect of using un-sintered powder on the MFR and mechanical properties.

In the following experiments, the samples of composite material of cement/PA12 were built on a DTM Sinterstation 2000 machine. After running the first build, it was necessary to break out the parts and separate the un-sintered powder that could be easily broken up as used powder. Because a huge amount of powder remained un-sintered during the SLS, this powder and overflow powder from the same build was sifted by an intensive shaking procedure, using a manual sifter to avoid powder agglomerates. The powder was then mixed mechanically in a Drum mixer, BS 125 with a mixing speed of 30 r.p.m. for 5 minutes. Later, the tensile and compressive parts were examined using a Testomeric M500 machine with a small amount of the un-sintered powder from the first build taken to measure and record their MFR. The powder was returned to the SLS for another build. This procedure was repeated for six builds.

The results of these experiments are shown in a bar chart format in Figures 5.23 to 5.25. Figure 5.23 illustrates the relationship between the MFR of the composite material of cement/PA12 and the number of builds via SLS. The results prove to be similar to those obtained from simulating the deterioration of the composite powder during the SLS process, as mentioned earlier in 4.6.2.3. This indicates that the powder exposed to oven temperatures with a nitrogen atmosphere can simulate the powder run by SLS. It is therefore clear from the figures there is a rapid decrease in

MFR with repeated heat exposures during the SLS process for the first two builds, and then a leisurely decline. As molecular weight increases through exposure of the powder to temperatures, the viscosity of the powder increases directly, thus finally leading to decreased melt flow rate. Figures 5.24 and 5.25 show the cement/PA12 tensile and compressive strength, respectively, as opposed to the number of builds. These results show a clear trend of substantial decline in tensile and compressive strength following the new builds, then a reduction for the next three builds, before quickly dropping. As shown from these Figures, tensile and compressive strength are in direct proportion to MFR. Therefore, with the degradation of the powder due to exposure to various temperatures for an extended period of time through the SLS system, a decline in tensile and compressive strength is observed.

The indications of the mechanical properties and MFR tests recommend that there is a relationship between results obtained from the melt flow rate index and tensile and compressive strength. As the powder degrades following exposure to temperatures for prolonged period through the SLS system, the tensile and compressive strength weakens. In addition, quality and surface finish of specimens become poorer. Tensile and compressive assessment and visual evaluation of components from the six builds indicate that the first two builds are excellent, the next three builds are acceptable and the rest builds are unacceptable. Consequently the amount of virgin power to be added to achieve the target melt index has therefore varied from 25 to 42 per cent. The melt flow rate index has ultimately proved to be a good indicator of mechanical properties.

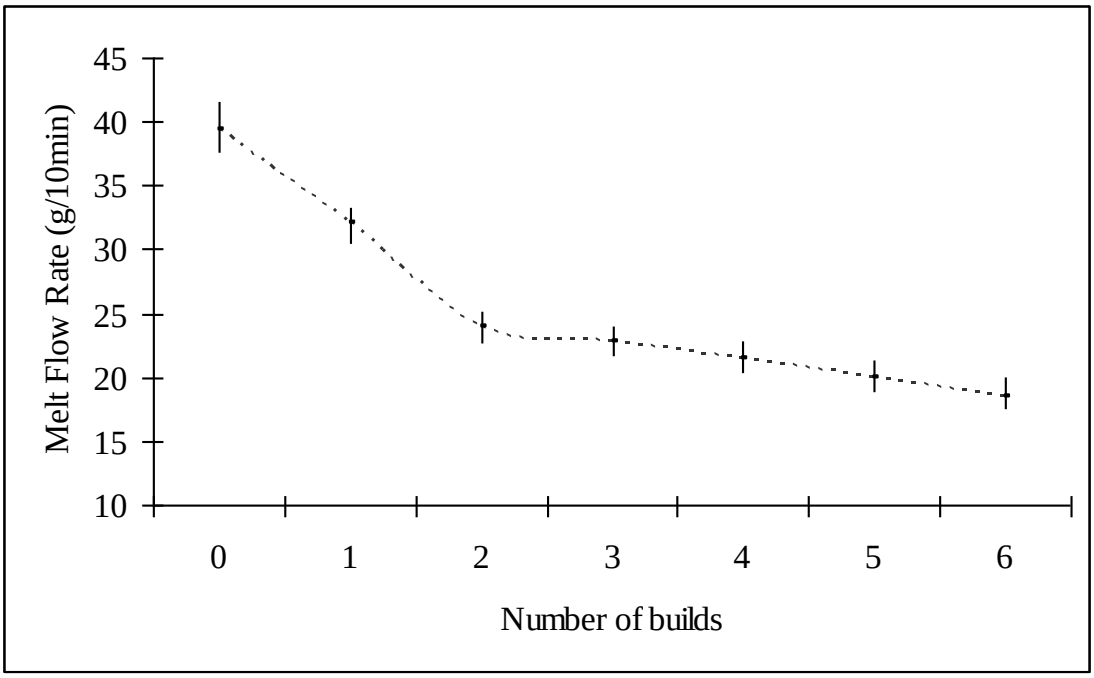

Figure 5.23: Variation of MFR of composite of cement/Polyamide 12 powder with number of builds.

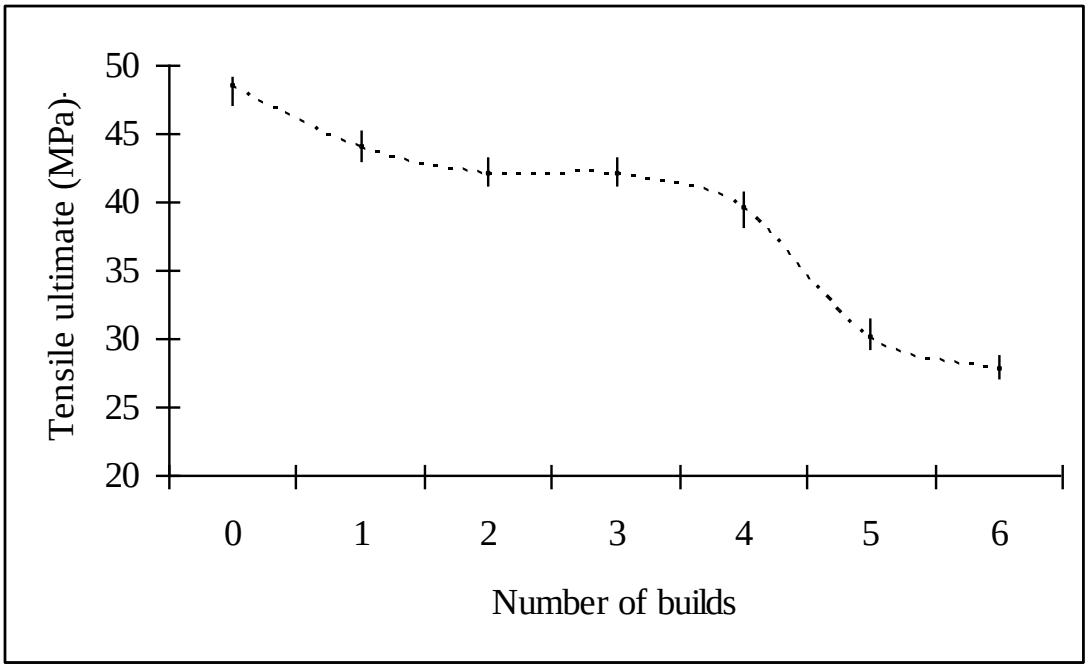

Figure 5.24: Variation of tensile strength of composite of cement/Polyamide 12 powder with number of builds.

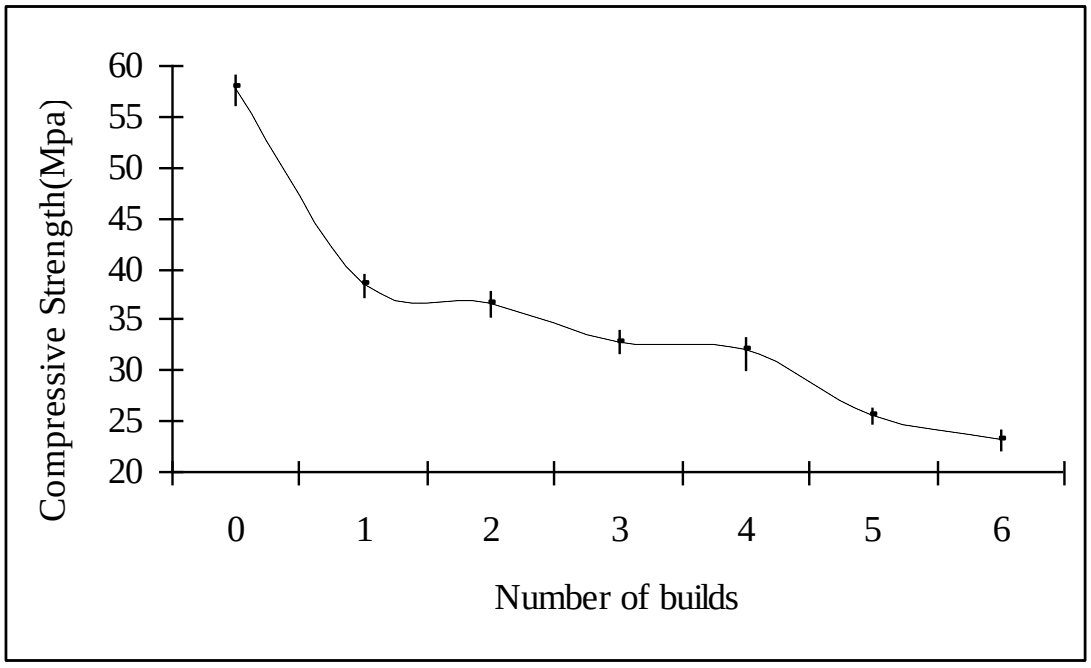

Figure 5.25: Variation of compressive strength of composite of cement/Polyamide 12 powder with number of builds.

5.4.2.8 Comparison of actual parts with data-sheet values

The main reason for comparing the mechanical properties of actual parts produced by SLS Sintersation 2000 with data-sheet values supplied by EOS for Polyamide 12 material is to have the assurance that the Sintersation 2000 used in this research is capable of consistently producing parts with mechanical properties comparable to the data-sheet. Table 5.5 shows the mechanical properties of the SLS parts produced in this research, and the values obtained from the manufacturer's data-sheet.

It can be seen that the measured values differ from those of the data-sheet. In the case of tensile strength and Young's modulus, the difference is relatively small (with the measured value only 3% and 6% higher, respectively, than the data-sheet value) which can be considered an acceptable level of variation. However, the other measured values differed from the data-sheet values by amounts ranging from 19% (flexural modulus) to as high as 36% (elongation at break). While in the case of impact strength, the difference was significant (with the measured value 71% higher than the data-sheet value). From the results obtained, this suggests that the manufacturer data-sheets of mechanical properties for parts produced via SLS vary from machine to machine, although the data of measured values exceeded that of the data-sheet value. This indicates that the SLS Sintersation 2000 used in this research is reliable for the production of parts with consistent mechanical properties.

Table 5.5: Mechanical properties of actual parts and data-sheet values.

Mechanical Properties	Actual parts	Data-sheet
Tensile Strength, Ultimate(MPa)	49.49	48
Young's Modulus (Mpa)	1975	1850
Elongation at break (%)	9.6	15
Flexural Modulus (GPa)	1710	1370
Notched impact strength (KJ/m²)	15.33	4.4

5.4.3 Morphology and microstructure

In order to carry out this investigation, the material morphology of parts produced from a composite of Polyamide 12 and cement SLS has been explored using different EDs. The research explains the effects of various EDs on composite material properties by examining the physical construction of the specimens.

Figure 5.26 shows surface images of samples made from composite material PA12/cement with different EDs. The ED used to produce the SLS specimens is shown underneath each image. The surface of the specimen built under an ED 0.043 J/mm² is porous. These porosities are formed due to low ED exposure to the powder and consequently, the part is likely to have insufficient bonds between Polyamide 12 particles, thus causing voids and weak parts (see Figure 5.26 A). If the ED level increases to a level between 0.047 J/mm² and 0.051 J/mm², the fusion of Polyamide 12 particles is better from the outset. It results in decreased porosity, thus enabling a more compact structure to be built (see Figure 5.26 B and C). Excessively high EDs of over 0.054 J/mm² lead to degradation of the Polyamide 12, roughness, cracks and a dark colour on the surface of the part through overheating (see Figure 5.26D).

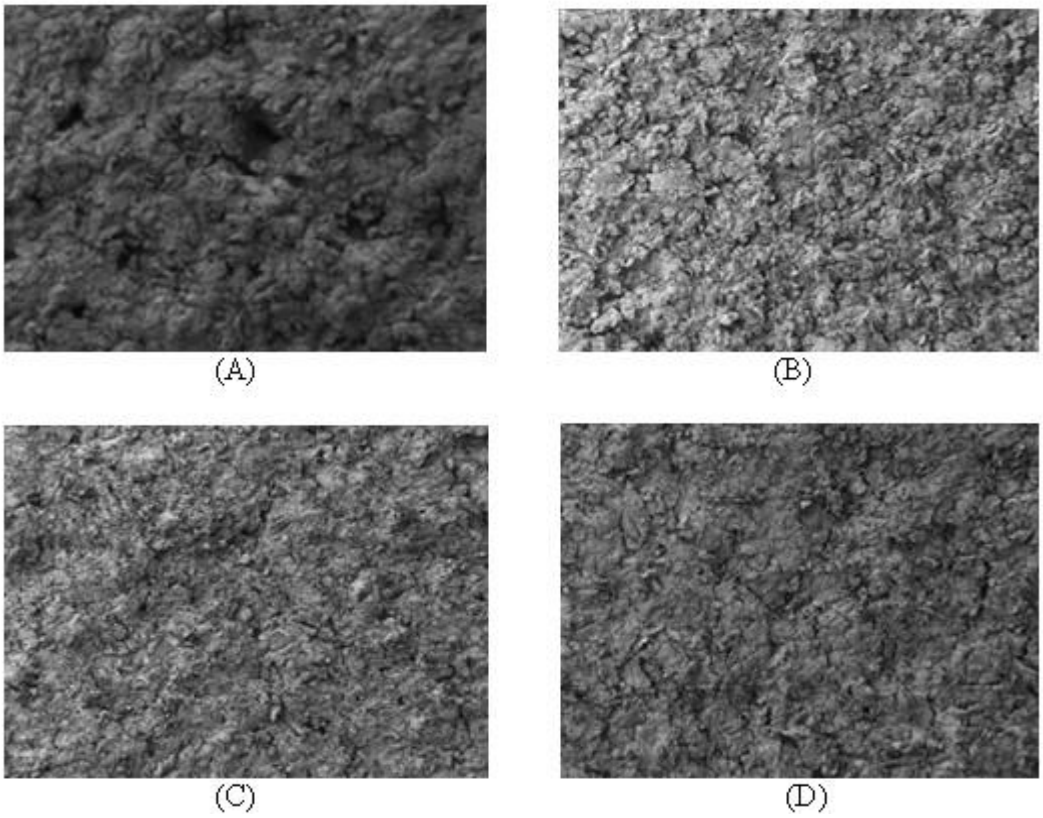

Figure 5.26: Surface image sintered specimens built at energy densities of (a) 0.043, (b) 0.047, (c) 0.051 and (d) 0.058 J/mm².

Fracture surface images are presented in Figure 5.27. These fracture surface images of the parts reveal how ED affects the material morphology. From Figure 5.27 A, it can be observed that at lowered EDs, there are partially melted Polyamide 12 particles but the majority of particles can be recognised individually because they have maintained their original shape rather than melting. This confirms findings with respect to the surface image at low ED, which resulted in the production of a composite part with defects and porosities and so would influence a preference for the stronger specimens.

When ED increases beyond 0.047 J/mm², the fusion of particles seems to be homogeneous and particles cannot be seen independently (see Figure 5.27 B and C). Due to excessive exposure of the ED to the powder at a level above 0.054 J/mm², Figure 5.27 D shows degradation of the powder and when the images are enlarged x 200, it is also clear that the fracture surfaces are rough. This therefore confirms that findings which relate to surface images where ED is excessively high, displaying degradation of the Polyamide 12 and a dark colour on the surface of the part from overheating with high ED.

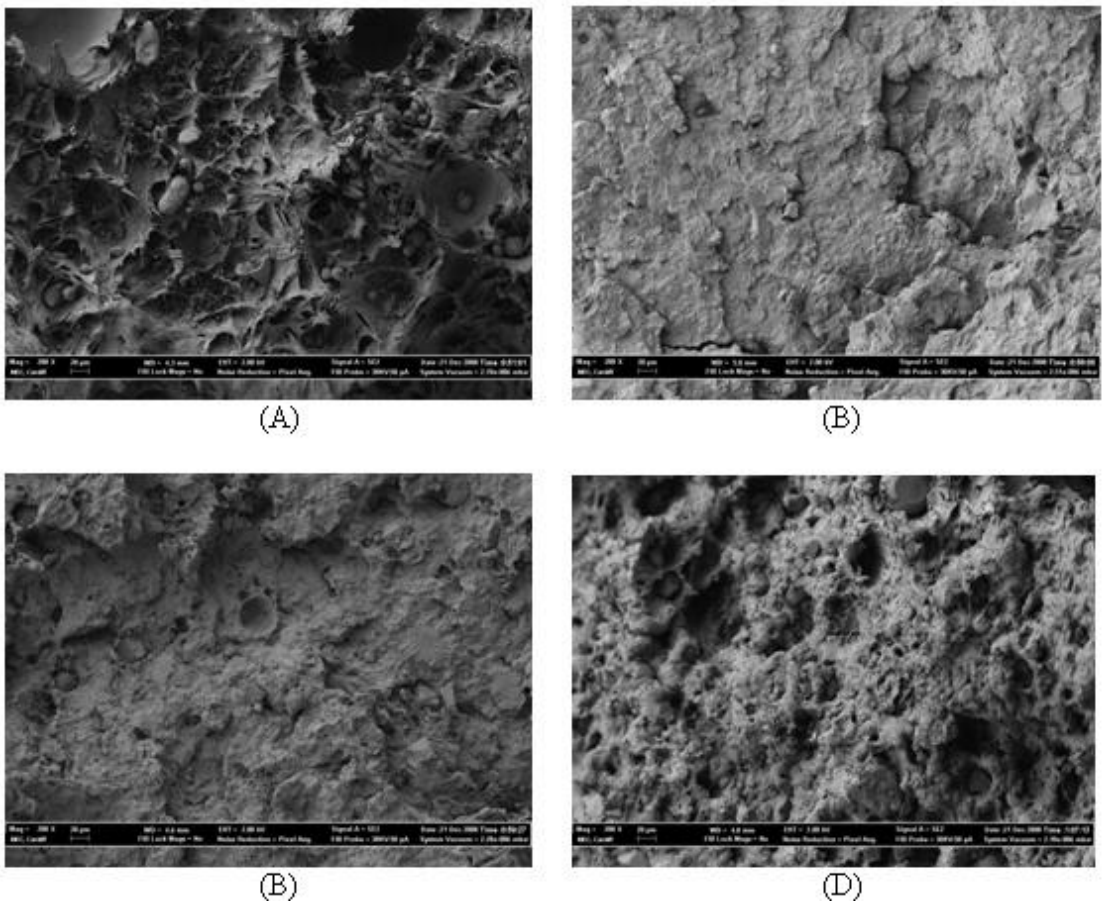

Figure 5.27: Fracture surface image sintered specimens built at energy densities of (a) 0.043, (b) 0.047, (c) 0.051 and (d) 0.054 J/mm².

5.5 Summary

The comparison of the mechanical properties of the measured and data-sheet values for pure Polyamide 12 has shown that, values for the actual parts produced by SLS Sintersation 2000 demonstrate values which exceed those of the data-sheet. This indicates that the SLS Sintersation 2000 used in this research is reliable for producing parts with consistent mechanical properties. The results from the data of the mechanical properties of parts produced by SLS reveal that the composite material has a significant effect on the mechanical properties of sintered specimens. Additionally, the energy density (ED) of the laser beam has a major influence effect on the dimensions, density and mechanical properties of sintered parts.

The comparison between pure Polyamide 12 powder and the composite material has demonstrated that there is an improvement from addition of cement filler to PA12, in terms of Young's modulus, flexural strength, compression strength and tensile strength in the sintered specimens. However, the addition of cement particles to Polyamide 12 weakens the impact strength of the composite. Density and mechanical properties are observed to increase as ED is increased. They peak at ED 0.051 J/mm^2 and then decrease as ED is increased even further.

It has been found that the amount of virgin power that must be added to used powder to achieve good, consistent mechanical properties of the fabricated SLS specimens can vary from 25% to 42%. The melt flow rate index has also proved to be a good indicator of mechanical properties. Sintered parts are porous and weak if the ED is

low, but become denser and stronger as ED increases to a specific point and then are weakened through degradation of the binder at excessive ED. This is confirmed by examining the physical construction of the sintered specimens.

Chapter 6

Mechanical Properties of Cast Parts Cement and Polyamide 12 Composite

6.1 Preliminaries

Selective Laser Sintering can be expensive and time-consuming when testing new materials (e.g. because of machine set-up, preheating, building, cool-down and cleaning the machine properly to avoid corruption when swapping materials). In addition, the large amount of material required to produce parts using SLS leads to high costs for the powder material, even when producing a test part (Majewski et al., 2008). This chapter presents a method of casting to produce parts with mechanical properties similar to those achieved by SLS in order to reduce the amounts of time and material required. This method was used to produce parts for tensile, Young's modulus, flexural and compression tests to assess the effects of varying the proportion of composite material of cement additive to Polyamide 12 on the mechanical properties of specimens. The mechanical properties of parts produced using the casting method are compared with the parts manufactured using SLS with the same materials. The main purpose of work reported in this chapter is to investigate whether or not a correlation could be made between the mechanical

properties of parts produced via the casting method and those manufactured with SLS.

6.2 Casting Process

A variety of processes, such as tape casting, slip casting, moulding, extrusion and injection moulding are used to produce parts with powder and require a firing treatment to instil strength in the shaped powder, which is known as sintering. Sintering may be considered the process by which an assembly of particles, compacted under pressure or simply confined in a container, chemically bond themselves into a cohesive body under the influence of elevated temperature (Hirschhorn, 1969; German, 1996; Majewski et al., 2008). The casting method was used in this research, without externally applied pressure to support the internal structure, so that it was most like pressureless sintering, i.e. the sintering of a powder compact (sometimes at very high temperatures, depending on the powder) without applied pressure.

In many cases, sintering is associated with an increase in compact density due to lowered surface energy, and this through a reduction in the surface area and concomitant formation of interparticle bonds. The bonds grow through various mechanisms that occur at the atomic level. The bonding between the particles of many metals and ceramics occurs through solid state diffusion, while with other materials, melting particles appear during liquid phase sintering, resulting in a solid

liquid mixture during the thermal cycle. Liquid phase bonding therefore contributes a capillary force and usually enhances the rate of mass transport in comparison with solid state processes (Hirschhorn, 1969; German, 1996).

During the stages of sintering, a basic step is completed at a constant temperature and the time is varied to obtain certain results. Consequently, time plays an essential role in describing the six possible stages of sintering.

The first stage is the initial bonding among particles, which takes place very early in the sintering process as the material warms up. This is followed by the diffusion of atoms, leading to the development of grain boundaries. During this stage, the sintering does not lead to any changes in the dimensions of the material. Neck growth is considered to be the second stage of the sintering process and is associated with the first stage. The initial sintering stage therefore usually occurs during heating and is characterised by rapid growth of the interparticle neck. Neck growth requires the transport of material with sinter mass but does not involve any decrease in porosity, so no shrinkage occurs at this stage (see Figure 6.1).

Pore channel closure is the third stage of sintering, and this stage explains changes in the nature of the porosity of the sinter mass from interconnected to isolated porosity (see Figure 6.2). Neck growth is considered to be one of the causes of pore channel closure. In addition, pore shrinkage can also lead to channel closure, so blocking of the tortuous and interconnected pore channels leads to the development of isolated

porosity. There are several methods for determining isolated porosity, such as measuring the density of the poured solid and also filling the interconnected porosity with a fluid. The fourth stage is called 'pore rounding' and it is considered to be a natural consequence of neck growth. The pores become more rounded in the neck region. In addition, the rounding process is associated with interconnected and isolated porosity. Pore rounding starts to occur at a high sintering temperature. This stage is considered to be one of the most important sintering stages in its effect on mechanical properties.

The most important sintering stage is called 'pore shrinkage' or 'densification' and it follows the pore rounding stage. This stage may well result in densification of the sinter mass if it remains at the required temperature for sufficient time. The process of pore shrinkage leads to a decrease in the volume of the sinter mass, which involves movement of the solid into porosity. Any gas in the porosity is consequently transferred to the external surfaces.

The final stage is called 'pore coarsening'. This stage usually occurs when most of the sintering stage has been completed. During this stage, the process includes the shrinkage and elimination of small isolated pores (Hirschhorn, 1969; German, 1996; Pacheco & Campos, 2009).

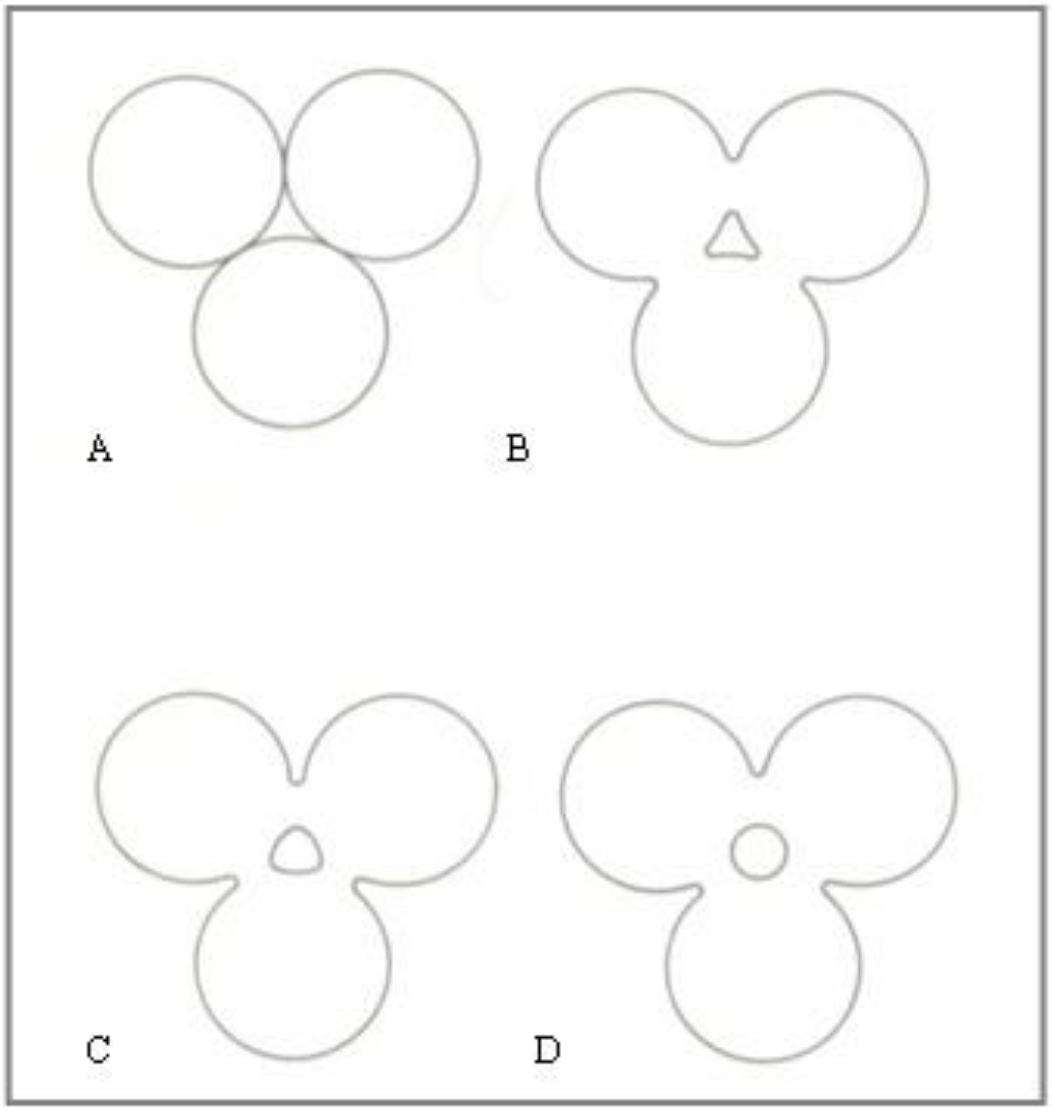

Figure 6.1: Three sphere sintering model (A) original point contacts; (B) neck growth, (C), and (D) pore rounding (Hirschhorn, 1969).

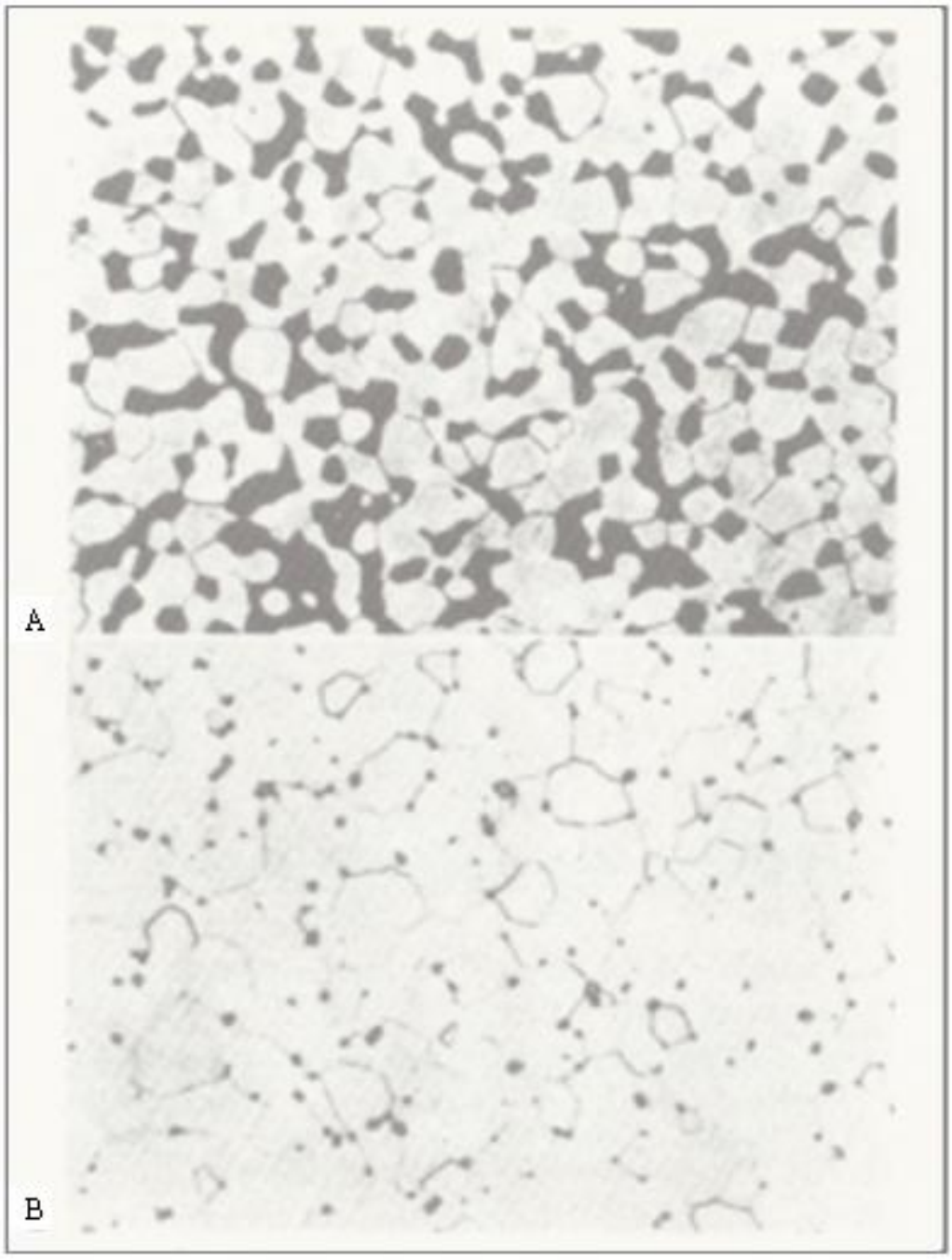

Figure 6.2: Photomicrographic illustration of change from interconnected to isolated porosity, (A) early phase with interconnected porosity; (B) later phase with closed porosity (Hirschhorn, 1969).

The casting structure strongly depends on the thermal properties of the material, the mould, the temperature of the mould, superheats of the mould, grain shape and grain size. Three distinct regions or zones with different grain structures can be recognised in most cast polycrystalline solids (Davies, 1973; Flood & Hunt, 1988; Martin, 2006). These zones are the chill zone, the intermediate columnar zone, and the central equiaxed zone, as shown in Figure 6.3.

The chill zone is placed in a boundary layer, near the mould wall with small equiaxed crystals and random orientation. This zone is known as the 'chill' zone because the mould wall chills the material. The fastest solidification therefore begins with cast polycrystalline solids in this zone. The chill zone is considered to form as a result of numerous nucleation observed in the undercooling region next to the mould wall. Thermal conditions at the mould wall, together with the efficiency of the mould wall as a substrate for heterogeneous nucleation, are mostly responsible for the extent of nucleation.

The second zone of columnar crystals develops from the chill zone. As the temperature decreases, the grains grow towards the centre of the casting until growth is interrupted by central equiaxed grains. Columnar structures are normally long columns with dendritic growth, perpendicular to the mould wall and parallel with the heat flow direction. As shown in Figure 6.3, the spread in orientation decreases as the columnar zone extends and at the same time the average size of the grain increases.

The equiaxed zone is located in the centre of the casting, as shown in Figure 6.3. The crystals in this zone usually have a grain size larger than that of the chill zone because the temperature in this zone is higher, thus leading to a decrease in the number of equiaxed grains and an increase in the size of the grain. The equiaxed zone has spherical crystals and their orientation is effectively random. The relationship between the degree of superheat and the equiaxed grain is only valid in small ingots.

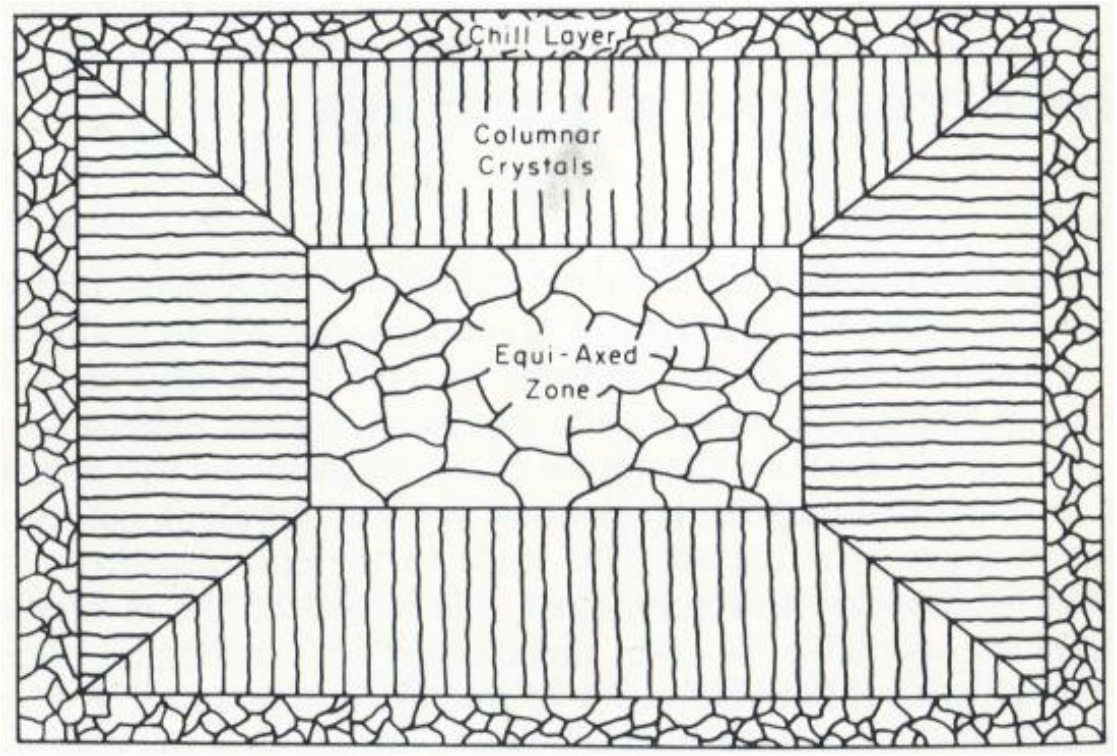

Figure 6.3: Schematic illustration of the casting structure (Davies, 1973).

6.3 Methodology

6.3.1 Sample preparation

An aluminium die to cast specimens was machined using the AGIE AGIECUT EXCELLENCE wire cutting machine, (see Figure 3.10, Ch. 3). The die consists of two pieces, with a base 4 mm thick and cavities for the cast specimens, machined to obtain tensile, flexural and compression specimen parts, as shown in Figure 6.4. Three dies were used and each die had two specimens of each kind. In order to correct shrinkage, the cavities were made twice and the depth was 14mm. The specimens were then post-machined to 4mm thickness using XYZ MACHINE TOOLS LIMITED EDGE 3000 (see Figure 3.11, Ch. 3) to meet British Standard specifications, reference ISO 527.2 for tensile specimens; ISO 178 for flexural specimens, and ISO 604 for compression specimens.

Composite of cement additive with Polyamide 12 was sifted to avoid agglomerates of powder. After this, composite powder was mechanically mixed according to a determinate formulation (see Table 5.1, Ch 5) in a high-speed mixer for 20 minutes, to obtain homogeneous powder mixtures and uniform colour. The blended powder was poured into the die cavities, which were then vibrated manually and compacted using a specimen of the same geometry as the cavity itself. Additional powder was then added to fill the cavity, before being compacted one final time.

6.3.2 Casting experiments

In order to simulate the conditions of the SLS process to produce the mechanical properties of specimens, three aluminium dies were filled with the composite material of cement filler with Polyamide 12, using varying filler content of cement from 0 wt% to 40 wt%, which was then placed in the oven (Heraeus Instruments Vacutherm, Type 6060M) without any externally applied pressure to assist in part formation. This took place in an atmosphere with optimum levels of nitrogen, in order to prevent the powders from oxidising (yellowing) and at a specified temperature of approximately 190ºC to ensure that the particles attracted each other and self-compressed to eliminate pores. However, the melting temperature of Polyamide 12 powder is about 185 ºC (see Section 3. 3.2). The thermocouple was embedded in the powder in order to monitor the temperature of parts so that the powder was held above its melting point. After many samples had been heated in the oven for different periods, the most effective timeframe was ascertained as at least 6 hours for powder melt, and so after this period, the oven was switched off and the powder allowed to cool naturally before the die was removed from the oven.

6.3.3 SLS experiments

Specimens were produced using Sinterstation 2000. The SLS process begins with the transfer of CAD data files in STL file format to the SLS machine, where they are sliced to produce a sintering component. Build parameters are controlled by data

processed by a computer system. In this chapter, the optimum parameters for producing the mechanical properties of SLS parts are cited, as shown in Table 6.1. The SLS process applies nitrogen, which creates an inert atmosphere that prevents powder oxidation. The powder in the part-bed is heated to just below the melting point of the Polyamide 12 material and laser power (7w) is used to fuse particles in each consecutive layer during the construction of components. The sintered powder forms the parts while a huge amount (about 80% to 90% of the powder) remains un-sintered in the part-build during fabrication to surround and support the parts. It could be reused, depending on its properties. Once the fabricated parts are completed, the temperature starts to drop and the parts are removed from the un-sintered powder.

6.3.4 Measurement and test specimens

The tensile, flexural and compression cast specimens were measured using a micrometer and tested using a Testomeric M500 machine, determined with reference to ISO 527.2, ISO 178 and ISO 604 respectively, with the same conditions as the SLS specimens described in Chapter 5 (3.4).

Table 6.1: Sintering parameters.

Scan spacing (mm)	0.15
Laser power (W)	7
Spot size (mm)	0.4
Scan speed (m/s)	0.914
Layer thickness (mm)	0.1
Part bed temperature (°C)	177
Right and left feed temperature (°C)	95

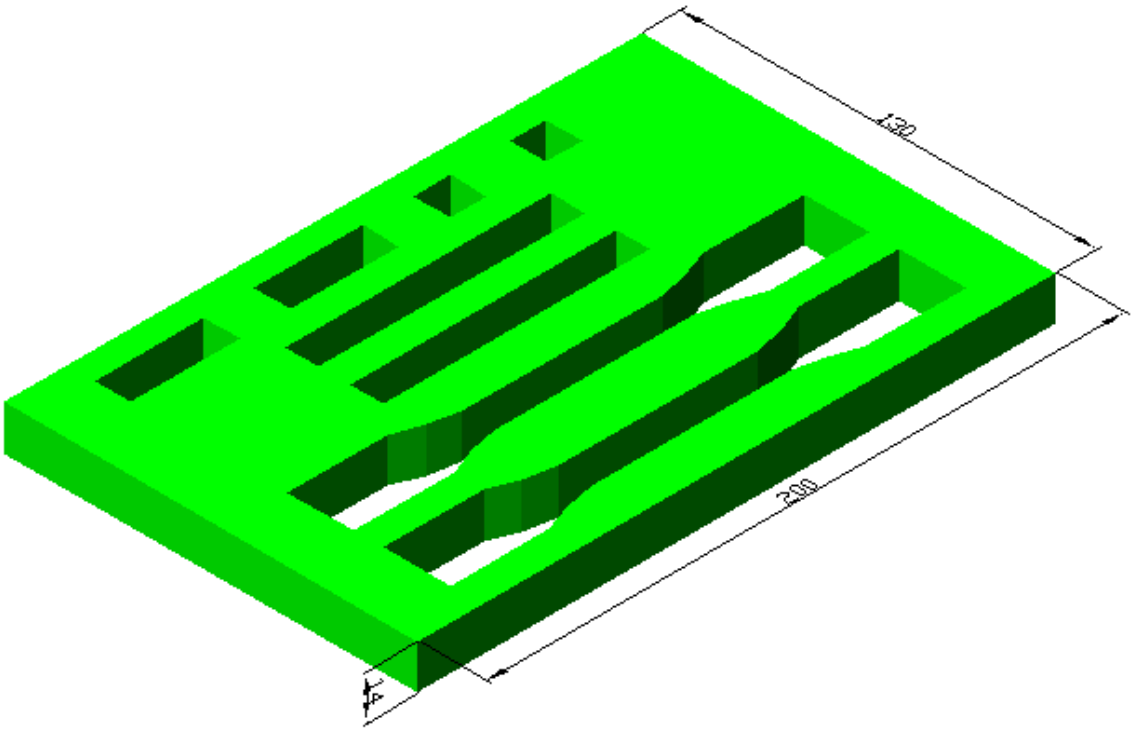

Figure 6.4: Die for the production of cast specimens.

6.4 Results and discussion

6.4.1 Tensile strength

Figure 6.5 displays a comparison of the ultimate tensile strength of the composite specimen for various wt% of cement filler added to Polyamide 12, produced via SLS and the casting method. It can be seen that the measured values of tensile strength for both methods indicate only a relatively small difference. The biggest discrepancy is a value 3.853565% higher than that of the SLS method at 5% cement filler, while the smallest difference is 0.929752% higher than for the SLS method at 25% cement filler. The average difference in measured values of tensile strength between the SLS and the casting methods for all weight fractions of cement additive with Polyamide 12 is 1.56393%, which can be considered an acceptable level of variation.

In order to prove the correlation between the results for SLS and cast specimens of ultimate tensile strength, Figure 6.6 plots all data to show a trendline. The trendline has been plotted through the entire data set, as displayed in the relevant graph. The coefficient of determination (R^2) value for tensile property has also been displayed. The R^2 value is used in statistical models to predict future outcomes on the basis of other related information, where the values vary from 0 to 1. A value of 0 signifies that there is absolutely no linear relationship between the independent and dependent variables, and a value of 1 indicates that the relationship between independent and dependent variables is perfectly linear. It can be seen from Figure 6.6 that all tensile

strength data from both the SLS and cast specimens fits the trendline with an R^2 value of 0.947265, indicating that the trendline produces a relatively accurate linear illustration of the effect of increasing cement filler in specimens created using both methods. From the results obtained, this suggests that the tensile strength value produced by the casting method would allow for acceptably accurate predictions of the SLS method.

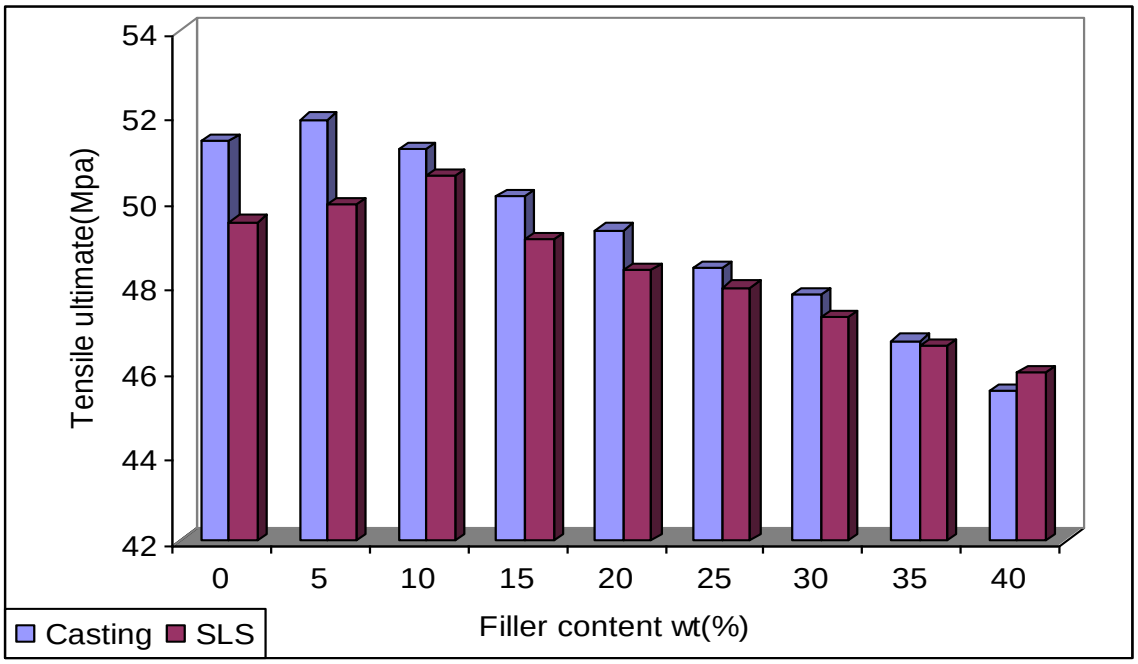

Figure 6.5: Variation in tensile ultimate with cement content for different methods (SLS; casting).

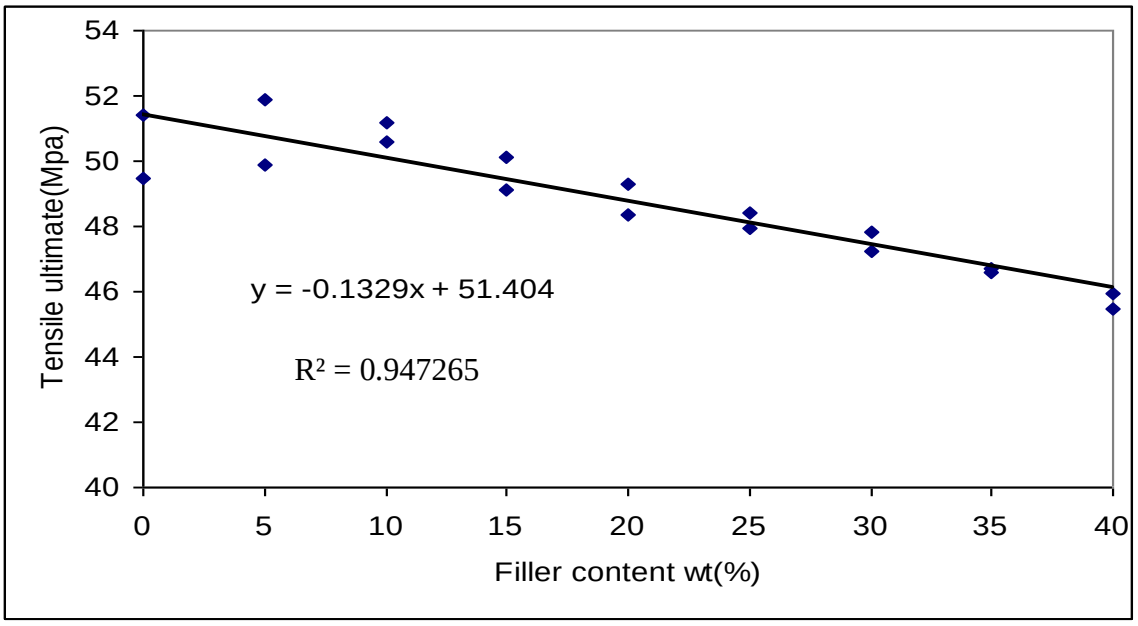

Figure 6.6: Correlation between the result of the cast and SLS specimens for tensile ultimate.

6.4.2 Elongation at break

In Figure 6.7, the elongation at break curve shows considerable influence from various wt% of cement filler for both SLS and the casting method. The elongation at break decreases with an increase in wt% of cement filler. This Figure also illustrates a comparison of the elongation at break of the samples produced using SLS and casting methods for various wt% of cement filler added to Polyamide 12. It can be seen from the Figure that the data of elongation at break for both sets does not differ greatly. The biggest disparity was a value 1.1% higher than that of the SLS method at 5%, 15% and 20% of cement filler, while the smallest dissimilarity was in a value 0.02% higher than that of the casting method at 40% of cement filler. The average difference in the elongation at break value between SLS and the casting method for various weight fractions (from 0% to 40%) of cement filler is 0.492222% and this indicates an acceptable level of variation for both sets.

Figure 6.8 shows a single trendline plotted through all data-points for elongation at break of the specimens produced using SLS and the casting method, with an R^2 value of 0.988102 to confirm the correlation between the elongation at break results obtained from both methods. This suggests that the effect on elongation at break when amounts of cement filler are increased in both the cast and SLS specimens is comparatively similar and the casting method used to produce the tensile samples is acceptable for predicting specimens produced through the SLS method.

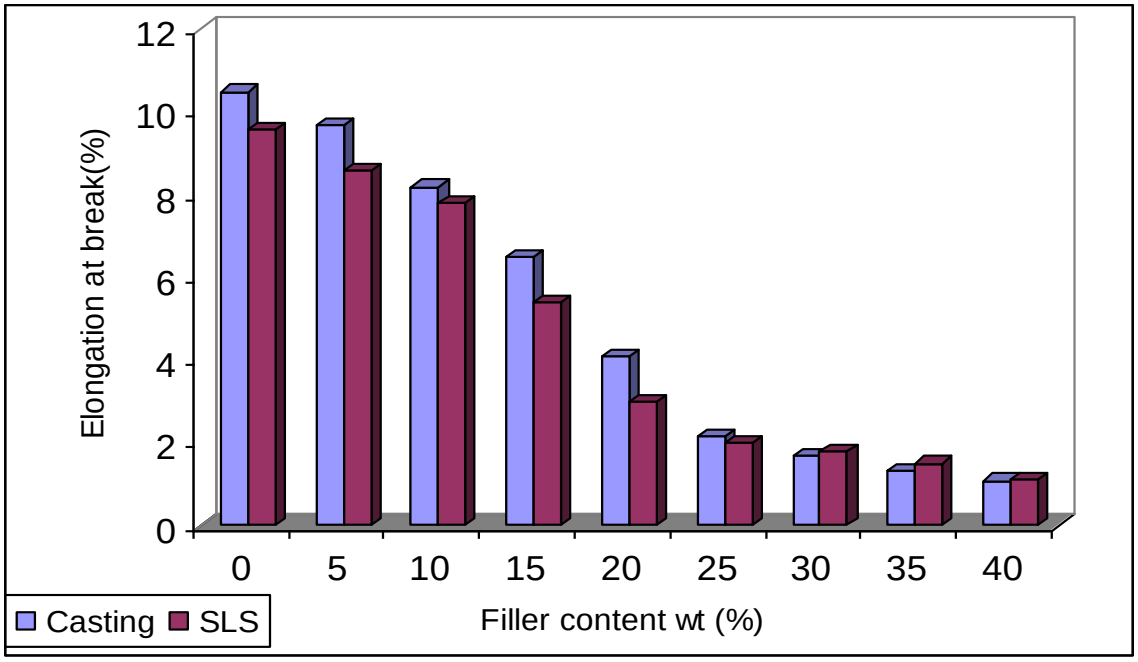

Figure 6.7: Variation of elongation at break with cement content for different methods (SLS; casting).

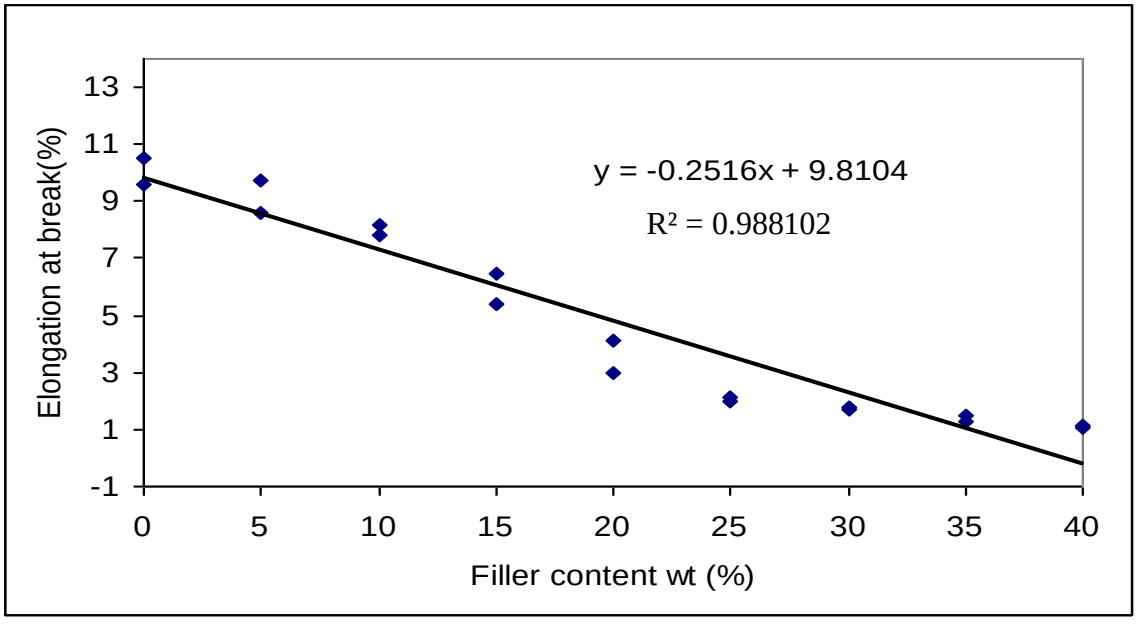

Figure 6.8: Correlation between results of the cast and SLS specimens for elongation at break.

6.4.3 Young's modulus

Figure 6.9 illustrates Young's modulus results plotted against the proportions of cement filler additive with Polyamide 12 for both casting and the SLS method, in order to draw comparisons. As shown in the Figure, the Young's modulus of the composite increases alongside greater wt% of cement filler in both the cast and SLS specimens. In addition, it is clear from the graph that the Young's modulus data for both methods indicates near parity, where the biggest difference in values is represented by a value 4.713462% higher than for the SLS method at 40% of cement filler and the smallest inequality is demonstrated as 0.02% higher than the SLS method, at 0% of cement filler. Moreover the average disparity between the results of the casting and SLS specimens of Young's modulus for various wt% of cement filler is 3.386019%. This shows there is a good correlation between the two methods in terms of Young's modulus.

Figure 6.10 demonstrates that the Young's modulus data all fits a single trendline. Therefore, in order to prove a relationship between the results for the Young's modulus SLS and cast specimens, the R^2 value 0.992921 indicates that the model accounts for more of the inherent variation than for the tensile strength. From the results obtained, it could be concluded that the Young's modulus values produced by two methods of SLS and casting would allow for a comparatively precise prediction of each other.

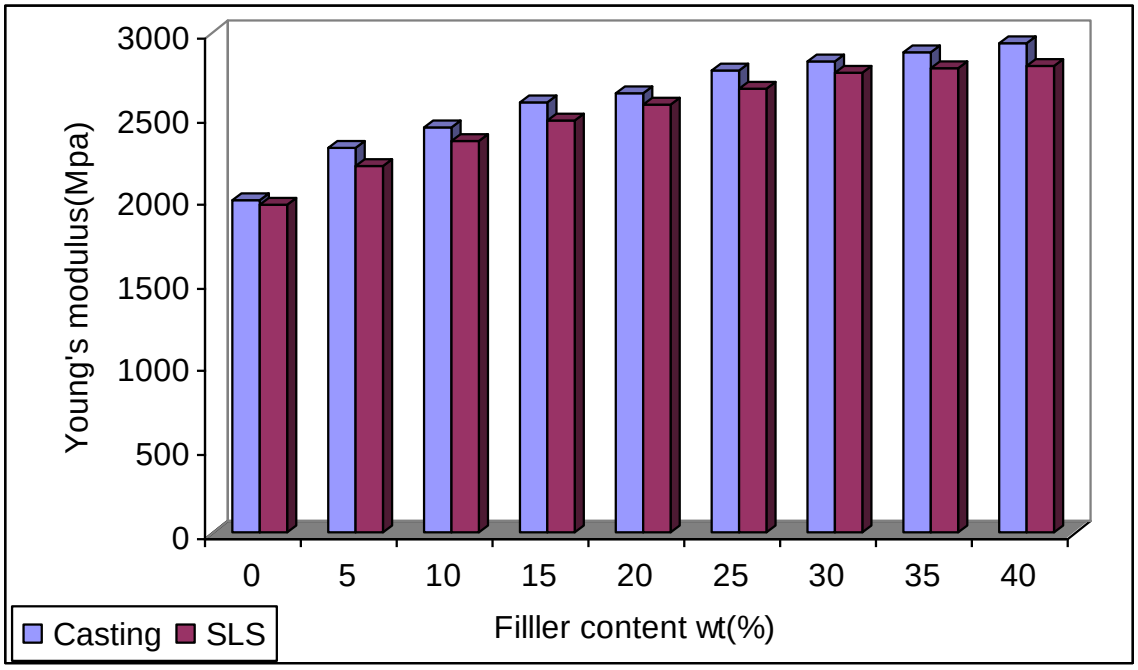

Figure 6.9: Variation of Young's modulus with cement content for different methods (SLS; casting).

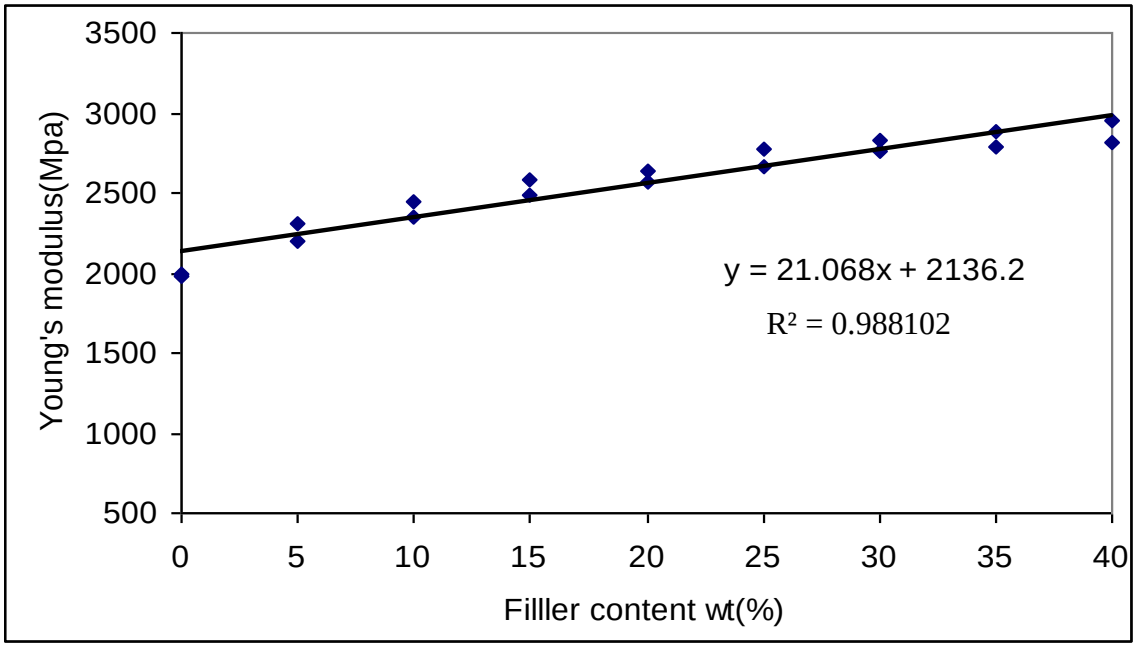

Figure 6.10: Correlation between the results of the cast and SLS specimens for Young's modulus.

6.4.4 Flexural modulus

Figure 6.11 displays the influence of various weight fractions (wt%) of cement filler on flexural modulus for SLS and the casting method. In addition, a comparison of the flexural modulus of samples was made between the casting and SLS methods. It can be seen from the Figure that flexural modulus increases with greater wt% and the difference in measured values of flexural modulus for both methods is comparatively small. The greatest difference in value is demonstrated by 4.612979 at 40% of cement filer, whilst the lowest discrepancy in value is found to be 0.854701 at 20% of cement filler. Furthermore the average difference in measured values of flexural modulus between the SLS and casting methods for all weight fractions ranging from 0% to 40% of the cement additive with Polyamide 12 is 1.56393, thus indicating an excellent interrelation between both methods.

It can be seen from Figure 6.12 that a single trendline through all data-points for flexural modulus specimens was produced by SLS and the casting method, with an R^2 value of 0.983307 to demonstrate the relationship in terms of flexural modulus between the results obtained through both methods. From the results obtained, it is suggested that the effect of increasing amounts of cement filler on the flexural modulus of cast and SLS specimens is comparatively analogous and the casting method used to produce samples of flexural modulus is admissible to predict specimens produced using the SLS method.

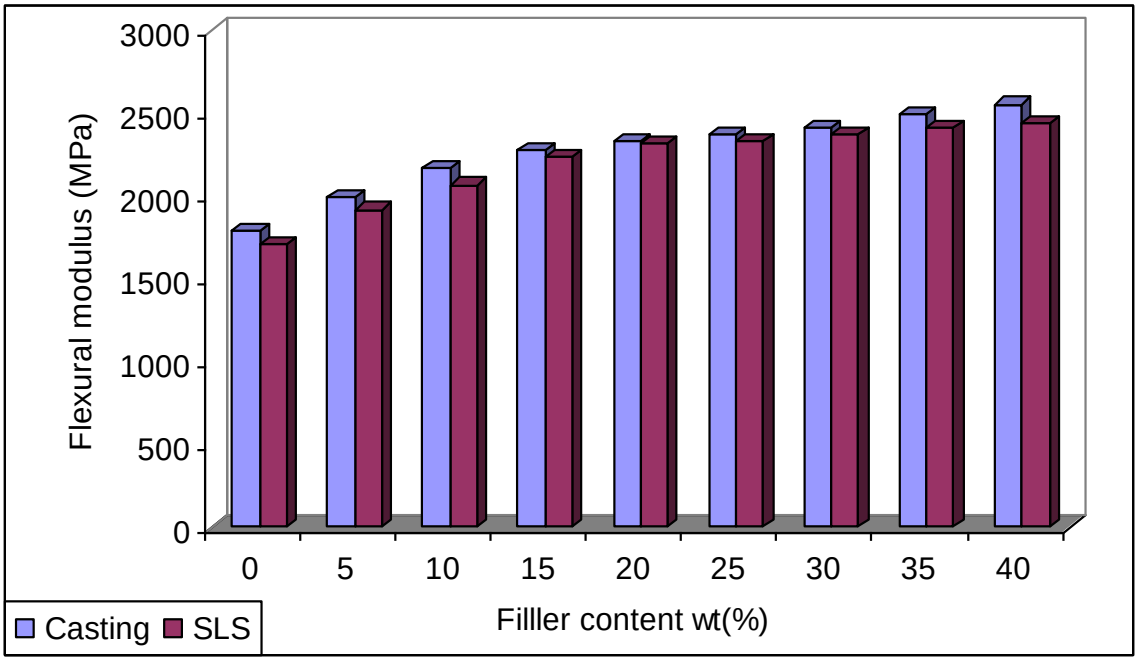

Figure 6.11: Variation of flexural modulus with cement content for different methods (SLS; casting).

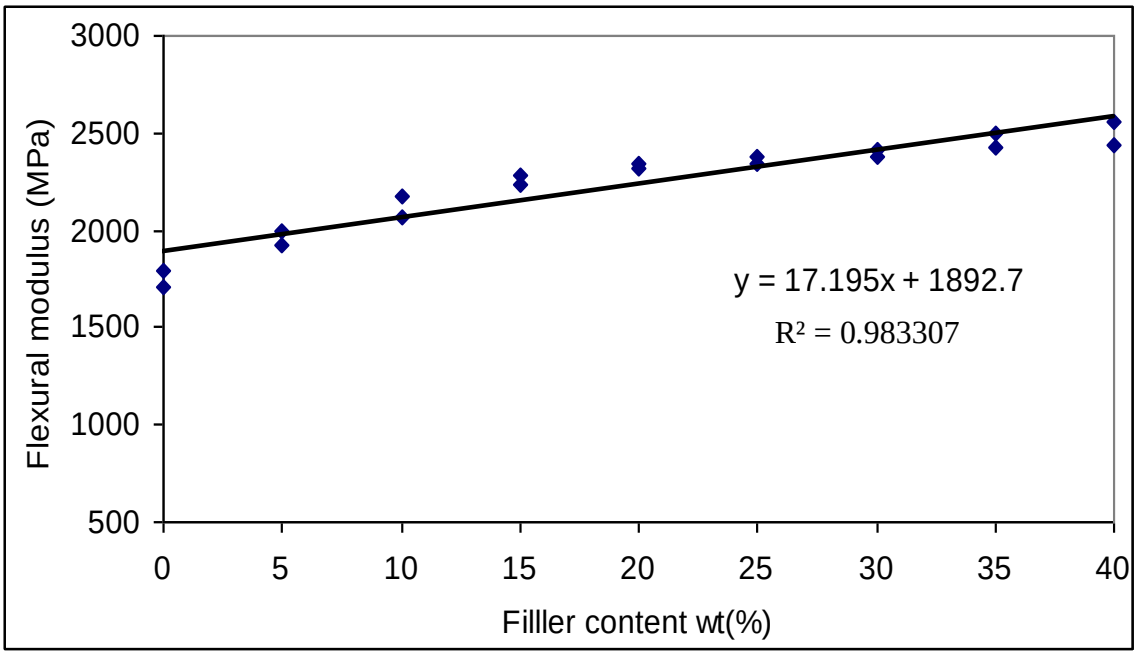

Figure 6.12: Correlation between the results of the cast and SLS specimens for flexural modulus.

6.4.5 Flexural yield strength

From Figure 6.13, the various wt% of cement filler's influence on flexural yield strength of the samples produced through SLS and the casting method may be observed. As the wt% of cement filler increases, so does the flexural yield strength. From the Figure, what can also be seen is a comparison of flexural yield strength for both methods across various wt% of cement filler added to Polyamide 12. The difference in measured values is almost equivalent. The greatest disparity is a value 4.97979% higher than for the SLS method at 40% of cement filler, while the smallest variation is 1.642105% higher than for the casting method at 0% of cement filler. The average difference in flexural yield strength values between SLS and the casting method for all wt% of cement filler is 3.137744%, signifying an acceptable level of variation for both sets in terms of flexural yield strength.

It can be seen from Figure 6.14 that flexural yield strength data from the specimens produced through SLS and the casting method fits the trendline with an R^2 value of 0.97009, demonstrating that the trendline produces a relatively precise linear illustration of the effect of increasing cement filler in both methods of manufacturing specimens. This suggests that the effect of increasing amounts of cement filler on the flexural yield strength of both the cast and SLS specimens is comparatively similar and the casting method used to produce flexural yield samples is acceptable to predict specimens produced using the SLS method.

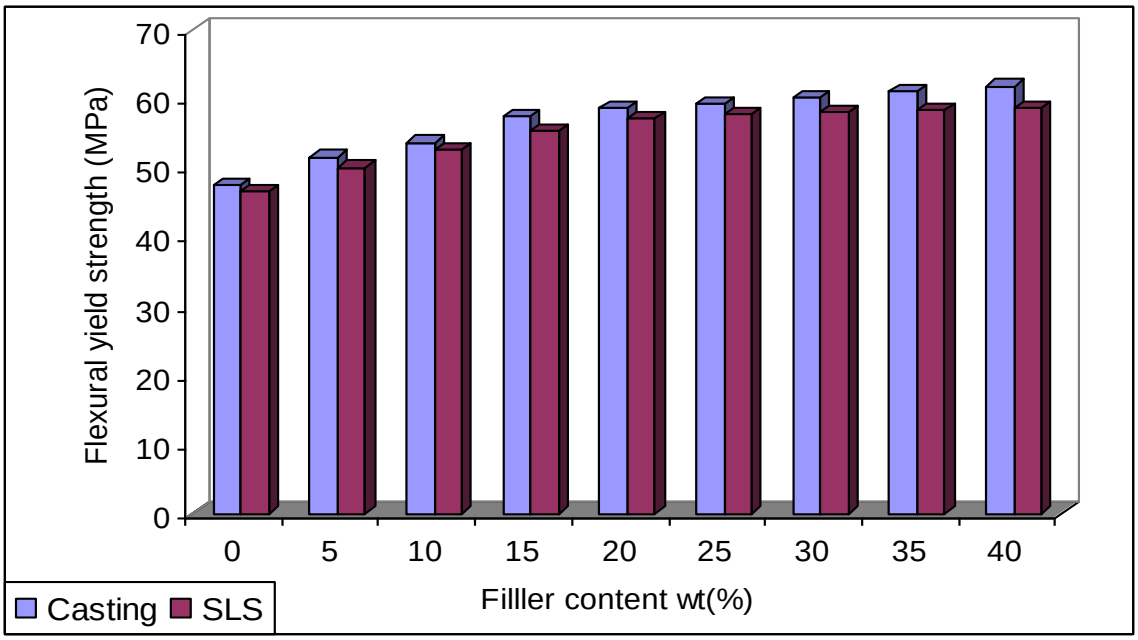

Figure 6.13: Variation of flexural yield strength with cement content for different methods (SLS; casting).

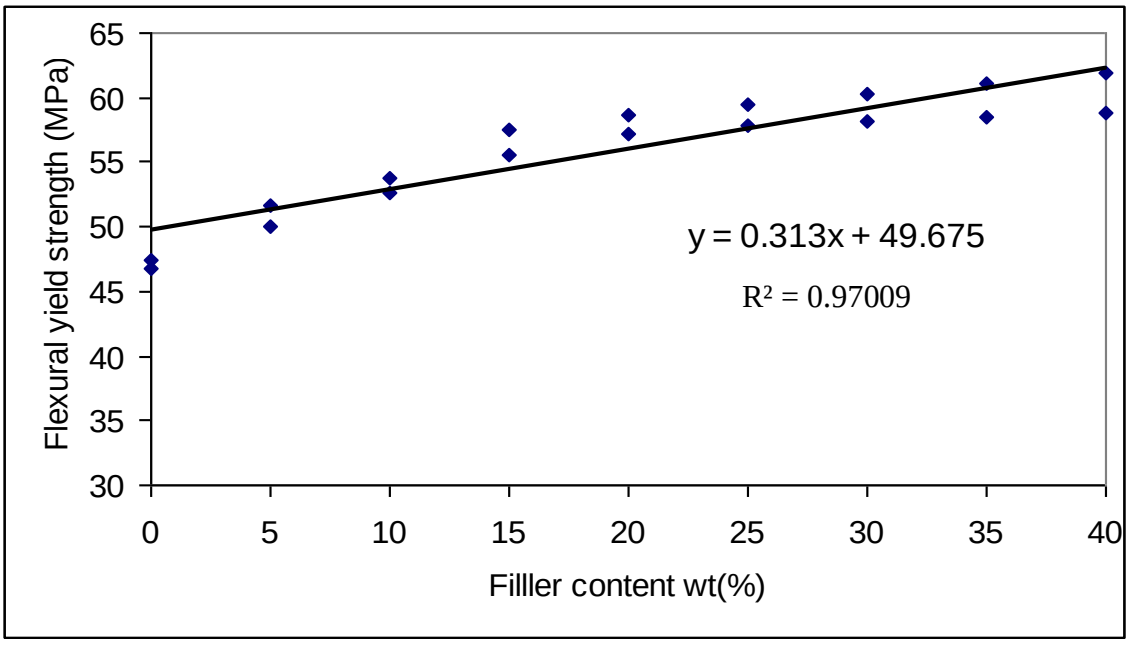

Figure 6.14: Correlation between the results of the cast and SLS specimens for flexural yield strength.

6.4.6 Compressive strength

For the purposes of comparison, Figure 6.15 demonstrates that compressive strength results were schemed against the proportions of cement filler additive with Polyamide 12 for specimens produced via the casting and SLS methods. As shown in the Figure, the compressive strength of the composite specimens increases with greater wt% of cement filler for both the cast and SLS methods and from the same Figure. It is clear from the results for compressive strength in both methods that the difference is comparatively small. The greatest difference in values for compressive strength between both methods is indicated for the SLS method with a value 4.8583% higher at 0% of cement filler, whilst the lowest disparity is a value 1.197822 % less than in the SLS method at 10% of cement filler. Furthermore the average difference between all results of compressive strength for the casting and SLS methods is 2.579453%, which indicates that there is a good correlation between the two methods in terms of compressive strength.

Figure 6.16 shows a schemata with a single trendline through all data-points for the compressive strength of samples manufactured using the casting and SLS methods, with an R^2 value of 0.98196 to corroborate the correlation between the results obtained for compressive strength in both methods. From these results, it may be suggested that the effect of increasing amounts wt% of cement filler on the compressive strength for both methods is relatively similar. This allows for an acceptably accurate prediction regarding the SLS and casting methods.

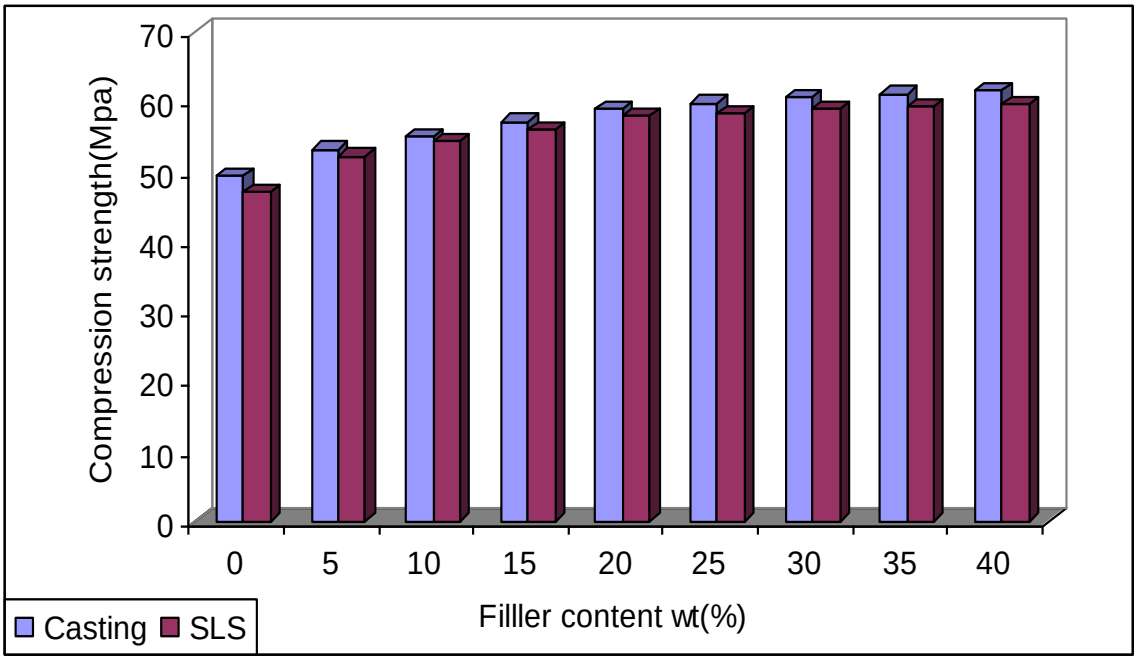

Figure 6.15: Variation of compression strength with cement content for different methods (SLS; casting).

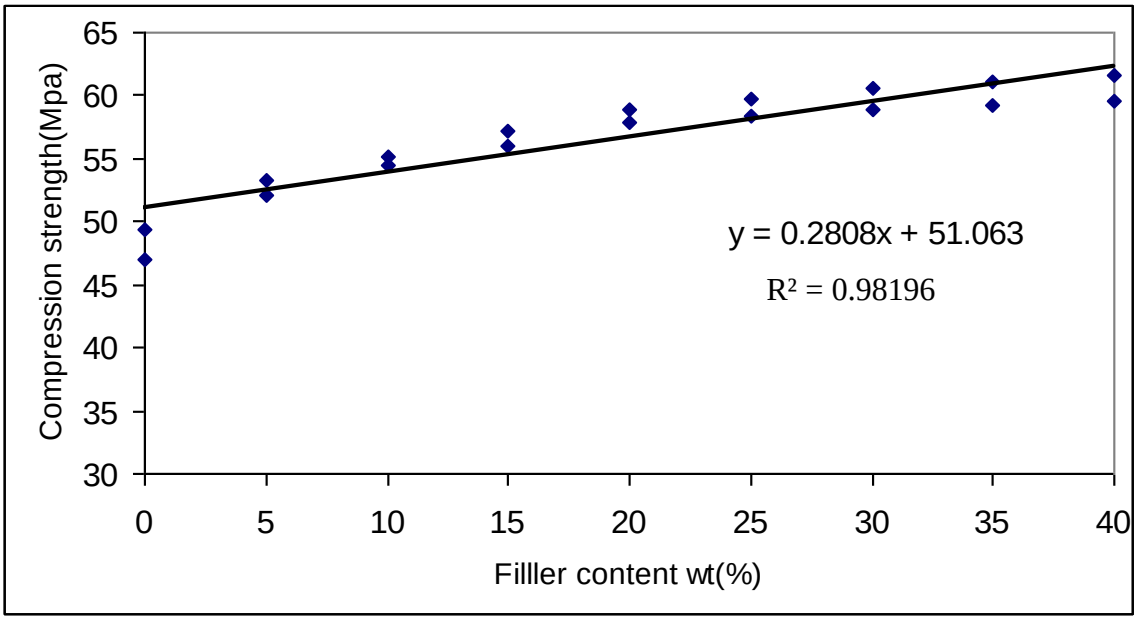

Figure 6.16: Correlation between the results for cast and SLS specimens in terms of compression strength.

6.5 Summary

This chapter presents a comparison between data on the mechanical properties of specimens produced through SLS and casting at atmospheric pressure, in order to investigate whether the latter method is suitable for producing parts with mechanical properties similar to those of SLS specimens in the same material. The comparison of the cast and SLS data-sets has shown that the tensile strength, elongation at break, Young's modulus, flexural modulus, flexural yield modulus and compressive strength obtained from specimens produced using casting were greater than in the SLS specimens. In addition, the data for the mechanical properties of both methods indicated a relatively small difference. This was proved by statistical models of coefficient of determination, indicating that cast specimens could be used to predict the properties of SLS parts produced in the same material. This would reduce the length of time consumed and save large amounts of material.

Chapter 7

Contributions, Conclusions and Future Work

7.1 Contributions

The development of a new composite material from cement additive with Polyamide 12 has been performed, in order to improve the mechanical properties of the sintered specimen and reduce the cost of the Polyamide 12 through the addition of cement.

An investigation of the thermal properties of composite material of cement and Polyamide 12 of the virgin powder has been carried out with different proportions of cement filler for controlling SLS parameters and obtaining consistent quality of fabricated SLS specimens.

A method of casting to produce specimens with properties similar to those of SLS parts has been examined with the aim of reducing the amount of time consumed and the large amounts of material used.

A methodology for controlling the proportion of additive cement filler to Polyamide 12 has been projected.

The possibility of using un-sintered powder exposed to high temperature for an extended period in the SLS system has been examined, and the development of a methodology for controlling the amount of virgin powder to be added to used powder has been investigated.

The relationship between mechanical properties and the melt flow rate (MFR) indicates that MFR is a proven good indicator of powder fitness and mechanical properties.

7.2 Conclusions

Applications of rapid prototyping are expanding to new domains. This is particularly true of the selective laser sintering (SLS) process. In order for that process to be competitive and become a strong candidate for new applications, such as rapid manufacturing, the material used needs to be improved. This research attempts to bring about SLS material improvement by creating new composite material from cement additive with Polyamide 12, so as to reduce the cost of Polyamide 12, as well as considerably improving the mechanical properties of the sintered specimen through the addition of cement.

The thermal properties of the powder play an essential role in obtaining proper SLS parameters, so a better understanding of the thermal properties of composite material of cement with PA12 of the virgin and used (un-sintered) powder is helpful in

controlling SLS parameters and obtaining consistent quality in the fabricated SLS specimens. In addition, the physical properties of virgin and used or un-sintered powder are studied to expand a methodology for controlling the proportion of filler additives to Polyamide 12 and organising the amount of virgin powder to be added to the used powder, in order to obtain consistent, good quality and fine mechanical properties.

The combined indications of the differential scanning calorimeter (DSC) suggest that the different proportions of cement added to the Polyamide 12 do not affect the glass transition temperature, *Tg*, melting temperature, *Tm*, or crystallisation temperature, *Tc* and this leads to a part-bed temperature fixed at 177 °C with different proportions of cement added to the Polyamide 12, while the melt flow rate index test proposes that the addition of cement particles to Polyamide 12 affects the melt flow rate of the composite. As the proportion of cement increases, so does the viscosity of the composite, due to a decrease in melted Polyamide 12. In addition, the gap between the cement particles becomes narrower, so that the extruded material becomes more viscous. This is a sign of a decrease in the MFR index and it ultimately affects the quality of surface finish of the fabricated SLS specimens. Therefore, an acceptable proportion of additive filler of cement to Polyamide 12 was established as 30%. This was found to be the maximum proportion required to produce sufficient surface finish of sintered specimens.

Large amounts (80% to 90%) of powder, remain un-sintered during the SLS process and could be reused, depending on its properties. However, the properties of un-sintered powder deteriorate through exposure to high temperatures, just below the melting point of the composite material for an extended period throughout SLS building and cool-down stage. The temperature and heating time to which the un-sintered powder are exposed are the most significant parameters for powder aging and deterioration of material properties.

The melt flow rate index tests intend that the temperature at which the un-sintered composite powder was exposed and the duration of this exposure affect the melt flow rate of the composite. The MFR of the composite material decreases by 18-25 g/10min with powder usage and this was attributed to the increased molecular weight, which leads to increased viscosity and then decreasing MFR. The powder without exposure to temperature has the lowest viscosity and highest MFR, while the powder exposed to the highest temperatures over the longest periods has the highest viscosity and lowest MFR. The molecular weight and melt flow rate of the samples subjected to continuous and cyclic heating is less significant than the temperature and heating time of the SLS process on material deterioration.

The differential scanning calorimeter DSC suggests that the temperature and heating time at which the un-sintered powder is exposed affect the glass transition temperature, *Tg*, melting temperature, *Tm* and crystallisation temperature, *Tc* and this generates changes in the part-bed temperature with different grades of powder. The

melting temperature of the composite material increases by 0.5-1 ºC with each build or cycle until it reaches 4ºC at the longest period of exposure of the powder to the part-bed temperature. The fabrication parameters in the SLS process are mainly dependent on the properties of powder used, so changing the fabrication parameters as the aging powder changes can give consistent and good quality fabricated SLS specimens.

The indications of the mechanical properties and MFR tests recommend that there is a relationship between results obtained from the melt flow rate index and tensile and compressive strength measures. As the powder degrades due to exposure to high temperatures for an extended period through the SLS system, the tensile and compressive strength deteriorates. Therefore, the amount of virgin power to be added to achieve the target melt index has varied from 25% to 42%. The melt flow rate index has proved to be a good indicator of powder fitness and mechanical properties.

It was also found that optimum energy density (ED) was obtained using a Sintersation 2000 machine with composite material from cement additive with Polyamide 12 at 0.051 J/mm². It was clear that ED has a major effect on the density and mechanical properties of sintered parts.

The density of sintered parts increases as ED increases until it reaches optimum energy density and then decreases as ED is increased even further. Sintered parts are porous and weak if the ED is inferior, but become denser and stronger as ED

increases to a certain degree and then are weakened through degradation of the binder at excessive exposure to ED.

In order to carry out and confirm the effect of ED on the density of sintered parts produced from composite material of cement additive with Polyamide 12, the research has endeavored to explain the effects of various ED on the density of composite material by examining the physical construction of the specimens through using scanning electron microscopy (SEM).

SEM discloses that sintered specimens built with low ED under 0.043 J/mm² have partially melted Polyamide 12 particles but the majority of these particles can be recognised individually because they have maintained their original shape rather than melting, thus leading to defects and porosities. SEM illustrates that the sintered parts built with higher levels of ED between 0.047 J/mm² and 0.051 J/mm² become denser and the fusion of the Polyamide 12 particles is better; the particles seem to be homogeneous and cannot be seen independently, which results in decreased porosity, therefore enabling a more compact structure to be built. Due to excessive exposure of ED to the powder at a level above 0.054 J/mm², SEM explains the degradation of the Polyamide 12 and a dark colour on the surface of the part due to overheating caused by ED.

A comparison was applied between the mechanical properties of measured values of actual parts produced by SLS Sintersation 2000, and data-sheet values supplied by

EOS for pure Polyamide 12, in order to ensure that Sintersation 2000 was capable of producing consistent parts. Compared with the data-sheet, results confirmed that the Sintersation 2000 used in this research was reliable to produce parts with consistent mechanical properties.

Composite material of cement additive with Polyamide 12 plays an essential role in the development of mechanical properties of sintered parts built using SLS Sintersation 2000. To a certain extent, adding cement filler to Polyamide 12 gives superior Young's modulus, flexural strength, compression strength and tensile strength to some extent in sintered specimens, but in terms of impact strength, the addition of cement particles to Polyamide 12 weakens the impact of the composite. To obtain consistency, good surface quality and fine mechanical properties in the fabricated SLS specimens, the suitable proportion of cement added to the Polyamide 12 proved to be 30% by weight, illustrated in the production of the garlic crusher.

Numerous materials and certainly, any material that can be triturated, may be used in the SLS process. However, with continuity and the increase of new powder and composite materials for use in SLS, limitations could arise, caused by the time-consuming nature of the SLS process itself when testing new materials (machine set-up, preheating, building, cool-down and cleaning the machine properly). In addition, there is the problem of the enormous amount of material required to produce parts using SLS. The casting method is therefore used in this research to simulate the mechanical properties of SLS parts, while reducing the amount of time and massive

amount of material involved when testing new materials. It was found that the casting method was suitable for predicting the mechanical properties of SLS specimens in the same material, as the data of mechanical properties for both methods does not differ a great deal, as proven by statistical models of the coefficient of determination.

The research mainly focused on the mechanical properties of the new composite material and specimens made from that material, but it should be obvious that the new material will be cheaper than pure Polyamide 12, as cement is much less expensive than Polyamide 12 (see Appendix C for a brief analysis of the cost of different materials).

7.3 Future work

One possible future research direction is the study of a phenomenon termed ‘curling’, which occurs due to temperature differences in different regions of the fabricated part, leading to uneven shrinkage. Shrinkage causes the surfaces of the part to display a curved profile when they are supposed to be flat.

In the SLS process, the sintered parts also exhibit varying degrees of inherent porosity, due to the nature of layer-by-layer construction. Through the sintering process, bonds between particles occur. Therefore, blocking tortuous and interconnected pore channels leads to the development of isolated porosity. This is usually an undesired trait, as the part integrity decreases with increased porosity. The

porosity phenomena could generate further work to investigate, eliminate or reduce the porosity in sintered components.

Finally, another possible further investigation course is the study of the effect of proportion of cement additive to Polyamide 12 and SLS processing parameters on the surface quality of sintered components. The most important factors considered to be an influence on the surface roughness are layer thickness (powder thickness of each layer in the part-cylinder) which leads to 'stair-stepping', laser power, laser beam speed, laser beam offset, beam diameter, scan spacing and part bed temperature.

Appendix A Equations used to find the value of mechanical properties

Equations used to find the value of mechanical properties

A.1 Flexural stress

$$\sigma_f = \frac{3FL}{2bh^2}$$

Where:

σ_f is the flexural stress expressed in megapascals.

F is the force applied concerned in Newton.

L is the span expressed in millimetres.

b is the width of the specimen expressed in millimetres.

h is the thickness of the specimen expressed in millimetres (BS EN 2746, 1998).

A.2 Flexural modulus

$$E_f \quad \frac{L^3}{4bh^3} \quad \frac{\Delta F}{\Delta d}$$

Where:

E_f is the modulus expressed in megapascals.

ΔF is a chosen difference in force concerned, in Newton.

Δd is the difference in deflection corresponding to the difference in force ΔF expressed in millimetres (BS EN 2746, 1998).

A.3 Stress calculations of tensile and compressive

$$\sigma = \frac{F}{A}$$

Where:

σ_f is the stress expressed in megapascals.

F is the measured force concerned, in Newton.

A is the initial cross-sectional area of the specimen expressed in square millimetres (ISO 527.2, 1996).

A.4 Elongation

$$\varepsilon\,(\%) = \frac{\Delta L_o}{L_o} \times 100$$

Where:

ε is the strain value expressed as a dimensionless ratio, or in percentage.

L_o is the original length of the test specimen expressed in millimeters.

ΔL_o is the increase in the specimen length between the gauge marks, expressed in millimetres (ISO 527.2, 1996).

A.5 Izod impact strength of notched specimens

$$a_{iN} = \frac{Ec}{h \,.\, b_N} \times 10^3$$

Where:

a_{iN} is the Izod impact strength of notched specimens expressed in kilojoules per square metre.

E_c is the corrected energy absorbed by breaking the test specimen expressed in joules.

h is the thickness of the test specimen in millimetres expressed in millimeters.

b_N is the remaining width of the test specimen expressed in millimeters (ISO 180, 2001).

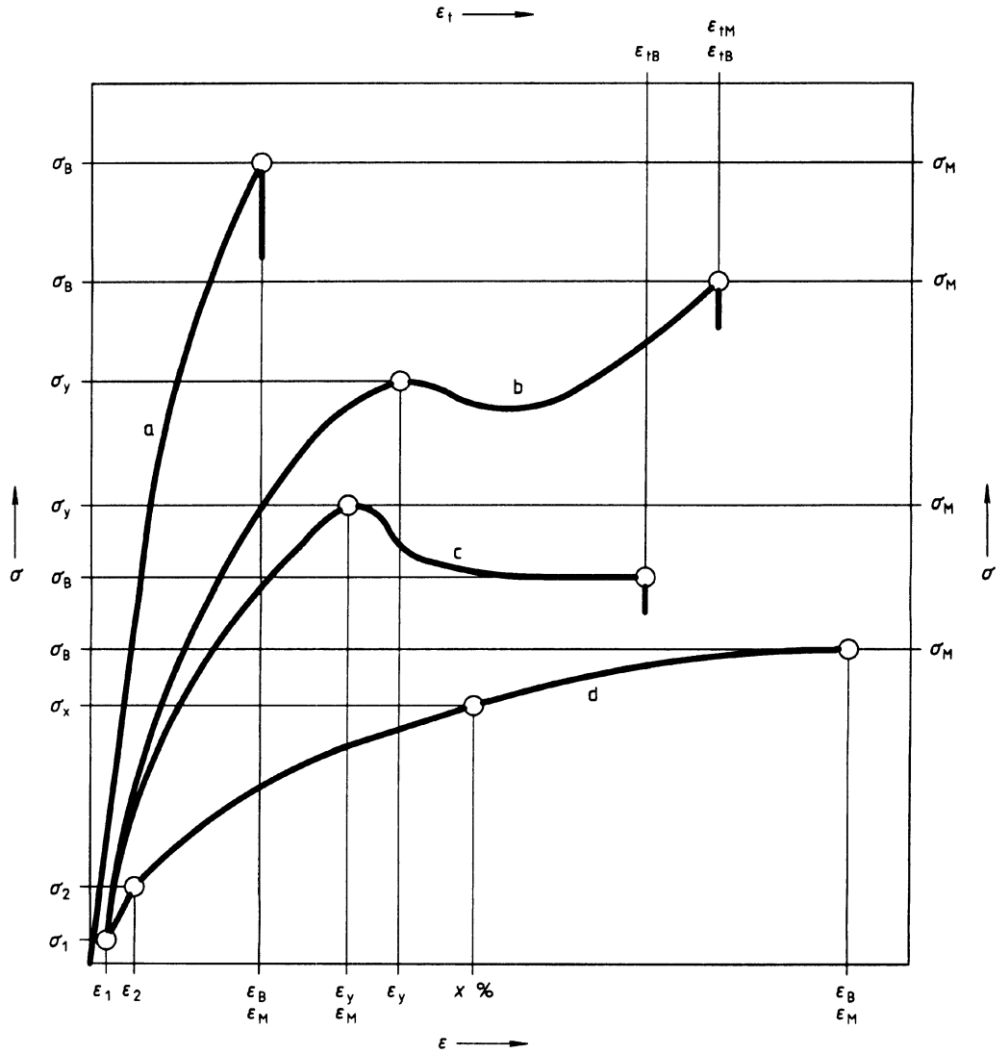

Figure A.1: Stress / Strain curves (a) Curve of brittle materials (b) Curve of tough materials with yield point (d) Curve of tough materials without yield point (ISO 527.2, 1996).

Appendix B The history and manufacture of Portland cement

Portland cement was developed from natural cements in the early part of the nineteenth century by Joseph Aspdin, and its name is derived from the place Isle of Portland in Dorset located in South West England.

Portland cement is considered the common type of cement used at present. It is made by heating raw materials of limestone and clay to high temperature to form clinker, and then the particles of clinker are ground down to small particles. Usually the Portland cement is manufactured in a four step process.

The first step is quarrying limestone or chalk and clay or shale and brought them to the cement plant with smash the limestone to small pieces less than 25 mm. These raw materials contain significant quantities of component of lime ($CaCO_3$), silica (SiO_2), alumina (Al_2O_3) and ferrous oxide (Fe_2O_3).

The second process is considered raw material preparation to form a consistent clinker. So the proportions of limestone and clay should be chosen by high precision to get good composite to form high-quality clinker after burn them.

The third step is heat treatment whereas the raw materials are fed into a rotating kiln and then they are started to dry and heat by high temperature of around 1200-1400 ^oC. After that the chemical reactions start to occur to form clinker which contains four main minerals are tricalcium silicate (C_3S) formed 65% of cement, dicalcium silicate (C_2S) formed 15% of cement, tricalcium aluminate (C_3A) formed 7% of cement and

last one tetracalcium alumino-ferrate (C_4AF) formed 8% of cement. Once the clinker is produced the cool down stage started and then transport to a storage area.

Last step is called cement milling in this process the particles of clinker is big size. So it is ground to get a fine powder, and then mixed with gypsum (hydrated calcium sulphate) which acts as a set regulator (retarder) (Barnes, 1983; Varas et al., 2005; Bramante et al., 2008).

Appendix C Cost of materials

C.1 Effect of cement additive on the price of Polyamide 12.

Figure C.1 illustrates the cost of cement filler composite material with Polyamide 12 in various types of cement filler content from 0 wt% to 40 wt%. It is clear from the graph representation that the cost of composite material is influenced by various weight fractions (wt%) of cement. It can be seen that the percentage of money saved on composite material increases with a rise in weight fractions of cement. This result confirms that the addition of cement particles to Polyamide 12 saves money by over 20% when 40wt% cement filler is added and this satisfies the market demand for cost-cutting on sintered components.

C.2 Comparison of the cost between composite material of (cement/PA12) and (GF)

Figure C.2 demonstrates how percentage cost results were plotted against different composite materials. The first composite material is cement filler additive with Polyamide 12 and the second composite is glass bead filler additive with Polyamide 12 for the purpose of comparison. As shown in the Figure, the cost decreases as weight fractions (wt%) of cement filler are increased and the cost increases with a rise in the proportion of glass bead filler. It is clear from the graph that the data on percentage costs differs between both composite materials. The cost of glass filler is always higher than that of composite material of cement filler with added Polyamide 12. This percentage difference in cost starts from 7% at proportion 5 and continues to

increase until it reaches 45.1% at weight fraction 40, thus demonstrating that the cost of composite material of cement additive with Polyamide 12 is cheaper than that of glass bead filler.

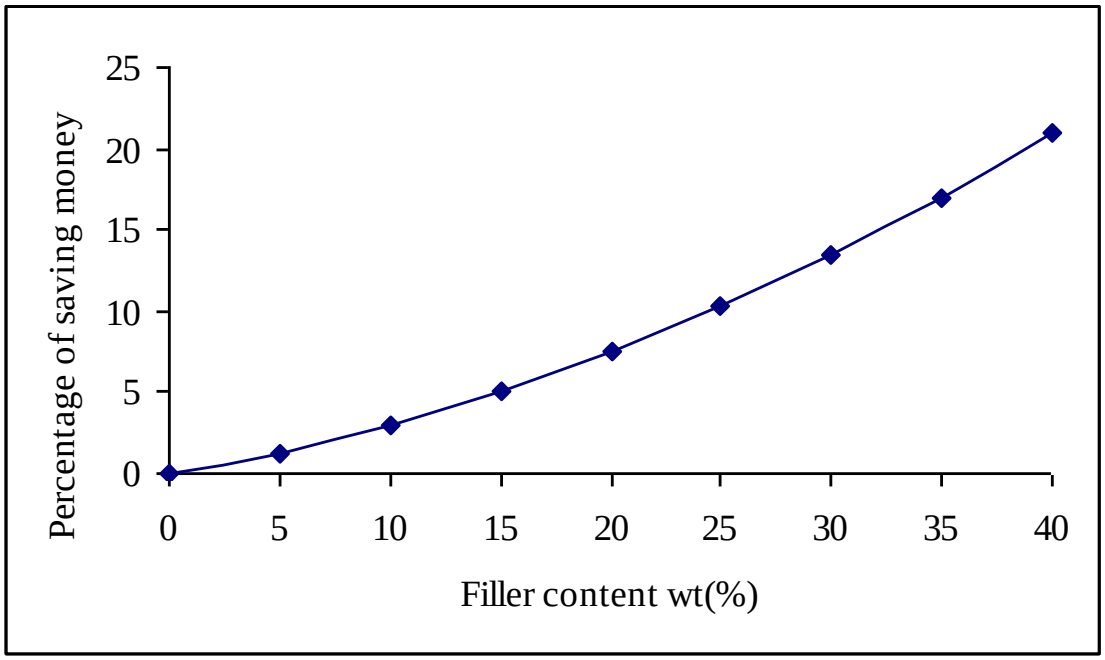

Figure C 1: Effect of cement filler and Polyamide 12 on relative cost.

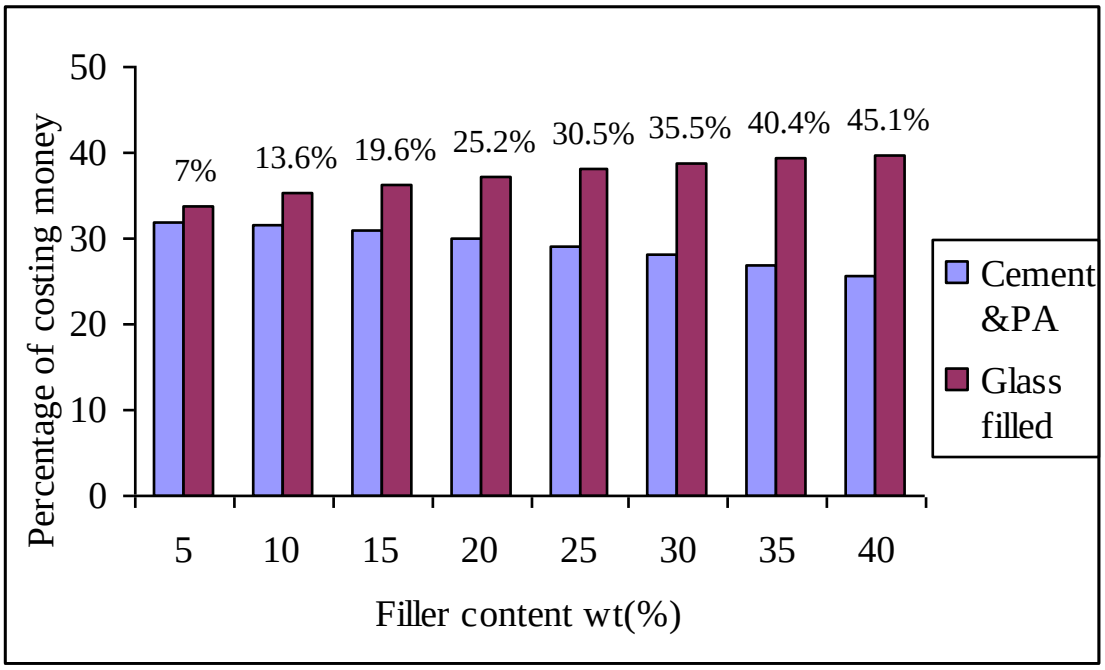

Figure C 2: Comparison of the cost of composite material of cement & PA12 and GF.

Appendix D Case study

D.1 Case study

The purpose of this experiment is to implement the optimal parameters of SLS and the highest proportion of cement additive composite material with Polyamide 12 to produce part of a garlic crusher with consistent, good quality and at a low cost. For this reason, the optimal energy density of 0.051 J/mm² and the highest proportion of 30%-40% of composite material weight fractions were employed in this experiment.

The SLS Sintersation 2000 was employed to produce three parts of a garlic crusher, each one in a separate run with the same parameters and varying proportions (see Figure D.1). The surface quality of the sintered parts of the garlic crusher was assessed through observation and touch on the part surface. It was found from the three components that all parts were classified as having acceptable consistent, good quality surface finish. However, it was seen that the roughness of the surface finish of components increased alongside increases in the proportion of cement filler.

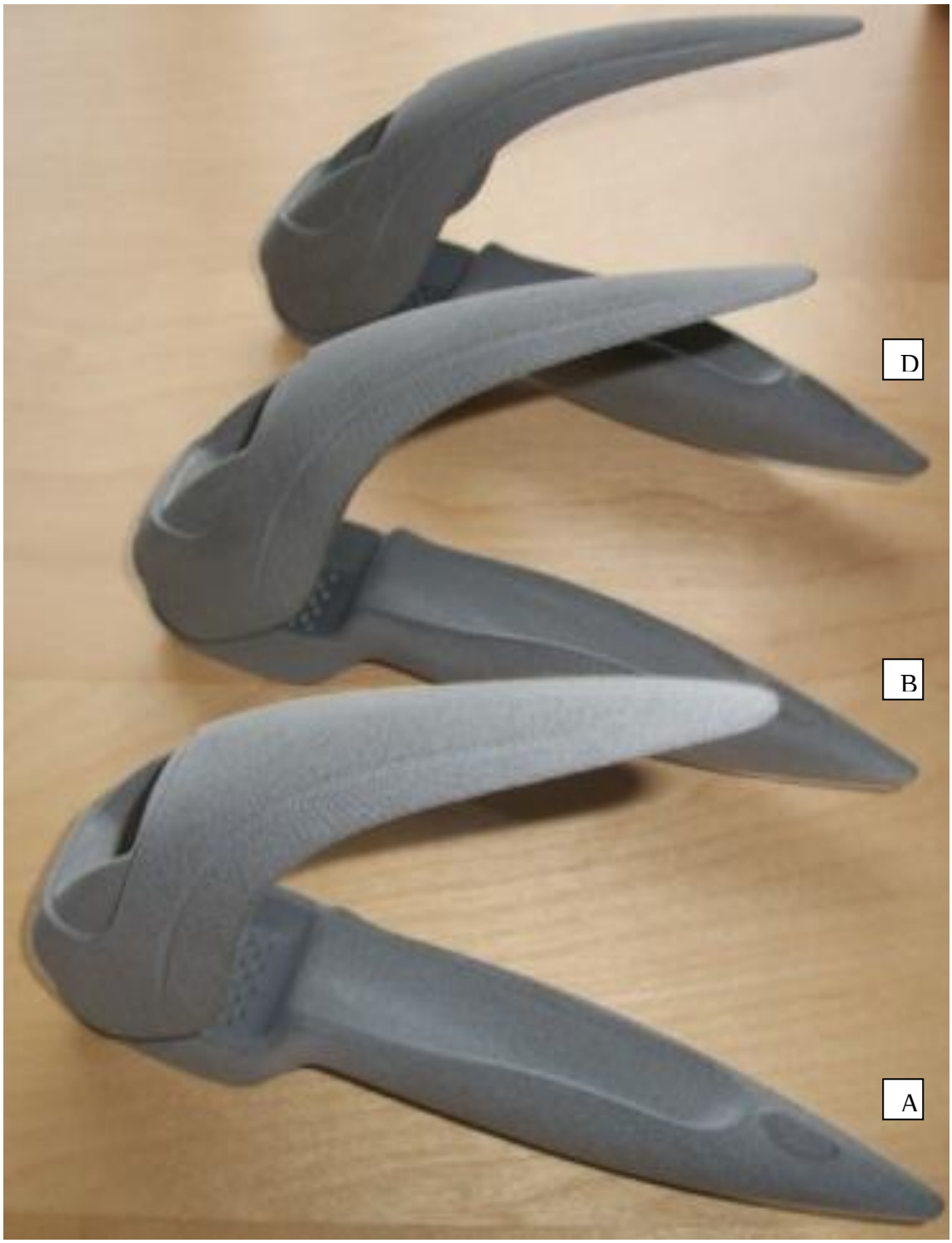

Figure D 1: Illustration of a garlic crusher made of composite material of cement filler with Polyamide 12 (A): 30% cement filler (B) 35% cement filler (D) 40% cement filler.

References

Abid, M. 2009, *Investigation of orange peel phenomenon related to powder deterioration and relevant process parameters*. PhD Thesis, Cardiff University.

Ajoku, U. Saleh, N. Hopkinson, N. Hague, R. and Erasenthiran, P. 2006. Investigating mechanical anisotropy and end-of-vector effect in laser-sintered nylon parts. *Journal of Engineering Manufacture.* 220(7) pp 1077-1086.

Barnes, P. 1983. *Structure and Performance of Cements.* London: Applied Science.

Beal, V. E. Paggi, R. A. Salmoria, G. V. and Lago, A. 2009. Statistical evaluation of laser energy density effect on mechanical properties of polyamide parts manufactured by selective laser sintering. *Journal of Applied Polymer Science*. 113 (5) pp 2910-2919.

BS EN 2746:1998. *Glass fibre reinforced plastics — Flexural test — Three point bend method.* British Standard Aerospace Series.

Beaman, J.B. Barlow, J.W. Bourell, D.L. Crawford, R.H. and Marcus, H.L. 1997. *Solid Freeform Fabrication: A New Direction in Manufacturing.* Dordrecht: Kluwer Academic Publishers.

Bertrand, P. Bayle, F. Combe, C. Goeuriot, P. and Smurov, I. 2007. Ceramic components manufacturing by selective laser sintering. *Applied Surface Science*. 254(4) pp 989-992.

Berzins, M. Childs, T.H.C. and Ryder, G.R. 2007. The Selective Laser Sintering of Polycarbonate. *CIRP Annals - Manufacturing Technology*. 45(1) pp 187-190.

Boivie, K. 2000. SLS Application of the Fe-Cu-C System for Liquid Phase Sintering [online]. Available at: http://74.125.155.132/scholar?q=cache:fSQhHwoBHEYJ:scholar.google.com/&hl=en&as_sdt=2000 [Accessed: 15 June 2008].

Bramante, C. M. Demarchi, A. Moraes, I. G. and Bernadineli, N. 2008. Presence of arsenic in different types of MTA and white and gray Portland cement. Mosby, Inc. 106(6) pp 909-913.

Brydson, J. 1999. Plastics Materials. 7th ed. Oxford: Butterworth Heinemann.

Castle, I. 2008. Fused Deposition Modelling [online]. Available at: http://home.att.net/~castleisland/fdm_int.htm [Accessed: 5July2008].

Caulfield, B. McHugh, P.E. and Lohfeld, S. 2007. Dependence of mechanical properties of polyamide components on build parameters in the SLS process. *Journal of Materials Processing Technology*. 182(1-3) pp 477-488.

Chen, X. Wang, C. Xiao, Y. and Huang, S. 2001. Direct Slicing from PowerSHAPE Models for Rapid Prototyping. *The International Journal of Advanced Manufacturing Technology*. 17(7) pp 543-547.

Childs, T.H.C. Tontowi, A.E. 2001. Selective laser sintering of a crystalline and a glass-filled crystalline polymer: experiments and simulations. *Journal of Engineering Manufacture*. 215(11) pp 1481-1495.

Cooper, K.G. 2001. *Rapid Prototyping Technology Selection and Application*. New York: Marcel Dekker, Inc.

Cowie, J.M.G. 1973. *Polymer: Chemistry & Physics of Modern Materials*. Guildford: Billing.

Crawford, R.J. 1987. *Plastics Engineering*. 2nd ed. Oxford: Pergamon Press.

Davies, G.J. 1973. *Solidification and Casting*. London: Applied Science Ltd.

Dewidar, M. M. Dalgarno, K. W. and Wright, C.S. 2003. Processing conditions and mechanical properties of high-speed steel parts fabricated using direct selective laser sintering. *Journal of Engineering Manufacture part B.* 217(12) pp 1651-16663.

Dewidar, M. M and Dalgarno, K. W. 2001. Direct selective laser sintering of high-speed steel, *17th National Conference on Manufacturing Research*, pp 181-186.

Dimov, S.S. Pham, D.T. Dotchev, K.D. and Ivanov, A.I. (2005), Dimensional accuracy of castform polystyrene patterns produced by selective laser sintering, *Proc. of the 2nd International Conference on Advanced Research in Virtual and Rapid Prototyping, October 2005, Leiria*, pp.229-304.

Doehler, H.H. 1951. *Die Casting*. New York: McGraw-Hill Book Company, Inc.

Dotchev, K. and Soe, S. 2006. Rapid manufacturing of patterns for investment casting: improvement of quality and success rate. *Rapid Prototyping Journal.* 12(3) pp 156-164.

DSC. 2005. *Differential scanning calorimetry* [Online]. Available at: http://pslc.ws/macrog/dsc.htm [Accessed: 10 February 2009].

DTM Corporation. 1996. *The Sinterstation@ System 2500, Guide to Materials for Nylon Compounds.* DCN:8001-10003.

DTM Corporation. 1997. *The Sinterstation® System, Guide to materials: DuraForm™ Polyamide, 1611 Headway Circle, Austin, Texas 78754.* DCN:8001-10014.

3D Systems. 2006. CastForm PS material for use with all selective laser sintering(SLS)system[online].Availableat:http://www.3dsystems.com/products/datafiles/lasersintering/datasheets/CastForm-PS-material-A4_UK.pdf [Accessed: 16 June 2008].

EOS, Electro Optical Systems GmbH [online].Available at: http://www.eos.info/en/home.html [Accessed: 20 July 2008].

Fan, K.M. Cheung, W.L. and Gibson, I 2005. Movement of powder bed material during the selective laser sintering of bisphenol-A polycarbonate. *Rapid Prototyping Journal*. 11(4) pp 188-198.

Flood, S.C. and Hunt, J.D. 1988. Columnar to equiaxed transition. *ASM International, ASM Handbook.* 15 pp 130-136.

German, R.M. 1996. *Sintering Theory and Practice.* New York: John Wiley & Sons, Inc.

Gibson, I. and Shi, D. 1997. Material properties and fabrication parameters in selective laser sintering process. *Rapid Prototyping Journal.* 13(4) pp 129-136.

Gill, T. J. and Hon, K. K. B. 2004. Experimental investigation into the selective laser sintering of silicon carbide polyamide composites. *Proc Instn Mech Engrs, Part B: Journal of Engineering Manufacture*, 218(10) pp 1249-1256.

Gubbels, F. Jerome, R. Vanlathem, E. Deltour, R, Calderone, V. Parente, J. and Bredas, L. 1994. Selective Localization of Carbon Black in Immiscible Polymer Blends: A Useful Tool To Design Electrical Conductive Composites. *Macromolecules.* 27(7) pp 1972-1974.

He, D and Jiang, B. 1993. The Elastic Modulus of Filled Polymer Composites. *Journal of Applied Polymer Science.* 49(4) pp 617-621.

Hirschhorn, J.S. 1969. *Introduction to Powder Metallurgy*. New York: American Powder Metallurgy Institute.

Hon, K.K.B. and Gill, T.J. 2003. Selective Laser Sintering of SiC/Polyamide Composites. *Journal of CIRP Annals Manufacturing Technology*. 52(1) pp 173-176.

Ho, H.C.H. Cheung, W.L. and Gibson, I. 2002. Effects of graphite powder on the laser sintering behaviour of polycarbonate. *Journal of Rapid Prototyping.* 8(4) pp 233-242.

Ilkgun, O. 2005. *Effects of Production Parameters on Porosity and Hole Properties in Laser Sintering Rapid Prototyping Process*. PhD Thesis, Middle East Technical University.

ISO1133, 2005. *Plastics Determination of the Melt Mass Flow Rate (MFR) and the Melt Volume Flow Rate (MVR) of Thermoplastics*. Cardiff: British Standard.

ISO11357-6, 2008. *Plastics - Differential scanning calorimetry (DSC)*. Cardiff: British Standard.

ISO16014, 2003. *Plastics-Determination of average molecular mass and molecular mass distribution of polymers using size-exclusion chromatography.* Cardiff: British Standard.

ISO 178, 2003. *Plastics. Determination of flexural properties.* Cardiff: British Standard.

ISO 180, 2001. *Plastics — Determination of Izod impact strength*. Cardiff: British Standard.

ISO 1183-3, 1999. *Plastics. Methods for determining the density of non-cellular plastics. Gas pyknometer method.* Cardiff: British Standard.

ISO527-1, 1996. *Plastics —Determination of tensile properties — Part 1: General principles.* Cardiff: British Standard.

ISO 604, 2003. *Plastics. Determination of compressive properties.* Cardiff: British Standard.

Jain, P.K. Senthilkumaran, K. Pandey, P.M. and Rao, P.V.M. 2006. ADVANCES IN MATERIALS FOR POWDER BASED RAPID PROTOTYPING. *International Conference on Recent Anvances in Materials and Processing.* PSG-tech. Coimbatore, INDIA. pp 1-8.

Jamal, N. M. 2001. *Finite Element Analysis of Curl Development in the SLS process*. PhD Thesis, Leeds University.

Kai, C.C. and Fai, L.K. 1997. *Rapid Prototyping: Principle & Application In Manufacturing*. New York: John Wiley & Sos, Inc.

Katstra, W. E. Palazzolo, R. D. Rowe, C. W. Giritlioglu, B. Teung, P. and Cima, M. J. 2000. Oral Dosage Forms Fabricated by Three Dimensional Printing. *Journal of Controlled Release.* 66(1) pp 1-9.

Kietzman, J. 1999. *RAPID PROTOTYPING POLYMER PARTS VIA SHAPE DEPOSITION MANUFACTURING*. PhD Thesis, Stanford Unoversity.

King, D. and Tansey, T. 2003. Rapid Tooling: selective laser sintering injection tooling. *Journal of Materials Processing Technology.* 132(1-3) pp 42-48.

King, D. and Tansey, T. 2002. Alternative materials for rapid tooling, *Journal of Materials Processing Technology*, 121 pp 313-317.

Kohan, M.K. 1995. *Nylon Plastic Handbook.* New York: Hanser.

Kruth, J.P. Mercelis, P. Vaerenbergh, J. Froyen, L. and Rombouts, M. 2005. Binding Mechanisms in Selective Laser Sintering and Selective Laser Melting, *Rapid Prototyping Journal, Emerald.* 11 (1) pp 26-36.

Kruth, J. P. Wang, X. Laoui, T. and Froyen, L. 2003. Lasers and materials in selective laser sintering. *Journal of Assembly Automation.* 23(4) pp 357-371.

Kumar, V. and Dutta, D. 1997. An assessment of data formats for layer manufacturing. *Journal of Adv. Engng Software* 28(3), pp.151- 164.

Kumar**,** S. 2009. Manufacturing of WC–Co moulds using SLS machine. *Journal of Materials Processing Technology*. 209(8) pp 3840-3848.

Lea, F.M. 1970. *The Chemistry of Cement and Concrete.* 3rd ed. Glasgow: Edward Arnold Ltd.

Levy, G.N. and Schindel, R. 2002. Overview of layer manufacturing technologies, opportunities, options and applications for rapid tooling, *Proc Instn Mech Engrs, Part B: Journal of Engineering Manufacture*, 216, pp 1621-1634.

Liang, J. Z. 2005. Tensile and Flexural Properties of Hollow Glass Bead-filled ABS Composites. *Journal of Elastomers and Plastic*. 37(4), pp.361-370.

Liao, Y.S. Li, H.C. and Chiu, Y.Y. 2005. Study of laminated object manufacturing with separately applied heating and pressing. *The International Journal of Advanced Manufacturing Technology.* 27(7-8) pp 703-707.

Maeda, K. and Childs, T.H.C. 2004. Laser sintering (SLS) of hard metal powders for abrasion resistant coatings. *Journal of Materials Processing Technology.* 149(1-3) pp 609–615.

Majewski, C.E. Zarringhalam, H. Toon, D. Ajoku, U. Hopkinson, N. Caine, M.P. 2008. The use of off-line part production to predict the tensile properties of parts produced by Selective Laser Sintering. *Journal of Materials Processing Technology*. 209(6) pp 2855-2863.

Mangonon, P.L. 1999. *The Principles of Materials Selection for Engineering Design.* New Jersey: Prentice Hall.

Mareri, P. Bastide, S. Binda, N. and Crespy A 1998. Mechanical Behaviour of Polypropylene Composites Containing Fine Mineral Filler: Effect of Filler Surface Treatment. *Composites Science and Technology.* 58(5) pp 747-752.

Martin, J.W. 2006. *Materials for engineering.* 3rd ed. Cambridge: Woodhead Publishing Ltd.

Mazzoli, A. Moriconi, G. Pauri, M. G. 2006. Characterization of an aluminum-filled polyamide powder for applications in selective laser sintering. *Journal of Materials and Design.* 28 pp 993-1000.

MettlerToledo. *Thermal Analysis Excellence.* [Online]. Available at: http://us.mt.com/us/en/home/products/Laboratory_Analytics_Browse/TA_Family_Browse.html [Accessed: 2 July 2008].

Min Hur, S. Hyun, K. Hee, S and Keun, P. 2001. Determination of fabricating orientation and packing in SLS process. *Journal of Materials Processing Technology*. 112(2-3) pp 236-243.

Mueller, B and Kochan, D. 1999. Laminated object manufacturing for rapid tooling and patternmaking in the foundry industry. *Journal of Computers in Industry* 39(1) pp 47-53.

Nakamoto, T. Shirakawa, N. Miyata, Y. and Inui, H. 2009. Selective laser sintering of high carbon steel powders studied as a function of carbon content. *Journal of Materials Processing Technology.* 209(15-16) pp 5653-5660.

Neal, P. J. 1994. Rapid Prototyping Using the Selective Laser Sintering Process. *Rapid Prototyping Journal.* 14(2) pp 14-17.

Nelson, J.C. Xue, S. Barlow, J.W. and Beaman, J. 1993. Model of the selective laser sintering of bisphenol-A polycarbonate. *Industrial & Engineering Chemistry Research*. 32(10) pp 2305-2317.

Pacheco, L.F. and Campos, M. 2009. Bonding Evolution with Sintering Temperature in Low Alloyed Steels with Chromium. *Science of Sintering,* 41 pp 161 173.

Paramount, 2009. SLS Material, Selective Laser Sintering Materials [online]. Available at: http://www.paramountind.com/selective-laser-sintering-material.html [Accessed: 17 June 2009].

Parnes, P. 1983. *Structure and Performance of Cements.* London: Applied Science.

Partanen, J. P. Zheng, N. and Bishop, R. J. 2010. Laser sintering process chamber gas curtain window cleansing in a laser sintering system. [online].Available at: http://www.freepatentsonline.com/7807947.html [Accessed: 20 Jan 2011].

Pham, D.T. and Dimov, S.S. 2000. *Rapid Manufacturing: The Technologies and Applications of Rapid Prototyping and Rapid Tooling*. London: Springer.

Pham, D. T. and Dimov, S. S. 2003. Rapid Prototyping and Rapid Tooling – the key enablers for rapid manufacturing. *Journal of Mechanical Engineering Science* 217(1),pp. 1-23.

Pham, D. T. Dotchev, K. D. and Yusoff, W. A. Y. 2008. Deterioration of polyamide powder properties in the laser sintering process. *Journal of Mechanical Engineering Science.* 222(11) pp 2163-2176.

Pham, D.T. and Gault, R.S. 1998. A comparison of rapid prototyping technologies. *Journal of Machine Tools and Manufacture* 38(10) 1275-1287.

Pintea, A. (no date) Heat Transfer Behaviour of the Parts Manufacturing by Selective Laser Sintering (SLS). [online]. Available http://imtuoradea.ro/auo.fmte/files-2006/TCM_files/Adina%20Pintea%201.pdf [Accessed: 22 June 2010].

Queijo, L. Rocha, J. Barreira, L. and Barbosa, T. 2010. A surgical training model manufacture using rapid prototyping technology. *CRC Press.* [online]. Available at: http://hdl.handle.net/10198/1800 [Accessed: 15 Jan 2011].

Salmoria, G. V. Leite, J. L. Ahrens, C. H. Lago, A. and Pires, A. T. N. 2007. Rapid manufacturing of PA/HDPE blend specimens by selective laser sintering: Microstructural Characterisation. *Journal of Polymer Testing* 26(3), pp. 361-368.

Salmoria, G. V. Leite, J. L. and Paggi, R. A. 2009. The microstructural characterization of PA6/PA12 blend specimens fabricated by selective laser sintering. *Journal of Polymer Testing.* 28 (7) pp 746-751.

Schmidt, M. Pohle, D. and Rechtenwald, T. 2007. Selective Laser Sintering of PEEK. *Journal of CIRP Annals Manufacturing Technology.* 56(1) pp 205-208.

Shirley, D.E. 1986. *Introduction to Concrete.* 3rd ed. Slough: Cement and Concrete Association.

Shi, Y. Chen, J. Wang, Y. Li, Z. Huang, S. 2007. Study of the selective laser sintering of polycarbonate and postprocess for parts reinforcement. *Journal of Materials: Design and Applications.* 221(1) pp 37-42.

Sichina, W.J. 2000. DSC as Problem Solving Tool: Measurement of Percent Crystallinity of Thermoplastics, *PerkniEimer, Inc*.

Subramanian, K. Vail, N. Barlow and Marcus, H. 1995. Selective laser sintering of alumina with polymer binders. *Rapid Prototyping Journal*. 1(2) pp 24-35.

ThermoHaake. 2000. *Instruction Manual SWO of Meltfiler MT*.

3T RPD. 2008. Selective Laser Sintering (SLS) for Rapid Prototyping [online].Available at: http://www.3trpd.co.uk/sls.htm [Accessed: 17 June 2008].

Unal, H. 2004. Morphology and mechanical properties of composites based on polyamide 6 and mineral additives. *Materials & Design.* 25(6) pp 483-487.

Vail, N. K. Balasubramanian, B. Barlow, J.W. and Marcus, H.L. 1996. A thermal model of polymer degradation during selective laser sintering of polymer coated ceramic powders. *Rapid Prototyping Journal.* 2(3) pp 24-40.

Vail, N. K. Barlow, J. W. and Marcus, H. L. 1993. Silicon Carbide Preforms for Metal Infiltration by Selective Laser Sintering (TM) of Polymer Encapsulated Powders. *Solid Freeform Fabrication Proceedings,* The University of Texas, Austin. pp 204-214.

Varas, M. J. Alvarez, M and Fort, R. 2005. Natural cement as the precursor of Portland cement: Methodology for its identification. *Cement and Concrete Research*. 35(11) pp 2055-2065.

Wang, X. 1999. Calibration of shrinkage and beam offset in SLS process. *Rapid Prototyping Journal.* 5(3) pp 129-133.

Xpress 3D . 2005 [online]. Available at:http://www.xpress3d.com/Zcorp3DP.aspx [Accessed: 9 June 2008].

Yan, C. Z. Shi, Y. S. Yang, J. S. and Xu, L. 2009. Preparation and Selective Laser Sintering of Nylon-12-Coated Aluminum Powders. *Journal of Composite Materials*. 43(17) pp 1835-1851.

Young, R.J. 1981. *Introduction to Polymers*. London: Chapman and Hall.

Yusoff, W.A.Y. 2007. *An investigation of the "Orange Peel" Phenomenon*. PhD Thesis, Cardiff University.

Zein, I. Hutmacher, D.W. Tan, K. C. and Teoh, S. H. 2002. Fused deposition modeling of novel scaffold architectures for tissue engineering applications. *Journal of Biomaterials*. 23(4) pp 1169-1185.

Zhou, J. Zhang, Y. and Chen, J.K. 2009. Numerical Simulation of Random Packing of Spherical Particles for Powder-Based Additive Manufacturing. *Journal of manufacturing science and engineering.* 131(3) pp 1-8.

Zhou, W. Y. Lee, S. H. Wang, M. Cheung, W. L. and Lp, W. Y. 2007. Selective laser sintering of porous tissue engineering scaffolds from poly(L lactide) /carbonated hydroxyapatite nanocomposite microspheres. *Journal of Material Science*. 19(7) pp 2535-2540.